Title

THE (3He,p) AND **-_ ,d), TWO-NUCLEON STRIPPING REACTIONS ON 12C AND l60: MECHANISM AND NUCLEAR SPECTROSCOPY

Author

Mangelson, Nolan Farrin.

Publication Date

1967-08-01

UCRL-17732

eg. 2

University of California

Ernest O. Lawrence Radiation Laboratory

THE (^{3}He, p) AND (α, d), TWO-NUCLEON STRIPPING REACTIONS ON ^{12}C AND ^{16}O: MECHANISM AND NUCLEAR SPECTROSCOPY

Nolan Farrin Mangelson

(Ph. D. Thesis)

August 1967

Berkeley, California

DISCLAIMER

UCRL-17732

UNIVERSITY OF CALIFORNIA

Lawrence Radiation Laboratory
Berkeley, California

AEC Contract No. W-7405-eng-48

THE (^{3}He,p) AND (α,d), TWO-NUCLEON STRIPPING REACTIONS ON ^{12}C AND ^{16}O: MECHANISM AND NUCLEAR SPECTROSCOPY

Nolan Farrin Mangelson

(Ph. D. Thesis)

August 1967

THE (^{3}He,p) AND (α,d), TWO-NUCLEON STRIPPING REACTIONS ON ^{12}C AND ^{16}O: MECHANISM AND NUCLEAR SPECTROSCOPY

Contents

FIGURE CAPTIONS

THE (^{3}He,p) AND (α,d), TWO-NUCLEON STRIPPING REACTIONS ON ^{12}C AND ^{16}O: MECHANISM AND NUCLEAR SPECTROSCOPY

Nolan Farrin Mangelson

Lawrence Radiation Laboratory
University of California
Berkeley, California

August 1967

ABSTRACT

Spectra and angular distributions were obtained for the reactions and conditions listed: $^{12}C(^3He,p)^{14}N$ at $E(^3He) = 20.1$ MeV, from $\theta_{lab} = 8°$ to 170° for ^{14}N excited states below 13 MeV excitation; $^{12}C(^3He,^3He)^{12}C$ at $E(^3He) = 20.1$ MeV, from $\theta_{lab} = 8.5°$ to 62.5° for the ground state and 4.433-MeV state of ^{12}C; $^{16}O(^3He,p)^{18}F$ at $E(^3He) = 19.8$ MeV, from $\theta_{lab} = 9°$ to 170° for ^{18}F excited states below 11.3 MeV excitation; $^{16}O(\alpha,d)^{18}F$ at $E(\alpha) = 40.3$ MeV, from $\theta_{lab} = 8°$ to 80° for ^{18}F excited states below 12.7 MeV excitation.

Distorted-wave calculations of angular distributions and relative cross sections for the two (^{3}He,p) reactions were compared to experimental values. Agreement was found when a spin-independent interaction potential was used. Nuclear wave functions used in the calculations were discussed.

Spectroscopic and configuration assignments were made or confirmed on the basis of excitation energy, angular distribution, comparison of (α,d) and (^{3}He,p) results, relative total cross section, and comparison of experimental quantities to the DW calculations. The following assignments were made for ^{14}N. A spin and parity assignment of 2^- and a tentative assignment of 4^+ were made for the 9.388- and 10.85-MeV, T = 0 levels respectively. Suggested configurations were made for the 8.979-, 10.213- and 10.85-MeV levels.

Configurations and J^π values of 3^+ and 4^+ were suggested for ^{18}F levels at 3.358 and 5.594 MeV respectively. Configurations and $J^\pi T$ values were confirmed for some levels and T = 0 assignments were made for a large number of levels. A new ^{18}F level at an excitation energy of 8.596 MeV was identified.

I. INTRODUCTION

Two-nucleon transfer reactions are of value in the study of nuclear physics for several reasons.[1] (1) They can be used for the formation and study of nuclei which are two mass units removed from an available target nucleus. (2) Such reactions selectively populate states of the final nucleus which may be difficult to study by other means. For example two-nucleon stripping reactions preferentially populate states with large components of two particles coupled to the undisturbed target ground state. (3) It will be shown in the expressions of the next section that coherent effects and correlations between the two particles, which arise from angular momentum coupling and the residual interaction, make the two-nucleon transfer cross section sensitive to both the target ground-state wave function and the final-state wave function. This sensitive dependence upon wave functions makes the two-nucleon transfer reaction a valuable tool for testing nuclear wave functions.

Harvey et. al.[2,3] have shown that the (α,d) reaction on light nuclei is a powerful tool for obtaining nuclear spectroscopic information. As will be discussed in this report, a few workers[4,5] have used the $(^3He,p)$ reaction at ^3He energies near 20 MeV or greater as a spectroscopic tool. Inasmuch as transitions involving an isospin change are forbidden[1] in the (α,d) reaction and allowed in the $(^3He,p)$ reaction, a comparison of these two reactions between the same initial and final states may be used to make isospin assignments.

Because of above mentioned advantages of two-nucleon transfer reactions, this study of $(^3He,p)$ and (α,d) reactions was undertaken. The aim of this work was to obtain spectroscopic information both by examination of the data in comparison to other work and also by comparing distorted-wave cross-section calculations for the $(^3He,p)$ reaction to experimental cross-section data. The two-nucleon reaction formalism of Glendenning[1] was used for the calculations.

Targets for the study were ^{12}C and ^{16}O. This choice of targets allows an examination of the validity of the computational methods used for reaction calculations when applied to light nuclei. Several theoretical calculations for the wave functions of ^{14}N and ^{18}F, the product nuclei, were also available for use in the calculations. The levels of

^{14}N below 9-MeV excitation were understood and the reaction involving this nucleus could be used as a test of the proposed reaction mechanism and of the ^{14}N wave functions. The ^{18}F energy levels were not well understood and it was anticipated that spectroscopic information could be obtained for this nucleus.

II. DISCUSSION OF THEORY, SELECTION RULES AND SIMPLIFYING ASSUMPTIONS

The object of this section is to present in outline form the development of direct reaction theory with specific emphasis on two-nucleon transfer reactions. This section does not purport to call attention to all previous writings which are pertinent to the problems and questions discussed.

In order to avoid repetitious citing of references, ideas attributable to other workers will not always be specifically acknowledged; however, all sources used are referred to at least once.

A. Transfer Amplitude and Cross Section

The exact transfer amplitude for scattering problems has been formulated by Gell-Mann and Goldberger.[6] Approximations to the exact amplitude which are convenient for use in the theory of direct reactions have been discussed.[7-11] Let a direct reaction be represented by the following form.

$$A + a \rightleftharpoons B + b \tag{1}$$

A represents the target (product), B represents the product (target), and a and b represent light nuclides. B and a can be described in terms of A, b and x,

$$\begin{aligned} a &= b + x \\ B &= A + x \end{aligned} \tag{2}$$

where x is the portion of a transferred in the reaction. In the remainder of the discussion (1) will be assumed to proceed from left to right.

The transfer amplitude, t, is approximately:

$$t \approx \langle \chi^{(-)} | V | \chi^{(+)} \rangle \tag{3}$$

In (3) $\chi^{(+)}$ is an approximation to the exact wave function for the system in the entrance channel, $\underline{A} + \underline{a}$. In the distorted-wave approximation (DWA) $\chi^{(+)}$ is separated into three factors.

$$\chi^{(+)} = \psi^{(+)}(\vec{k}_1, \vec{R}_1)\psi_{J_1 T_1}(A)\psi_{J_a T_a}(b,x,\rho) \tag{4}$$

The wave function $\psi(A)$ is a function of the internal coordinates of the target $\underline{A}$. $\psi(b,x,\rho)$ is a function of the internal coordinates of $\underline{a}$. It is assumed that these internal coordinates are separable into $\underline{b}$, $\underline{x}$, and ρ, where ρ represents the relative coordinate (or coordinates) between $\underline{x}$ and $\underline{b}$. $\psi^{(+)}(\vec{k}_1, \vec{R}_1)$ is the distorted wave between $\underline{A}$ and $\underline{a}$ with wave number $\vec{k}_1$, and relative coordinate $\vec{R}_1$. An optical-model potential determined by fitting the elastic scattering of $\underline{a}$ on $\underline{A}$ is usually used to generate this distorted wave. $\psi^{(+)}$ has outgoing spherical waves.

Justification for approximating the entrance-channel interaction by the elastic-scattering optical potential is based on the observation that the elastic-scattering process, modified through coupling to other reactions as implied by the optical potential, is the dominant process between $\underline{a}$ and $\underline{A}$. It is assumed that a direct reaction into the channel to be studied may be treated as a perturbation of the elastic-scattering process.

As shown by Henley and Yu[10] the exact interaction between $\underline{A}$ and $\underline{a}$ is a sum of two-body potentials between the nucleons of $\underline{A}$ and $\underline{a}$. It is, therefore, to be expected that the optical-model potential chosen should approximate a sum of two-body potentials.

The interaction potential V is a sum of terms

$$V = V_{bx} + V_{bA} - U_{bB} \tag{5}$$

The potentials V_{bx} and V_{bA} are sums of two-body potentials between the nucleons of the respective nuclides. U_{bB} is an arbitrary potential used to give the asymptotic relationship between $\underline{B}$ and $\underline{b}$.

It is assumed that

$$V_{bA} - U_{bB} \approx 0 \tag{6}$$

leaving only the term V_{bx}. Inasmuch as V_{bA} and U_{bB} involve core nuclei differing by $\underline{x}$ it can be appreciated that this assumption should be more valid for heavy nuclei than for light nuclei. An optical-model potential determined from elastic scattering of $\underline{b}$ on $\underline{B}$ is usually used for U_{bB}.

On would expect U_{bB} to approximate a sum of two-body potentials in order to satisfy (6). For this reason and for reasons discussed in connection with $\psi^{(+)}$ some workers[12-14] have suggested that the optical-model potentials used for nuclear structure calculations should be sums of nucleon potentials or that optical-model well depths should be approximately n times the single-nucleon well depths, the number of nucleons in the light particle being n. It has been pointed out[7,13] that although the optical-model potential gives the proper asymptotic form to the wave functions $\psi^{(+)}$ and $\psi^{(-)}$ (see (7)) it may or may not give the proper form near or within the nucleus. It is, therefore, not unreasonable to consider some variation in the potential that will improve the scattering wave function in the nucleus but may destroy the fit to elastic scattering.

The exit-channel wave function is a product of three factors.

$$\chi^{(-)} = \psi^{(-)}(\vec{k}_2,\vec{R}_2)\psi_{J_2T_2}(A,x,\vec{R})\psi_{J_bT_b}(b) \tag{7}$$

The optical-model wave function $\psi^{(-)}$ between $\underline{B}$ and $\underline{b}$ has wave number $\vec{k}_2$, relative coordinate $\vec{R}_2$ and a boundry condition giving incoming spherical waves. The wave function dependent upon the internal coordinates of $\underline{B}$ is $\psi(A,x,\vec{R})$. It is assumed the coordinates of $\underline{B}$ can be separated into $\underline{A}$, $\underline{x}$, and $\vec{R}$, where $\vec{R}$ represents the relative coordinate (or coordinates) between $\underline{A}$ and $\underline{x}$. $\psi(b)$ is the wave function dependent on internal coordinates of $\underline{b}$. The transition amplitude can now be written using Eqs. (4) and (7).

$$t \approx J\int\psi^{(-)^*}(\vec{k}_2,\vec{R}_2)\langle\psi^*_{J_2T_2}(A,x,\vec{R})\psi^*_{J_bT_b}(b)\,|V_{bx}(\rho)|$$
$$\times\,\psi_{J_1T_1}(A)\psi_{J_aT_a}(b,x,\rho)\rangle\psi^{(+)}(\vec{k}_1,\vec{R}_1)d\vec{R}_1 d\vec{R}_2 \tag{8}$$

The Jacobian for transformation from the natural coordinates $\vec{R}$ and $\vec{R}_{bA}$ (see Fig. 1) to $\vec{R}_1$ and $\vec{R}_2$ is J. This Jacobian will not receive further consideration. Hereafter the symbol J will be used for a different purpose. Note also that strictly speaking the above expression should have definite magnetic quantum number designations. In keeping with the stated objectives of this section these quantum numbers together with their attendant sums will not be considered except in a few cases.

The factor $\langle \| \rangle$ in (8) is the matrix element of the interaction taken between the internal coordinates of the nuclides involved. The matrix element acts as an effective interaction between the initial and final states. Notice that only the interaction between b and x, the two parts of a, is responsible for the transition.

To facilitate calculation of the factor $\langle \| \rangle$ it is necessary to expand the nuclides' wave functions in terms of their respective parts.

$$\psi_{J_2T_2}(A,x,\vec{R}) = \sum_{JT\gamma J_cT_c\gamma'} \beta' {}_{JT\gamma J_cT_c\gamma'} [\psi_{J_cT_c\gamma'}(A)\Phi_{JT\gamma}(x,\vec{R})]_{J_2T_2} \qquad (9)$$

The core A is represented in the configuration γ' with total spin J_c and isospin T_c. The nucleons of x are in a configuration γ characterized by quantum numbers J and T. The square bracket indicates vector coupling, β' is a coefficient of fractional parentage (c.f.p.) times a recoupling constant if one is necessary. For example, the characterization of the nucleons in x might be in a jj scheme. In two-nucleon transfer it is necessary to transform from a jj to an LS scheme thus necessitating a transformation coefficient.

Also included is a statistical factor expressing the number of ways the particles of x can be drawn from identical particles of B. Assume x contains i nucleons and these can be drawn from i' identical nucleons in B (i' nucleons in a shell above a closed core for example). The statistical factor is then

$$\binom{i'}{i}$$

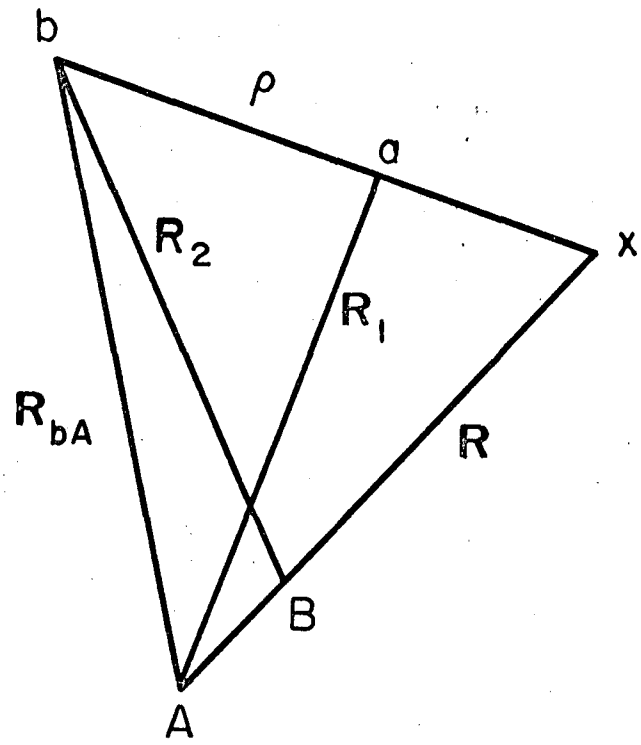

XBL678-3859

Fig. 1. Spatial relationship between the centers of mass of particles in a nuclear reaction.

If $\psi(A,x,\vec{R})$ is a wave function of mixed configuration the appropriate mixing coefficients are also included in β'.

The wave function of $\underline{x}$ must be further expanded.

$$\Phi_{JT\gamma}(x,\vec{R}) = \sum_{N\Lambda MS\gamma''} P_{N\Lambda SJT\gamma''} [U^{M}_{N\Lambda}(\vec{R})\chi_{ST\gamma''}(x)]_{JT} \qquad (10)$$

It is here assumed that $\Phi(x,\vec{R})$ can be expanded in terms of internal structure $\chi_{ST\gamma''}(x)$ and center-of-mass motion $U^{M}_{N\Lambda}(\vec{R})$ taken relative to $\underline{A}$. $P_{N\Lambda SJT\gamma''}$ are expansion coefficients defined by Eq. (10). These coefficients will be further discussed in Sec. II-B. The square bracket indicates vector coupling. The center-of-mass motion of $\underline{x}$ is characterized by principle quantum number N and angular momentum Λ. The z projection of Λ is taken to be M. S is the total intrinsic spin of $\underline{x}$ and T is the total isospin of $\underline{x}$. The internal relative motion of $\underline{x}$ is designated by γ''.

The light particle $\underline{a}$ must be expanded in terms of its space and spin components. Consideration will be restricted to $\underline{a}$ and $\underline{b}$ with four nucleons or less whose motion is relative S with respect to one another. The quantum number J_a of Eq. (4) then becomes S_a, the total intrinsic spin of $\underline{a}$.

Assume that the wave function of $\underline{a}$ is a product of space and spin terms. A Gaussian wave function is an example[1] of the desired type of function.

$$\psi_{S_aT_a}(b,x,\rho) = \chi_{S_aT_a}(b,x)\phi'(b)\phi'(x)\phi(\rho) \qquad (11)$$

$\chi(b,x)$ is the spin and isospin function of $\underline{a}$. $\phi(\rho)$ indicates the relative motion between $\underline{b}$ and $\underline{x}$. The other two factors indicate relative motion within $\underline{b}$ and $\underline{x}$.

It is assumed that the wave function of $\underline{b}$ in the exit channel can be expanded into a space and spin function. Because of the assumed relative S motion J_b now becomes S_b.

$$\psi_{S_bT_b}(b) = \chi_{S_bT_b}(b)\phi(b) \qquad (12)$$

The spin function is $\chi(b)$ and $\phi(b)$ is the spatial function.

The requirement of overlap between the initial and final channel imposes several restrictions on the expansions just discussed. The overlap of the core $\underline{A}$ with the target requires J_c and T_c equal J_1 and T_1 respectively. By assumption the internal motion of $\underline{x}$ in $\underline{a}$ is relative S only. Thus only relative S motion of $\underline{x}$ in $\underline{B}$ is allowed. It follows that the total orbital angular momentum L associated with $\underline{x}$ arises from the center-of-mass motion. Therefore Λ is set equal to L.

The factor $\langle\|\rangle$ of Eq. (8) can now be written.

$$\langle\|\rangle = \sum_{NLMSJT\gamma\gamma'} \beta'_{NLSJT\gamma\gamma'} P_{NLSJT\gamma} \times \langle [\psi_{J_1T_1\gamma'}(A)[U^M_{NL}(\vec{R})\chi_{ST\gamma}(x)]_{JT}]_{J_2J_2} \tag{13}$$

$$\times \chi_{S_bT_b}(b)\phi(b)|V_{bx}(\rho)|\psi_{J_1T_1}(A)\chi_{S_aT_a}(b,x)\phi'(b)\phi'(x)\phi(\rho)\rangle$$

The double sum on γ and γ'' is now redundant and has been replaced by a single sum on γ. Square brackets indicate vector coupling.

The overlap of several quantities can now be defined. First consider the core $\underline{A}$.

$$\sum_{\gamma'} \langle\psi_{J_1T_1\gamma'}(A)|\psi_{J_1T_1}(A)\rangle = \sum_{\gamma'} C_{\gamma'} \tag{14}$$

The index γ' refers to a single configuration of $\underline{A}$. The $C_{\gamma'}$ are mixing coefficients for the complete wave function of the target ground state. Let the coefficients $C_{\gamma'}$ be absorbed into the corresponding β' to give β and drop the subscript and sum over γ'.

The γ index on the function $\chi_{ST\gamma}(x)$ indicates the internal spatial function of $\underline{x}$ in $\underline{B}$. The overlap of this spatial function with $\phi'(x)$ can be designated Ω_γ. Let $\chi_{ST}(x)$ now represent the spin and isospin function of $\underline{x}$. The overlap of $\phi(b)$ with $\phi'(b)$ can be designated Ω_b. This manner of defining Ω_γ and Ω_b assumes that $V_{bx}(\rho)$ is independent of the relative spatial coordinates within $\underline{x}$ and within $\underline{b}$ thus allowing these overlap integrals to be evaluated without consideration of the interaction potential. An overlap of the spin and isospin functions of the light particles involved is defined by Eq. (15).

$$b'_{ST} = \langle \chi_{ST}(x)\chi_{S_bT_b}(b) | V_{bx}(\rho) | \chi_{S_aT_a}(b,x) \rangle \qquad (15)$$

V_{bx} is a sum of two-body potentials acting between the nucleons of $\underline{b}$ and $\underline{x}$. If the wave functions of the light particles are all spatially symmetric, the potential may be written as follows.

$$V_{bx} = \sum_{ij}^{bx} U_{bx}(\rho)[V^1_{ij} + V^0_{ij}] \qquad (16)$$

V^1_{ij} is the potential for the triplet spin interaction between nucleons i and j and V^0_{ij} is the potential for the singlet spin interaction. $U_{bx}(\rho)$ is that portion of the potential which depends only on the spatial coordinate ρ.

If it is assumed that the potentials discussed above are central potentials only and that the singlet potential is proportional to the triplet potential, b'_{ST} can be written as follows.

$$b'_{ST} = b_{ST}D(S)U_{bx}(\rho) \qquad (17)$$

$D(S)$ is a function of the spin S which is transferred in the reaction. The need for such a spin-dependent term has been discussed by Fleming et. al.[15] and by Hardy and Towner.[16]

It is also illustrative to consider specifically the Clebsch-Gordan coefficient for coupling the target, transferred and product isospins. Define C_{ST} as follows.

$$C_{ST} = \langle T_2\ T_{z_2}\ T\ T_z | T_1\ T_{z_1} \rangle b_{ST}D(S) \qquad (18)$$

Now (13) can be rewritten.

$$\langle \| \rangle \propto \sum_{NLMSJT\gamma} \beta_{NLSJT\gamma}\ P_{NLSJT\gamma}\ C_{ST}\ \Omega_b\ \Omega_\gamma \times U^M_{NL}(\vec{R})U_{bx}(\rho)\phi(\rho) \qquad (19)$$

The proportionality sign is now used because Clebsch-Gordan coupling coefficients have been neglected. Let a quantity G_{NLSJT} be defined as follows.

$$G_{NLSJT} = \sum_{\gamma} \beta_{NLSJT\gamma}\ P_{NLSJT\gamma}\ \Omega_\gamma \qquad (20)$$

The transition matrix now has the form shown in Eq. (21)

$$t \propto \Omega_b \sum_{LSJT} C_{ST} \sum_{MN} G_{NLSJT}$$

$$\times \int \psi^{(-)*}(\vec{k}_2,\vec{R}_2) U^{M*}_{NL}(\vec{R}) U_{bx}(\rho)\phi(\rho)\psi^{(+)}(\vec{k}_1,\vec{R}_1) d\vec{R}_1 d\vec{R}_2 \qquad (21)$$

If the integral over $\vec{R}_1$ and $\vec{R}_2$ is designated by $B^M_{NL}(\vec{k}_1,\vec{k}_2)$ Eq. (21) is in a form corresponding to the notation of Glendenning.[1]

By reference to Fig. 1 it can be determined that R and ρ are related to R_1 and R_2. R is proportional to $R_1-(b/a)R_2$ and ρ is proportional to $R_2-(A/B)R_1$.

The six-dimensional integral of Eq. (21) is difficult to evaluate. For this reason the zero-range approximation is often employed as indicated below.

$$D(\rho) = U_{bx}(\rho)\phi(\rho) \qquad (22)$$

Let $D(\rho)$ be approximated as follows.

$$D(\rho) \approx D_o \delta(\rho) \qquad (23)$$

A number of methods have been used[7,17-19] for the evaluation of $D(\rho)$ and of D_o. By reference to Fig. 1 it is seen that when the coordinate ρ goes to zero all other coordinate vectors become parallel.[20] The integration in Eq. (21) then becomes an integration over a one-coordinate vector only. Physically the zero-range model for the reaction means the "particle" x is captured at a point and b is emitted at that same point.

The square of the transition amplitude is proportional to the probability for the reaction with specified magnetic quantum number projections. The differential cross section is proportional to a sum of such amplitudes. The sum extends over the proper magnetic quantum numbers.

Under some assumptions the sum of Eq. (21) may be coherent in nature, but in general the sum on J is incoherent. If it is assumed there is no spin-orbit coupling, the sums on LSTM are also incoherent.

If proper account is now taken of factors neglected, Glendenning[1] has shown the cross sections to have the following form.

$$\frac{d\sigma}{d\Omega} = \frac{k_2}{k_1} \frac{2J_2 + 1}{2J_1 + 1} \left(\frac{d\sigma}{d\Omega}\right)_o \qquad \text{(stripping)} \qquad (24)$$

$$\frac{d\sigma}{d\Omega} = \frac{k_1}{k_2} \frac{2S_a + 1}{2S_b + 1} \left(\frac{d\sigma}{d\Omega}\right)_o \qquad \text{(pickup)} \qquad (25)$$

$$\left(\frac{d\sigma}{d\Omega}\right)_o = \frac{m_1^* m_2^*}{(2\pi\hbar^2)^2} \Omega_b^2 \sum_{LSJT} C_{ST}^2 \sum_M \left| \sum_N G_{NLSJT} B_{NL}^M \right|^2 \qquad (26)$$

A reduced mass is indicated by m*. It is important to note the formulation (26) allows for the separation of the kinematic factors B_{NL}^M from the spectroscopic factors.

Selection rules for transfer reactions are discussed by Penny and Satchler[21] and by Glendenning.[9] In order to evaluate B_{NL}^M the distorted waves $\psi^{(\pm)}$ are represented by a partial-wave expansion. Let L_a and L_b represent a partial wave of a and b respectively. The following triangular relationships must exist.

$$\begin{aligned}
\vec{L}_a - \vec{L}_b &= \vec{L} \\
\vec{S}_a - \vec{S}_b &= \vec{S} \\
\vec{T}_a - \vec{T}_b &= \vec{T} \\
\vec{L} + \vec{S} &= \vec{J} \\
\vec{J}_1 - \vec{J}_2 &= \vec{J} \\
\vec{T}_1 - \vec{T}_2 &= \vec{T}
\end{aligned} \qquad (27)$$

The quantum numbers L, S, J, and T designate the physical quantities transferred between the system of light particles and the system of heavy particles.

The change of parity in the reaction is determined by the over all change of motion. The parity will therefore change if the partial wave of b does not have the parity of the partial wave of a.

$$\pi_A \pi_B = \pi_a \pi_b = (-1)^{L_a + L_b} = (-1)^L \qquad (28)$$

This may also be written as

$$L_a + L_b + L = \text{even} \quad . \qquad (29)$$

These expressions are valid in two cases. First, they are always true in the zero-range approximation. Second, they are always true if a and b have relative S motion only (even in finite-range calculations). If the light particles contain components of motion other than relative S the orbital motion of these light particles must enter the first expression of (27) as well as (28) and (29).

B. Comparison of Single- and Double-Nucleon Transfer Reactions

The equations discussed will now be specialized to two cases; deuteron pickup or stripping and two-nucleon transfer. Comparisons of the two reactions will be noted.

If a represents a deuteron and the reaction involves transfer of a single nucleon, Ω_b and Ω_γ are both unity, $P_{NLSJT\gamma}$ is one, and $\beta_{NLSJT\gamma}$ will not include a recoupling coefficient.

The sum on nuclear configurations is possible in single-nucleon transfer if the wave functions of A and B involve mixed configurations such that a nucleon, bound in a single-particle state j, may be transferred between more than one combination of configurations in A and B. An example of such a case would be between states of intermediate coupling within a single shell.

If it is assumed that the single nucleon is transferred to (or from) a shell-model, single-particle, bound state, a single value of N and L describes the nucleon motion in that state. Thus the coherent sum on N is removed. A configuration-mixed state may have contributions from more than one L value however.

The spin S and isospin T of a single-nucleon transfer are restricted to a value of 1/2.

The spectroscopic factor $\mathcal{S}_L$ of single-nucleon reactions is then defined as follows.

$$\sum_{LSJT} C_{ST}^2 \sum_M \left|\sum_N G_{NLSJT} B_{NL}^M\right|^2 = C_{ST}^2 \sum_{LM} \mathcal{S}_L \left|B_{NL}^M\right|^2 \qquad (30)$$

$$\mathcal{S}_L = \sum_J G_{NLSJT} \qquad (31)$$

Theoretical treatment of two-nucleon transfer reactions has been developed by several workers.[1,9,10,22-31] The present work follows the development by Glendenning.[1] Consider the form of G in Eq. (20). β is a producet of the c.f.p. and statistical factor as indicated. If the c.f.p. is given in terms of j_1 and j_2, the shell-model single-particle states for the two transferred nucleons, these two j values must be recoupled to an LS description by use of the 9-j coefficients since an LS description is used for calculation of B_{NL}^M. This spin-recoupling coefficient is a factor in β. Glendenning discusses prescriptions for calculation of β in several cases.

A two-particle configuration may be coupled to give contributions from more than one L and S value. Multiple S values also imply multiple T values. This is in contrast to the single value of L, S and T contributing to a configuration in single-nucleon transfer reactions.

The spatial motion of the two particles must be expressed in terms of center-of-mass motion and relative motion. If $n_1\ell_1$ and $n_2\ell_2$ are the principle and angular-momentum quantum numbers of particles 1 and 2 respectively, an expansion in terms of the center-of-mass motion, described by quantum numbers $N\Lambda$, and the relative motion between 1 and 2, described by quantum numbers $n\ell$, is possible. The expansion[1] is a sum on $N\Lambda\, nl$ with coefficients

$$\langle n\ell,\ N\Lambda\ ;\ L | n_1\ell_1,\ n_2\ell_2;\ L\rangle = P_{NLSJT\gamma} \quad . \qquad (32)$$

If the single-particle wave functions are harmonic oscillator functions the coefficients are easily obtained.[32] Only the relative motion with

$\ell = 0$ is able to overlap with relative S motion in the light particle a. It therefore follows that $\Lambda = L$.

Relationship (33) must be satisfied for the expansion under discussion.

$$2(n+N) + \ell+L = 2(n_1+ n_2) + \ell_1 + \ell_2 \qquad (33)$$

When $\ell = 0$ a unique relationship exists between n and N as can be seen in (33). The overlap integral Ω_γ, dependent on relative motion, can be written Ω_n. A single sum on N is all that is now required for the expansion.

The sum on N is coherent (Eq. (26)) which may lead to an enhancement or a reduction in the cross section. The coherent effect may result in a simple addition of terms and in favorable or unfavorable or unfavorable form-factor characteristics. Glendenning[1] has shown the sum on N may enhance the magnitude of the form factor in the nuclear surface, a condition favorable for a direct reaction. The opposite effect is also possible. Single-nucleon transfer does not involve a coherent sum on N.

A second coherent effect arises from a sum over the configurations of the nuclear wave function as shown in Eq. (20). In two-nucleon transfer this sum is general because j_1 and j_2 couple to a resultant L thus allowing various combinations of j_1 and j_2 to contribute to an L value. In contrast, a sum over configurations in single-nucleon transfer is restricted as discussed above.

The following values of b^2_{ST} have been given by Glendenning.[1]

$$b^2_{ST} = \begin{cases} \delta_{S0}\delta_{T1} & , (t,p) \text{ or } (^3He,n) \\ 1/2(\delta_{S0}\delta_{T1} + \delta_{S1}\delta_{T0}) & , (t,n) \text{ or } (^3He,p) \\ \delta_{S1}\delta_{T0} & , (\alpha,d) \end{cases} \qquad (34)$$

The factor D(S) of Eq. (17) has been discussed by Fleming et. al.[15] and by Hardy and Towner.[16] If the singlet and triplet nucleon-nucleon potentials are assumed to be equal (i.e. a spin-independent force) D(S) is unity for both S = 0,1. Hardy and Towner[16] have evaluated the

ratio $R(S) = |D(1)/D(0)|^2$ for several spin-dependent potentials which were used as effective interactions in nuclear-structure calculations. The ratio has been found to be about 0.5.

Selection rules for two-nucleon transfer reactions have been discussed by Glendenning[1,9,22] and Newns.[23] In addition to the general selection rules (27)-(29) the following are of importance in two-nucleon transfer reactions. By expression (28)

$$\pi_A \pi_B = (-1)^L = (-1)^{\Lambda+\ell} \tag{35}$$

In the present formulation $\ell = 0$ and $\Lambda = L$ which means the angular momentum transfer L associated with the center of mass of the pair designates the parity change.

The jj to LS transformation coefficient vanishes unless

$$L = S = J = \text{even} \quad . \tag{36}$$

Now $\Delta\pi$ is odd or even as L and may be substituted for L in (36).

$$\Delta\pi + S + J = \text{even} \tag{37}$$

If $S = 0$

$$\Delta\pi + J = \text{even} \quad . \tag{38}$$

If $j_1 = j_2 = j$ the parity change is even and $S + J =$ even .

The transferred pair $\underline{x}$ must have a totally antisymmetric wave function. Their relative S motion dictates an even space function. The product of spin and isospin must therefore be antisymmetric. This requirement is seen in the delta-function requirements of expression (34). For (t,p) or (^{3}He,n) reactions $T = 1$ and only $S = 0$ is possible. For (α,d) reactions only $S = 1$ and $T = 0$ is possible. For (^{3}He,p) and (t,n) reactions either combination is possible and in some instances[15] both contribute to a given transition. Glendenning[1] tabulates these allowed combinations.

A few general remarks concerning two-nucleon transfer reactions will help to point out the characteristics and usefulness of such reactions. $\beta_{NLSJT\gamma}$ contains factors which measure the extent to which the product $\underline{B}$ can be expanded as $\underline{x}$ coupled to the parentage $\underline{A}$. The jj to LS coupling coefficient, also in β, measures the extent to which angular momentum of the two particles can couple[9] to transfer angular momentum L. For states where the two particles are correlated in such a way as to give a large coupling coefficient the cross section will be enhanced.

$P_{NLSTJT\gamma}$ is a coefficient measuring the degree to which the two particles are correlated such that their center-of-mass motion $U^M_{NL}(\vec{R})$ allows the proper L transfer. The proper correlation here also enhances the cross section. As an illustration, consider the case of $j_1 = j_2$. If the two are coupled to a minimum or maximum value, both coupling coefficients just discussed are enhanced to some degree in comparison to other possible couplings. Yoshida[31] has shown that collective motion enhances the two-particle correlations, thus enhancing the transition amplitude.

As was pointed out earlier in this section, there are two coherent sums in the transition amplitude of two-nucleon transfer reactions. The residual interaction acting between pairs of nucleons gives rise to configuration-mixed wave functions. The spectroscopic factor G (Eq. (20)), for each value of L and N transferred, is a coherent sum over the configurations of a wave function.

A second coherent sum, a sum on the principle quantum number N, is introduced in order to properly describe the complicated center-of-mass motion for two particles. The phases of the configuration mixing coefficients, therefore, affect the transition amplitude: first by affecting the phase and magnitude of G and second, through G, affecting the contribution of each $U^M_{NL}(\vec{R})$ to the radial form factor.

The above considerations have been concerned with one value of L only. Often each configuration (j_1,j_2) contributes to more than one value of L. The relative amplitudes of the allowed L transfers to a product state will strongly affect both the angular distribution and the total cross section for the state. In single-nucleon transfer, each configuration can contribute to only one L value.

This discussion suggests the two-nucleon transfer reaction will be selective, exciting predominantly states with strong two-particle (or two-hole) correlations. This selectivity is in fact observed experimentally. It is also clear that a comparison of two-nucleon transfer calculations with experiment can be expected to be a sensitive test, in some cases, of the details of the nuclear wave functions used in the calculations.

C. Examination of Assumptions and Other Reaction Mechanisms

Several simplifying assumptions have been made or are implied by the above development. A stripping or pickup reaction proceeding by a simple, single-step, direct mechanism has also been assumed. Some of the assumptions will be examined. Additional reaction mechanisms will also be discussed.

1. Zero-Range Approximation

This approximation was introduced in Sec. II-A in order to simplify the integration of Eq. (21). The effects of this assumption have been discussed by a number of workers. Two recent publications treat the general subject well. One is the presentation made by Satchler[7] at the Boulder Conference and the other is by Hiebert, Newman, and Bassel.[33] An earlier paper by Lee et al.[34] is also pertinent.

The zero-range approximation generally overestimates the cross section. As is indicated in Eq. (21) the magnitude of B^M_{NL} depends on the overlap of the two distorted waves and the radial wave function U^M_{NL}. All three of these functions are oscillating rapidly in the nucleus. This variation leads to cancellations in the overlap. The zero-range approximation causes correlations in these varying functions which reduce cancellation and hence it overestimates B^M_{NL}.

A simple correction factor known as the "local energy approximation" (LEA) smoothly damps the radial form factor within the nucleus. Its use is discussed in the works noted above. Smith[35] has developed an "effective-mass approximation" (EMA). His development produced second-order correction terms as well as first-order terms. In the (LEA) the cross section is shown to be a minimum when the following equality if approximately satisfied.

$$U_a(r) \approx U_x(r) + U_b(r) \tag{40}$$

The $U(r)$ are optical-model potentials. This, of course, suggests $U_a(r)$ as a potential formed by summation of the other two potentials. Such an idea is compatible with arguments given in Sec. II-A for use of summed potentials.

Calculations for single-nucleon transfer using correction factors indicate little change in angular distributions for most cases. Unpublished data by Bassel has been cited,[33] however, which shows definite effects of zero-range calculations on angular distributions. In general the magnitude of the cross section is changed 10 to 20 per cent. Some levels are clearly affected more than others suggesting that zero-range calculations may introduce some error in relative cross sections as well as in absolute magnitude.

The effects of the zero-range approximation become increasingly less important with increasing atomic number[7,35] in A and B. There are at least two reasons for this. First, the radial wave functions of heavy nuclei contain several nodes. The oscillating functions aid cancellation. Many light nuclei have only one node or two nodes. Second,[36] optical-model damping of partial waves is also greater in the nucleus of a heavy element than in a light element.

Reactions involving particles strongly absorbed in the nuclear surface are expected to be less affected by the approximation than particles penetrating the nuclear interior. The authors mentioned have pointed out that effects of the zero-range approximation will be more pronounced for large angular momentum transfer.

The effect of this approximation in two-nucleon transfer reactions has been examined by Bencze and Zimanyi[37] who have proposed corrections to be applied to the radial form factor. They suggest that zero-range effects will be more important in two-nucleon transfer than for single-nucleon transfer.

2. Local-Potential Approximation

The usual optical-model potential used is a local potential. The usual shell-model potential wells used are also local potentials. The effects of this assumption are discussed in the first three works[7,33,34] mentioned in Sec. II-C-1. Schenter[38,39] has also been concerned with this problem.

A nonlocal potential includes exchange effects and target polarization both of which are neglected in local potentials. One important consequence of the neglect of exchange effects is the violation of the Pauli exclusion principle. Target polarization refers to the distortion of the core wave function due to the presence of additional nucleons either in a bound or an unbound scattering state. The effect of a nonlocal potential as compared to a local potential is to decrease nuclear wave functions in the interior of the nucleus but often to increase the bound-state wave function in the nuclear surface region.

Each wave function is affected by the local potential approximation which means that both distorted waves and the functions for each transferred nucleon are modified. In the scattered wave function some of the nonlocal effects are accounted for by an energy dependence in the optical-model potential. A correction factor of the LEA type mentioned for zero-range corrections has been used to modify the radial form factor of the bound-state wave function thus reducing these functions 15 to 20 per cent in the nuclear interior. The combined effect of finite-range and nonlocal potentials can decrease the radial integral of the transition matrix element by 50 per cent in the nuclear interior.[7]

By the arguments of this section and the previous one several observation can be made concerning the local-energy approximation. Various transitions will be affected differently depending upon the importance of the nuclear interior vs. surface in the transition. Penetrating particles will be affected by the increased internal wave functions while those absorbed on the surface may be affected by the decreased surface wave function. Two (or more)-nucleon transfer reactions are expected to be more affected than single-nucleon transfer.

In single-nucleon transfer, calculations usually show little change in angular distributions when corrections for nonlocal potentials are made. However, Bassel[33] has found modifications in his calculations. In general changes in the magnitude of transitions on the order of 20 per cent have been found. These changes have both increased and decreased the magnitude as might be expected from the discussion above.

3. Use of Radial Cutoff

It has often been the practice to use a lower limit or cutoff radius in the radial integration of Eq. (21). The cutoff radius was frequently in the region of the nuclear surface. This has been justified on the grounds that it helped to compensate for the over estimation due to zero-range and local-potential approximations. A number of arguments can be advanced, however, which show this extreme method is not justified.

Correction factors are smooth damping factors and are poorly approximated by sharp cutoff. The increase of the bound-state wave function in the tail region due to the nonlocal potential is, of course, not reproduced by cutoff. The two approximations just discussed do not affect all transitions within a given system in the same way. This difference cannot be accounted for by cutoff. Interference effects between the interior and exterior regions are neglected if the integration does not extend into the nuclear interior. As has been stated above interior contributions are especially important in light nuclei. Satchler[7] has pointed out that interior effects in light nuclei may lead to phenomena such as pronounced backward peaking. Hiebert,[33] as well as other workers, have shown the use of radial cutoff strongly affects the magnitude of the transition matrix.

4. Concerning the Radial Form Factor of the Bound State

The problem of properly representing the radial form factor $U^{M}_{NL}(\vec{R})$ is one of major importance in nuclear-structure calculations. Through this factor the nuclear structure and the reaction mechanism are interdependent.[7,40] The development of Sec. II-A demonstrates how this factor arises from the bound-state configuration of the transferrred particles. The strength of the transition and the nature of the angular distributions are directly affected by the overlap of distorted waves with the radial form factor as indicated in Eq. (21).

Austern[41] has discussed proper characterization of the radial form factor. Pinkston and Satchler[7] have shown that the exact expression for a single-nucleon form factor based on one parent configuration of a state is related by a set of coupled equations to all other possible parent configurations. A simple shell-model form factor is perturbed by the residual interaction and thus related to all possible configurations. The form factor for a given L value should, therefore, be a sum over all principal quantum numbers (N) and all continuum states.[42]

The asymptotic shape of the form factor should be an exponential with a decay constant related to the binding energy.[40] The binding energy BE of $\underline{x}$ is defined in (41).

$$BE = E_B - E_A \tag{41}$$

The wave number K of the bound particles $\underline{x}$ may now be defined.

$$K^2 = \frac{2m^*_x \, BE}{\hbar^2} \tag{42}$$

The reduced mass of $\underline{x}$ is m^*_x. The asymptotic shape of the form factor of $\underline{x}$ is then proportional to exp(-KR). The proportionality constant is not well known.

Several methods are used to approximate the form factor. Most of them use an unperturbed, shell-model, single-particle potential. The Woods-Saxon (WS) finite, spherical well is often used. The DW program JULIE uses this well.[43] There are uncertainties in choosing the depth and radius parameter for the potential.[8] The tail of a WS radial wave function is a good approximation to exponential decay, particularly for single-particle bound states. Rost[44] has used a deformed WS potential well for transfer reactions.

An infinite, spherical harmonic oscillator (HO) potential well is often used for nuclear-structure calculations. This well has analytical properties which make it attractive for use; however, the tail of the well decays much faster than the desired exponential decay. To correct for this poor behavior[1,40] in the tail region a Coulomb or Hankel function, with decay based on the BE of $\underline{x}$, is often matched to the HO function at a point where the slopes of the two functions are equal.

Two methods are used to accomplish this matching. In one method[20] a matching radius R_m is chosen and the HO parameter $\hbar\omega$ is adjusted until the HO and tail functions have equal slopes at R_m. In a second method the value of $\hbar\omega$ is set equal to the value used in the nuclear structure calculation relevant to the problem. R_m is then adjusted to a value such that the slopes of the tail and HO are equal. In both methods the magnitude of the tail must be adjusted in order to establish an equality between the functions at R_m, and the overall function normalized to one. One does not know "a priori" how properly to adjust R_m and the tail magnitude.

The center-of-mass motion of two nucleons in two-nucleon transfer reactions has been treated by the several methods discussed above. Calculations made by Glendenning[1,45] have employed the HO plus tail where matching is accomplished according to the second method discussed.

Broglia and Riedel[46] have compared several methods for treating the form factor in a two-nucleon transfer reaction. They compare WS, HO, HO plus tail, and WS plus tail. Glendenning[45] has pointed out the WS well, when used for the center-of-mass motion of two particles, does not approximate the exponential decay as well as a coulomb or Hankel function tail. This is shown to be the case in the comparisons of Broglia and Riedel. Also included in these comparisons was a form factor obtained by taking the product of two single-particle WS form factors. Each particle was given one half the binding energy of the pair. A sum of such products was taken over the configurations of the wave function. This form factor had the proper asymptotic shape. This latter method was earlier used by Drisko and Rybicki.[47]

Rook and Mitra[30] have used a form factor based on the assumption that $\underline{x}$ is a point particle. They use a product of two single-particle WS form factors as described above. They, however, neglect the relative coordinate between the two nucleons. The two WS factors have, therefore, the same radial coordinate. This form factor was also examined by Broglia and Riedel and was shown to have two deficiencies. The factor is almost entirely of one sign. As a result cancellations in the integral of Eq. (21) cannot take place as they would for the proper integral which oscillates positive and negative. The factor is also much reduced in

the nuclear surface region, the region of most importance for stripping reactions. These same effects have been observed by Glendenning.[48]

5. Spin-Orbit Effects

Three spin-orbit effects are possible for transfer reactions: incident distorted wave, bound state, and exit distorted wave. Satchler[8] has developed a formalism for treating spin-orbit effects which allow spin flip in the distorted waves. Each of the distorted waves is designated by $\psi_{mm'}(\vec{k},\vec{R})$. The initial projection at infinity is m, and m' is the projection after interaction. In the case of no spin-orbit interaction a sum on m is purely statistical. With spin-orbit interaction a sum on both m and m' is necessary and the resulting coupling is correlated with the angular momentum of the partial wave.

The sum on L and S in expressions for the transition amplitude is coherent when a spin-orbit potential is included in the distorted waves. That this is reasonable can be seen as follows. Equation (27) indicates that the values of S and L are related to the corresponding quantum numbers in the distorted partial waves. Each coupling is weighted by the Clebsch-Gordan coefficients relating their spin projections. The spin-orbit force introduces a correlation between the orbital and intrinsic angular momentum spin projections. This correlation affects the transferred quantities L and S through coupling coefficients.

Angular distributions are affected to a minor extent[7] by the inclusion of spin-orbit effects. The distribution at large angles is most affected. In some cases observed j dependence is qualitatively reproduced. Cross section magnitude is changed by 5 to 20 per cent for sincle-nucleon reactions.

Spin-orbit coupling in the bound state[7] leads to modification of the wave function. The potential for the case of $\ell + 1/2$ is peaked in the nuclear surface allowing for an enhanced wave function and increased transition amplitude. For $\ell - 1/2$ the opposite is true. For single-nucleon transfer the difference in cross section magnitude between $\ell + 1/2$ and $\ell - 1/2$ has been found to vary from 10 to 50 per cent depending on the value of ℓ (more effect for larger ℓ) and the reaction.

6. Multiple-Step Processes

In the formulation of Sec. II-A the reaction was assumed to be a single-step process between the ground state of the target and the final state of the product. Many other mechanisms involving more than one step can be proposed. Several workers[21,49-52] have developed schemes for calculations involving inelastic excitation in the incident channel, transfer taking place between the excited target state and a product state, and inelastic excitation (de-excitation) in the exit channel. Figure 2 indicates the mechanisms considered.

Following the development of Penny and Satchler[21] the distorted waves must be labeled by two indices which account for possible inelastic excitation. For example the entrance channel distorted wave may be $\psi_{AA'}(\vec{k}_1,\vec{R}_1)$. Each of the possible reaction paths contribute coherently. The product GB of Eq. (26) must be summed over all possible reaction paths. G becomes the spectroscopic factor for transition between the two relevant states $A' \rightarrow B'$. The amplitude for the inealstic scattering will be determined by a coupled channel calculation for the corresponding distorted wave.

Additional selection rules are present in such multiple step processes. These have been discussed in detail by Penny and Satchler.[21] The general selection rules of Eqs. (27), (28) and (29) are still valid where the quantities refer to the total transferred quantities. Let L'_1 and L'_2 be the angular momentum transferrred by inelastic scattering in the entrance and and exit channels respectively. Let L' represent the angular momentum transferred during the transfer of $\underline{x}$ between A' and B'.

$$\vec{L}'_1 + \vec{L}' + \vec{L}'_2 = \vec{L} \tag{43}$$

Parity changes as follows:

$$\begin{aligned} \pi_A \, \pi_{A'} &= (-1)^{L'_1} \\ \pi_{A'} \pi_{B'} &= (-1)^{L'} \\ \pi_{B'} \pi_B &= (-1)^{L'_2} \\ \pi_A \, \pi_B &= (-1)^{L'_1 + L' + L'_2} = (-1)^L \end{aligned} \tag{44}$$

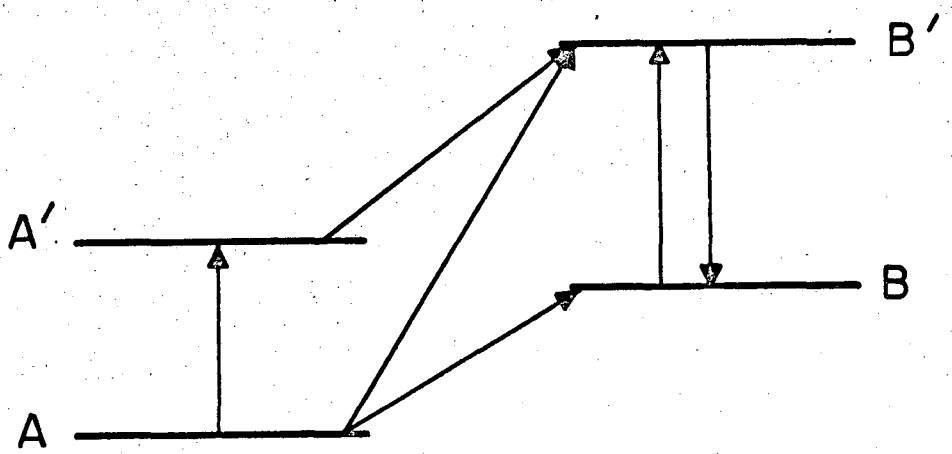

XBL678-3860

Fig. 2. Some nuclear reaction paths from target A to product B or B'.

Equation (43) indicates that a total angular momentum transfer L, which may not be allowed by a single-step process due to nuclear-configuration restrictions, may proceed through a multiple-step process. Equation (44) indicates that a reaction which by a single-step transition is parity forbidden, may proceed through multiple-step processes.

The workers noted above have calculated the effects of these processes. The angular distribution of a multi-step reaction is similar to the single-step but generally flatter. The magnitude of such processes is rather small compared to an allowed single-step process although the angular distribution is affected to some extent by addition of both mechanisms. The calculation of multi-step processes was found to be very sensitive to the optical-model parameters used.

Multi-step processes will, no doubt, be most important for transitions of small cross section[53] and transition which are forbidden for a single-step process.

7. Other Mechanisms

In addition to the reaction mechanisms discussed above others have been suggested which may contribute or interfere in a nuclear reaction. Compound-nuclear contributions are often important, particularly at low energies. Possible contributions from a compound-nuclear mechanism must, therefore, be considered in each particular case.

Recently DW calculations of a knockout mechanism for direct reactions have been made by Strobel.[54] Contributions from knockout were found to be small compared to stripping or pickup when both are allowed. When stripping or pickup were not allowed a knockout mechanism was still unable in most cases to account for the experimental observations. The calculated angular distributions were found to be very similar to those for stripping or pickup. Pehl[55] considered a possible knockout mechanism for two-nucleon transfer. He concluded the reactions could be equally well explained by other mechanisms.

The question of heavy-particle stripping often is raised in connection with backward-peaked[56] cross sections. Austern[57] has stated his belief that the existence of the mechanism has a sound theoretical basis but points out that proper treatment of the problem has not yet been

developed. Because of this, an accurate assessment of the importance of heavy-particle stripping has not been made. As was stated earlier, effects arising from the nuclear interior, especially in light nuclei, may also account for backward peaking.

III. EXPERIMENTAL EQUIPMENT

A. Cyclotron and Beam Line

The Berkeley 88-inch variable-energy cyclotron[58] was used to produce beams of ^{3}He and alpha particles for the experiments discussed in this report.

The principal active elements of the beam-transport system,[59] proceeding from the machine to the scattering chamber, were a pair of quadrupole-magnet lenses, a switching magnet, a second set of quadrupole-magnet lenses, the scatter chamber, and a Faraday cup. The first pair of lenses focused the beam at a position midway to the switching magnet. A radial and a vertical pair of slits located between the quadrupole magnets and the focus point were used to define the beam. The circular-pole, uniform-field, switching magnet bent the beam through 57° and created a focus at an analyzing slit.

A quartz target could be placed at the analyzing-slit position. The fluorescent glow of the quartz induced by the beam was observed with a television camera and used as an indication of beam focus. Current adjustments in beam-transport elements were made to give a raidal focus at the analyzing-slit position.

Beyond the analyzing slit a second pair of quadrupole-magnet lenses focused the beam at the center of the scatter chamber. A quartz target (see Fig. 3) with a slit cut out of the center was used to determine a proper focus in the scatter chamber. The beam current passing through the slit was maximized to ensure that the beam passed through the center of rotation of the chamber.

B. 36-inch Scatter Chamber and Associated Equipment

In Figs. 3 and 4 the scatter chamber (SC) and associated equipment are shown. Basically the SC was a cylindrical section 12 in. high and 36 in. in diameter. The chamber lid covered the entire cross section of the cylinder. A table which covered the entire floor of the chamber rotated 360 deg. The position of the table was given by digital voltmeter readout with an error of $\pm$ 0.1 deg.

Between the Faraday cup and the scatter chamber were located two foil wheels and a plunger-type foil holder. Aluminum foils in these devices together with the range-energy tables of Williamson and Boujot[62] were used to make an approximate determination of beam energy. The wheel nearest the scatter chamber contained a blank hole and nine foils weighing approximately 1.8 to 9.3 mg/cm^2. The other wheel contained a blank hole and nine foils weighing approximately 10 to 90 mg/cm^2. The plunger-type holder held one foil. The foil was placed in the beam for energy measurement and then withdrawn. The foil was easily changed through an air lock while the scatter chamber and beam line were maintained under vacuum.

On one side of the scatter chamber at an angle of 19 deg from the beam exit was located a port which held a monitor detector.

A gas-handling rack, used to fill or to evacuate the gas cell, was mounted on a cart for convenient use. The rack could be connected externally to the hollow, target-positioning rod. The rack contained a manometer to monitor target gas pressure. It also contained a mercury toepler pump for transfer of gasses.

C. Electronics

The basic electronic block diagram is shown in Fig. 5. A detection and identification system described by Goulding et al.[63,64] for use with charged particles was employed. This system employed a ΔE plus E solid-state detector telescope for energy detection which also permitted use of an empirical power-law range-energy relationship for particle identification. Phosphorus-diffused or lithium-drifted silicon semiconductor detectors were used for the ΔE detector. The latter type were used for the E detector. Goulding[65] has described the manufacture and characteristics of these devices.

The preamplifiers (P.A.) used were a charge-sensitive type designated as 11 × 3391-P3. A similar but improved type designated 11 × 4831-P1 has been described by Goulding et. al.[64] The preamplifiers were located inside the SC in order to reduce the cable capacitance between the detector and thus to improve the signal to noise ratio.

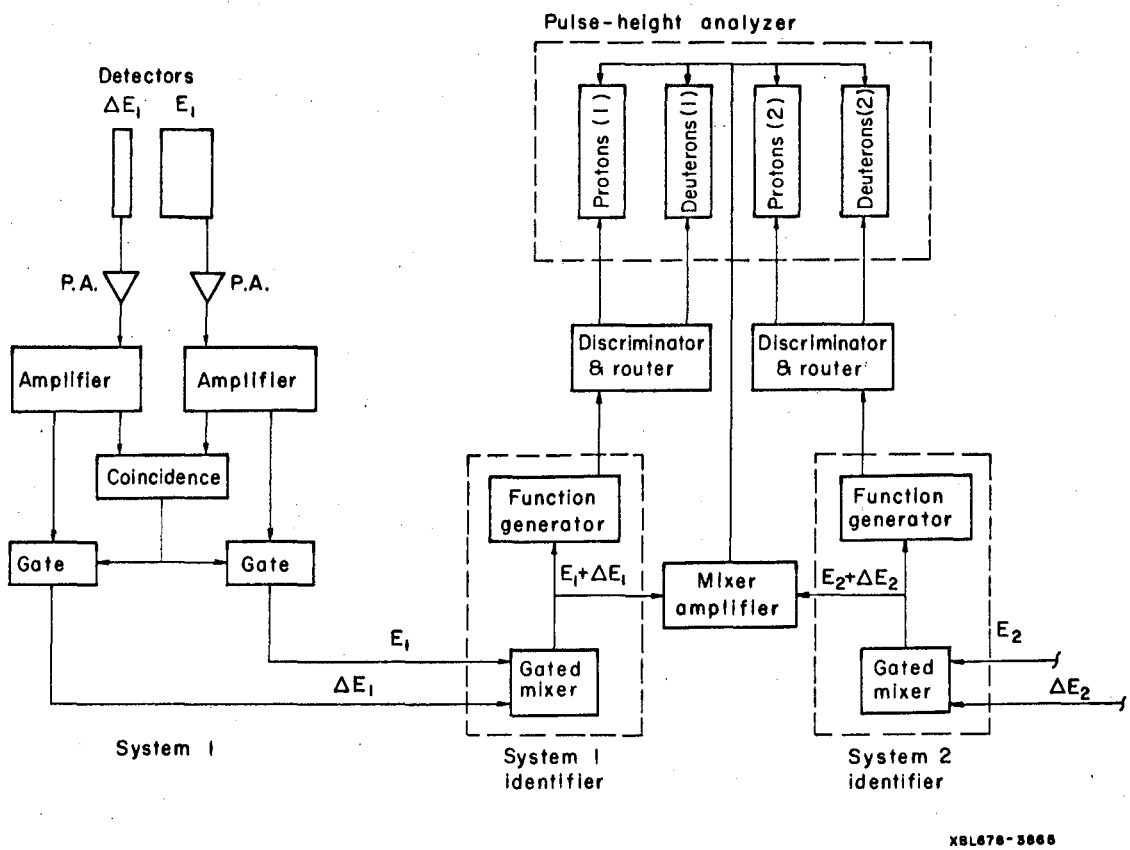

Fig. 5. Block diagram of electronics. System 2 is similar to system 1.

The amplifiers and all other electronic equipment not discussed above were located in a counting room area. The Linear Amplifier System 11 × 1980P[66] was used for further amplification of signals.

A Particle Identifier 11 × 2650-P2 as described in the references noted above added the ΔE and E signals to give a total energy signal. It also generated an identification pulse with voltage magnitude proportional to the product MZ^2 for a particle of mass M and charge Z.

The identification signal was fed into a 4 Channel Router and Mixer Amplifier 11 × 2790P-1 which contained four single channel analyzers (SCA). Each SCA could be set to select a single particle type. When a particle of a type corresponding to a given SCA setting was identified that SCA generated a signal to be used for routing the coincident total energy signal to the proper block of storage in the multichannel pulse-height analyzer.

As noted earlier two detection systems were operated simultaneously. This required mixing of the two total energy signals in a mixer amplifier in order to facilitate input into the same pulse-height analyzer. The identification pulse was analyzed and stored in a RIDL 400 channel analyzer in addition to its use in the routers.

A Nuclear Data multichannel pulse-height analyzer with a 4096 Channel Arithmetic Unit ND-160M was used for storage of total energy signals. This analyzer was interfaced with a PDP-5 computer built by the Digital Equipment Corporation. The PDP-5 had an 8K, 12 bit word memory. Robinson[67] has described this computer facility and its attendant equipment. Some associated external devices are CAL COMP plotter, typewriter, "micro" magnetic tape deck, IBM compatible tape deck, oscilloscope with accompanying light pen, paper tape reader, and paper tape punch. Light pen techniques were used for partial analysis of the data during the period of data collection.

A monitor system with a single detector located in the SC port described in Sec. III-B was used. No particle identification was made for the monitor system. The energy signals were stored in a 400 Channel RIDL analyzer. The number of counts per microcoulomb of integrated beam in a spectrum peak (usually the peak due to elastic scattering) were

monitored. In this way changes in target thickness could be noted. The channel number of the spectrum peak was also monitored. A change in beam angle could change both the peak channel number and the counts per microcoulomb.

IV. EXPERIMENTAL CONDITIONS AND RESULTS

A brief description of the experimental conditions and the methods of data reduction together with a presentation of the data in final form will be found in this section. An examination of the data and comparison to other work will be made in Sec. V. A comparison of the data with theoretical calculations will be made in Sec. VI.

A. Data Reduction Procedures

Upon transfer of an energy spectrum from the Nuclear Data analyzer to the PDP-5 computer, the spectrum data were stored on a "micro" magnetic tape. The spectrum was also plotted by means of the CAL COMP plotter.

Strong transitions or transitions to levels of particular interest were examined during the progress of the experiment. This was accomplished by first displaying the spectrum on an oscilloscope. A peak was selected and the counts in the peak integrated using light-pen controls. The computer was then used to calculate the differential cross section of the peak. In this manner the center-of-mass angular distribution of a level was obtained during the course of the run.

At the conclusion of an experiment the "micro" tapes were used to generate an IBM-compatible tape containing all spectra for use in further data analysis and for generating a numerical listing of the data.

For final analysis the number of counts in a spectrum peak and the analyzer channel number of the peak were obtained by one of two methods: (1) by inspection of the peak on the plotted spectrum together with a manual summation from the numerical listing of the spectrum or (2) by use of a computer program VFIT.[68] The program VFIT fitted peaks with Gaussian functions and then integrated the functions. Several Gaussians could be used simultaneously to allow the separation of contributions to peaks that were not fully resolved from one another. VFIT also determined the peak channel number and calculated the differen-tail cross section and center-of-mass angle.

The following equations were used for calculation of the differential cross section in the center-of-mass system.

$$\frac{d\sigma}{d\Omega}_{c.m.} = \frac{CJ(\theta_L)\ Z\ MR^2\ 2.660 \times 10^{-7}}{BNAt} \quad mb/sr \qquad (45)$$

:solid target

$$\frac{d\sigma}{d\Omega}_{c.m.} = \frac{CJ(\theta_L)\ Z\ (T+273)R^2\ SIN\theta_L\ 6.530 \times 10^{-7}}{BNP\ W_1W_2H_2(1+R_1/R_2)} \quad mb/sr \qquad (46)$$

:gas target

Quantities are defined as follows:

- C = number of counts in the peak
- $J(\theta_L)$ = Jacobian for the transformation from laboratory to center-of-mass system
- Z = charge of an incident particle in units of electron charge
- R = distance from the center of the target to the back of the detector slits
- B = total μCoulombs of beam charge integrated during measurement of the spectrum
- N = number of target nuclei per molecule
- M = molecular weight of the target in g/mole
- t = solid target thickness in mg/cm^2
- W_1 = width in inches of the gas-target defining slit
- W_2 = width of the detector slit
- H_2 = height of the detector slit
- A = $W_2 \times H_2$ = area of the detector slit
- R_1 = distance from the center of the gas target to the back of the gas-target defining slit
- R_2 = $R - R_1$
- T = target-gas temperature in C°
- P = target-gas pressure in cm of Hg
- θ_L = laboratory angle

The excitation energies of levels excited in a reaction were determined by use of a computer program, LORNA.[69] From the peak channel numbers and the excitation energies of well identified levels excited in a reaction and using a polynomial of arbitrary degree, LORNA constructed an energy scale of excitation energy vs. channel number. The peak

channel number of an unidentified level was then compared to this energy scale and the excitation energy of the level determined.

Data taken at several angles could be treated simultaneously by LORNA. The excitation energy of a level was then determined to be the average value obtained at the several angles. In practice, two or three levels of low excitation energy were taken as known values. Levels of a few MeV higher excitation energy could then be accurately assigned an excitation energy. One or two of these latter levels could then be included with the known levels and another calculation made to identify unknown levels at still higher excitation energy, etc. The number of counts in a peak could also be included as input to LORNA and then the differential cross section and center-of-mass angle were also calculated.

Center-of-mass angles and the corresponding differential cross sections were used as input data for a program, TSECT, which calculated the total cross section over specified angular limits by use of the trapezoidal rule for numerical integration.

B. $^{12}C(^{3}He,p)^{14}N$

The $^{12}C(^{3}He,p)^{14}N$ reaction was studied using an evaporated self-supported ^{12}C foil of 280 ± 25 $\mu g/cm^2$ thickness. A small contribution from the reaction $^{16}O(^{3}He,p)^{18}F$ to the 1.131- and 0.937-MeV levels of ^{18}F indicated 1-2% oxygen in the target. Data from ^{3}He elastic scattering on a similar ^{12}C target (see Sec. IV-C) were examined in order to estimate the amount of impurities in the target as evidenced by the presence of impurity peaks in the data. Oxygen was the most abundant impurity observed. On this basis it was estimated that less than 2% of the target mass was due to impurities other than oxygen and hydrogen. An additional uncertainty in the measured cross sections arises from possible nonuniformity of the foil.

The energy of the ^{3}He beam, as determined by the range of the particles in Al (see Sec. III-B), was 20.3 MeV. A comparison of the $(^{3}He,p)$ reaction on ^{1}H and on ^{12}C leading to several excited states of ^{14}N, as discussed below, indicated a ^{3}He energy of 20.1 MeV.

Two independent detector systems separated by 15° were used in the experiment. The smaller-angle system contained a 0.0043" thick phosphorus-diffused silicon ΔE detector and a 0.125" thick lithium-drifted silicon E detector with the latter placed at an angle of 40° to the scattered particle direction. The larger-angle system was similar, with 0.0032" and 0.125" ΔE and E detectors respectively. The solid angles subtended by the smaller- and larger-angle systems were 6.67×10^{-5} steradians and 7.25×10^{-5} steradians respectively.

An energy spectrum taken at $\theta_{lab} = 30.4°$ is shown in Fig. 6. The full-width at half maximum (FWHM) of a spectrum peak for a "sharp" level appeared to vary with proton energy (i.e. with analyzer channel number). The FWHM ranged from about 80 keV at channel number 300 to $\approx$ 150 keV at channel number 600. This may have been due to the increasing rise time of the energy pulse as protons penetrated deeper into the E detector.

The $^{12}C(^{3}He,p)^{14}N$ reaction Q-value is 4.7786 ± 0.0003 MeV.[70]

Background counts were arbitrarily subtracted from each spectrum as follows. No subtraction was made below an excitation of approximately 8 MeV. By inspection a line was drawn from zero counts at 8 MeV with a slope increasing in counts with excitation energy. The line was drawn below the valleys of the spectrum. A second line was similarly drawn with a sharper rise vs. excitation energy and intersecting the first at about 10.5 MeV. All counts below these two lines were subtracted as background.

The program LORNA was used to assign excitation energy values to the observed levels of ^{14}N. These experimentally determined values are listed in Table I. In addition to a few levels of ^{14}N which were assumed to be known, the reaction $^{1}H(^{3}He,p)^{3}He$ was also assumed known. A peak corresponding to this latter reaction is shown in Fig. 6. The use of this impurity reaction in the determination of the energy scale had two valuable consequences: (1) confidence was placed in the energy assignment of levels in the region of 12 MeV excitation energy and (2) an independent determination of the ^{3}He beam energy was made (see Sec. IV-A).

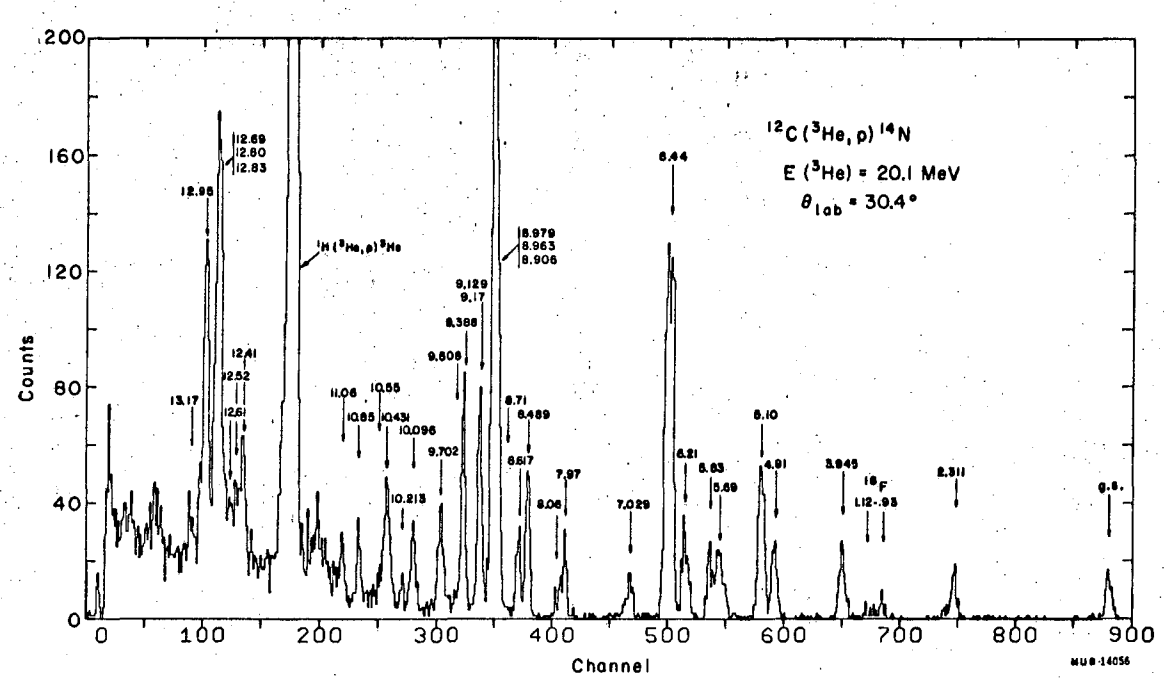

Fig. 6. Proton energy spectrum for the $^{12}C(^{3}He,p)^{14}N$ reaction at $E(^{3}He)$ = 20.1 MeV.

Angular distributions for a number of ^{14}N levels are shown in Figs. 15 to 19. Differential cross sections are tabulated in the Appendix. Errors on the experimental points represent statistical error only.

Total cross sections calculated between 10° and 70° center of mass are listed in Table I. The following estimated errors affect the relative cross sections: statistical error 5-10%, background subtraction 1-10% (for the states above 9 MeV). The errors for the strong states are the low limits. In addition to these errors the following would affect the absolute cross section: beam integration 3%, dead time and other electronic errors 2%, uncertainty in target thickness, 10%. From these estimates relative total cross sections are estimated to agree with 5% - 15%, depending on the strength of the state. The absolute cross sections are expected to vary from 15% - 20% for levels below 9 MeV and due to errors in background subtraction, from 20% - 30% for higher excited levels.

C. $^{12}C(^3He,^3He)^{12}C$

The $^{12}C(^3He,^3He)^{12}C$ reaction was studied using an evaporated, self-supporting ^{12}C foil of 280 ± 25 $\mu g/cm^2$ thickness. Target impurities were estimated as discussed in Sec. IV-B.

The energy of the ^3He beam, as determined by the range of the particles in Al (see Sec. III-B), was 20.1 MeV.

The detector system contained a 0.0035" thick phorphorus-diffused silicon ΔE detector and a 0.040" thick-lithium drifted silicon E detector. A solid angle of 7.19×10^{-5} steradians was subtended by the system. The FWHM of the elastic-scattering peak was approximately 160 keV. Angular distribution for ^3He particles scattered from the ground state (g.s.) and 4.433-MeV level of ^{12}C are shown in Fig. 13. Differentail cross ections are tabulated in the Appendix. Errors represent statistical error only. The following are estimated errors: beam integration 3%, uncertainty in the target thickness 10%, dead time and other electronic errors 2%, statistical and impurity peaks 3%. The absolute cross section of the g.s. is expected to be accurate within 15%. The cross sections of the two levels are expected to be within 5% relative accuracy.

D. $^{16}O(^{3}He,p)^{18}F$

The $^{16}O(^{3}He,p)^{18}F$ reaction was studied using O_2 gas and the gas target described in Sec. III-B. A gas pressure of 15.40 cm of Hg at 21.5°C was used. The gas was 99.7% ^{16}O. The addiational 0.3% was due to impurities and other oxygen isotopes. The purity was determined using the suppliers analysis and the natural isotopic abundance of ^{16}O. The energy of the ^{3}He beam, as determined by the range of the particles in Al (see Sec. III-B), was 19.8 MeV at the center of the gas cell.

Two independent detector systems separated by 20° were used in the experiment. The smaller-angle system contained a 0.0098" thick phosphorus-diffused silicon ΔE detector and a 0.120" thick lithium-drifted silicon E detector with the latter placed at an agle of 40° to the scattered particle direction. The larger-angle system was similar, with 0.0010" and 0.120" ΔE and E detectors respectively. The solid angles subtended by the smaller- and larger-angle systems were 7.19×10^{-5} steradians and 6.75×10^{-5} steradians respectively.

An energy spectrum taken at $\theta_{lab} = 25.1°$ is shown in Fig. 7. The FWHM of a spectrum peak for a "sharp" level was approximately 140 keV.

The $^{16}O(^{3}He,p)^{18}E$ reaction Q-value is 2.0334 ± 0.0009 MeV.[70]

Background counts were subtracted from each spectrum as follows. No subtraction was made below an excitation of approximately 6.5 MeV. By inspection, a line was drawn from zero counts at 6.5 MeV with a slope increasing in counts with excitation energy. The line was drawn below the valleys of the spectrum. All counts below this line were subtracted as background.

The program LORNA was used to assign excitation energy values to the observed levels of ^{18}F. These experimentally determined values are listed in Table II.

Angular distributions for a number of ^{18}F levels are shown in Figs. 21 to 24. Differential cross sections are tabulated in the Appendix. Errors on the experimental points represents statistical error only.

Total cross sections calculated between 10° and 82° center of mass are listed in Table II. The following estimated errors affect the

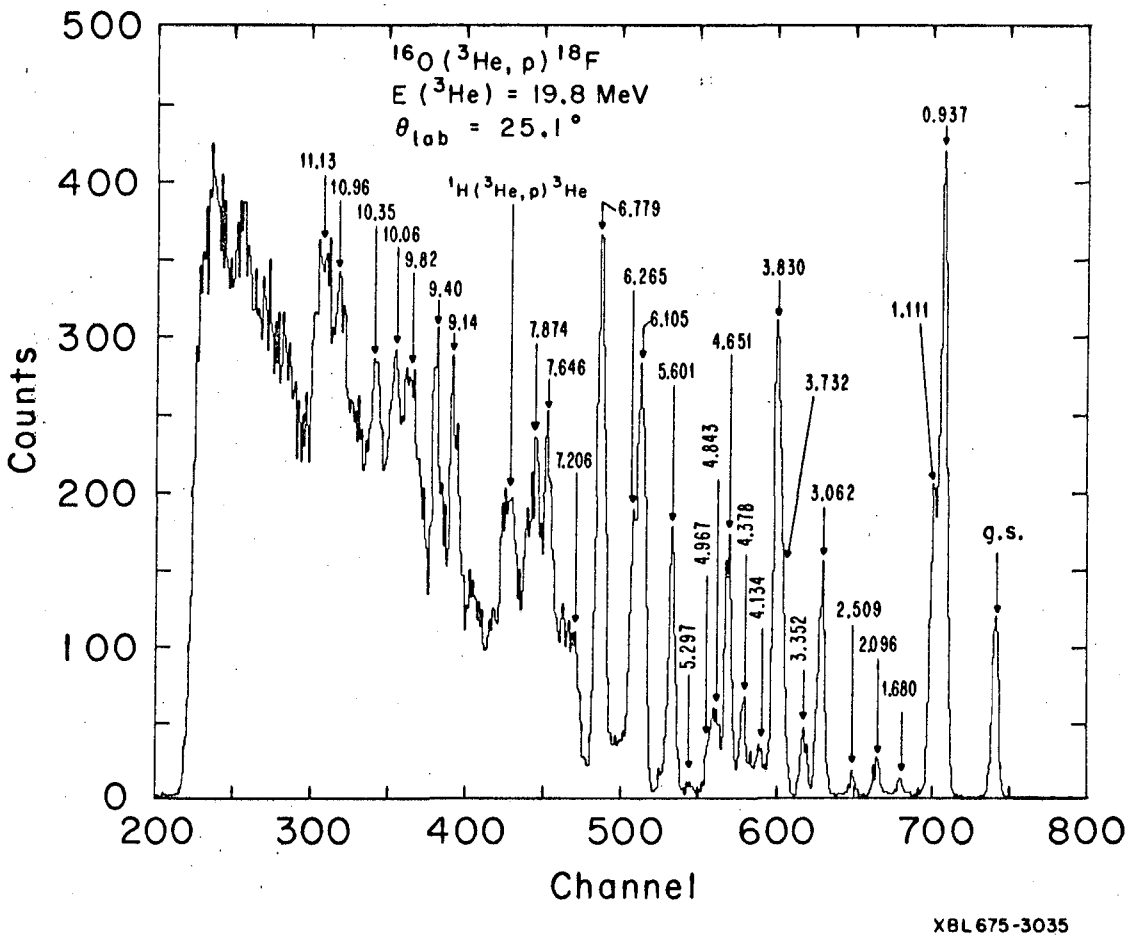

Fig. 7. Proton energy spectrum for the $^{16}O(^{3}He,p)^{18}F$ reaction at E(p) = 19.8 MeV.

cross sections: beam integration 3%, dead time and other electronic errors 2%, target thickness 1%, statistical and peak separation 5-30%, background subtraction 1-10%. Relative total cross sections are estimated from these to agree within 5% - 30% depending on the strength of the state. The absolute cross sections are expected to vary from 10% to 40% depending on the strength of the state and the background subtraction

E. $^{16}O(\alpha,d)^{18}F$

The $^{16}O(\alpha,d)^{18}F$ reaction was studied using O_2 gas and the gas target described in Sec. III-B. Gas with 99.4% ^{16}O and a pressure of 17.85 cm of Hg at 23.4°C was used. The additional 0.6% of the gas was due to impurities and other oxygen isotopes. The purity was determined using the suppliers analysis and the natural isotopic abundance of ^{16}O.

The energy of the α-particle beam, as determined by the range of the particles in Al (see Sec. III-B), was 40.3 MeV at the center of the gas cell.

The single detecting system subtended an angle of 7.17×10^{-5} steradians.

An energy spectrum taken at $\theta_{lab} = 20.4°$ is shown in Fig. 8. The FWHM of a spectrum peak for a "sharp" level was approximately 135 keV.

The $^{16}O(\alpha,d)^{18}F$ reaction Q-value is -16.3201 ± 0.0009 MeV.[70]

Background was subtracted from each spectrum as follows. No subtraction was made below an excitation of approximately 6 MeV. By inspection, a line was drawn from zero counts at 6.5 MeV with a slope increasing in counts with excitation energy. The line was drawn below the valleys of the spectrum. All counts below this line were subtracted as background.

The program LORNA was used to assign excitation energy values to the observed levels of ^{18}F. These experimentally determined values are listed in Table II. Total cross sections calculated between 10° and 82° center of mass are also listed in Table II. Differential cross sections are tabulated in the Appendix. Error on the experimental points

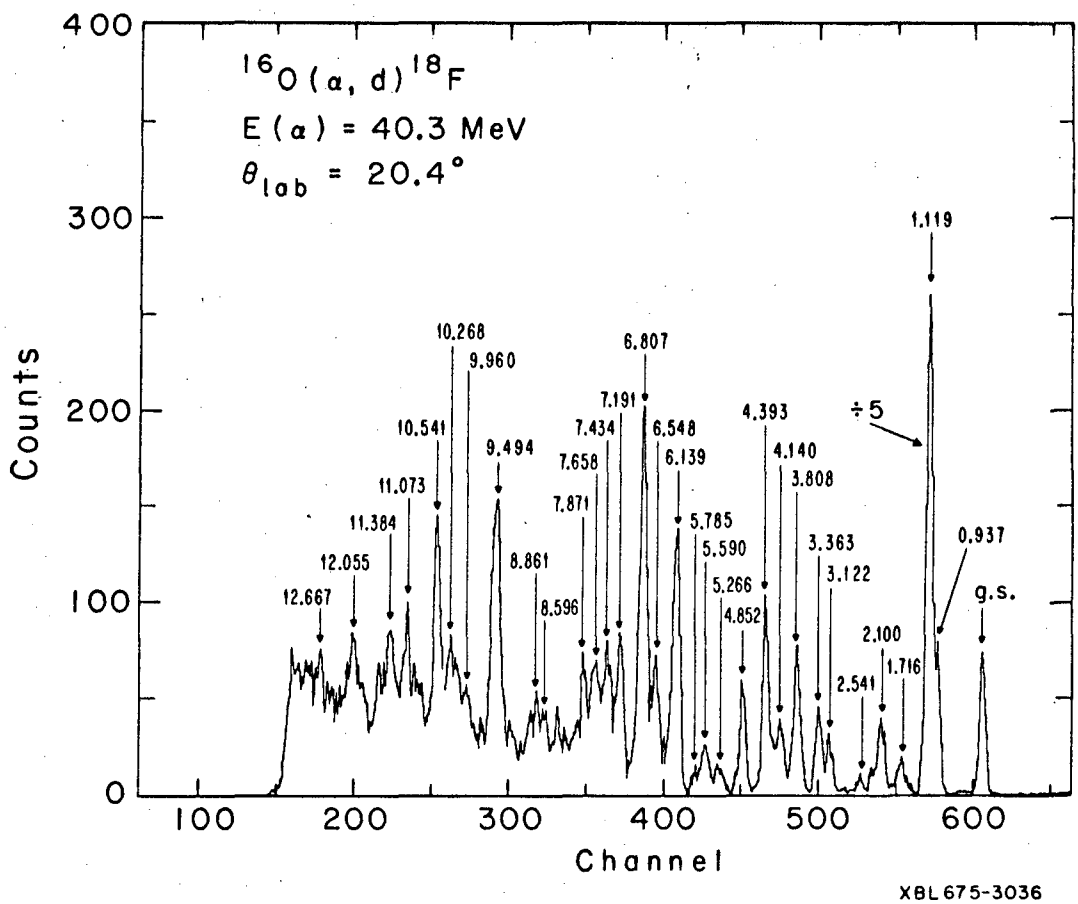

Fig. 8. Deuteron energy spectrum for the $^{16}O(\alpha,d)^{18}F$ reaction at E(α) = 40.3 MeV.

represents statistical error only. The following estimated errors affect the cross sections: beam integration 3%, dead time and other electronic errors 2%, target thickness 1%, background subtraction 1-5%, statistical and peak separation 5-15%. Relative total cross sections are estimated from these to agree within 5% - 10% depending on the strength of the state. The absolute cross sections are expected to vary from 10% to 20% depending on the strength of the state and this amount of background subtraction.

V. SPECTROSCOPY AND MECHANISM BY EXAMINATION OF DATA AND COMPARISON TO OTHER WORK

A. Discussion of Mechanism

The $^{12}C(^3He,p)^{14}N$ reaction has been studied by several workers. Holbrow et al.[71] and Priest et al.[72] studied this reaction at a ^3He energy of 14 MeV. The latter obtained angular distributions to the ground state and first two excited states of ^{14}N (see Figs. 9-11). Rivet[4] obtained angular distributions to the ground state and first two excited states of ^{14}N at a ^3He energy of 31 MeV.

Hinds and Middleton[73] obtained excitation functions at 10° laboratory for the ground state and six excited states of ^{14}N from the $(^3He,p)$ reaction at ^3He energies of 5.7 to 10.23 MeV. All excitation functions show strong fluctuations over this energy range. Angular distributions for these levels were taken at several energies. Angular distributions for the ground state of ^{14}N all peak at zero degrees except the angular distribution at $E(^3He)$ = 10.14 MeV (see Fig. 9). At this energy the angular distribution has a maximum at approximately 30° c.m. and then decreases at smaller angles.

At ^3He energies higher than 10 MeV the transition to the ^{14}N ground state continues to show an angular distribution decreasing at zero degrees with a first maximum moving from about 25°c.m. to 15°c.m. as the energy is increased from 14 MeV[72] to 31 MeV.[4] It will be shown in Sec. VI that the transition $^{12}C(^3He,p)^{14}N$ to the ^{14}N ground state, if a direction two-nucleon stripping transition, should proceed predominantly by an L = 2 transfer. The angular distribution shape just discussed is an L = 2 shape (see Fig. 17). The change in the form of the ground state angular distribution in the energy region of 5 to 10 MeV suggests a changing reaction mechanism in this region.

Angular distributions for ^{14}N states at 2.311 MeV (Fig. 10) and the 3.945 MeV (Fig. 11) also show a change in character between 5.98- and 10.14-MeV incident ^3He energies, although the change isn't as pronounced as in the case of the ground-state transition. It is also interesting to note that the envelope of the angular distributions for all energies is nearly flat for angles larger than 60° or 70° center of mass. If a constant cross section magnitude at back angles was due

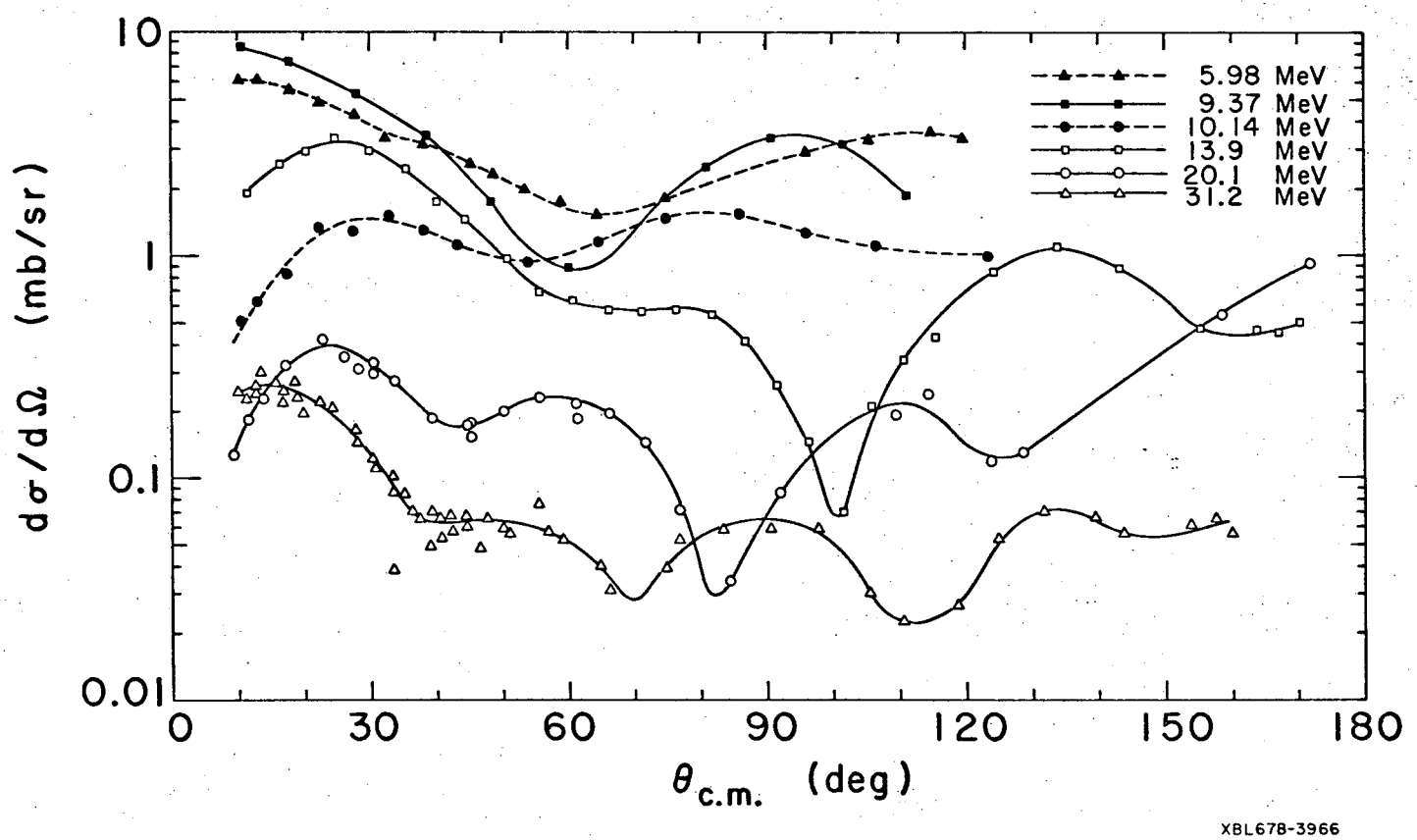

Fig. 9. Proton angular distributions for transitions to the ^{14}N ground state via a $^{12}C(^{3}He,p)^{14}N$ reaction at various energies: 5.98-, 9.37- and 10.14-MeV data by Hinds and Middleton;[13] 13.9-MeV data by Priest et al.;[12] 20.1-MeV data by this work; 31.2-MeV data by Rivet.[4]

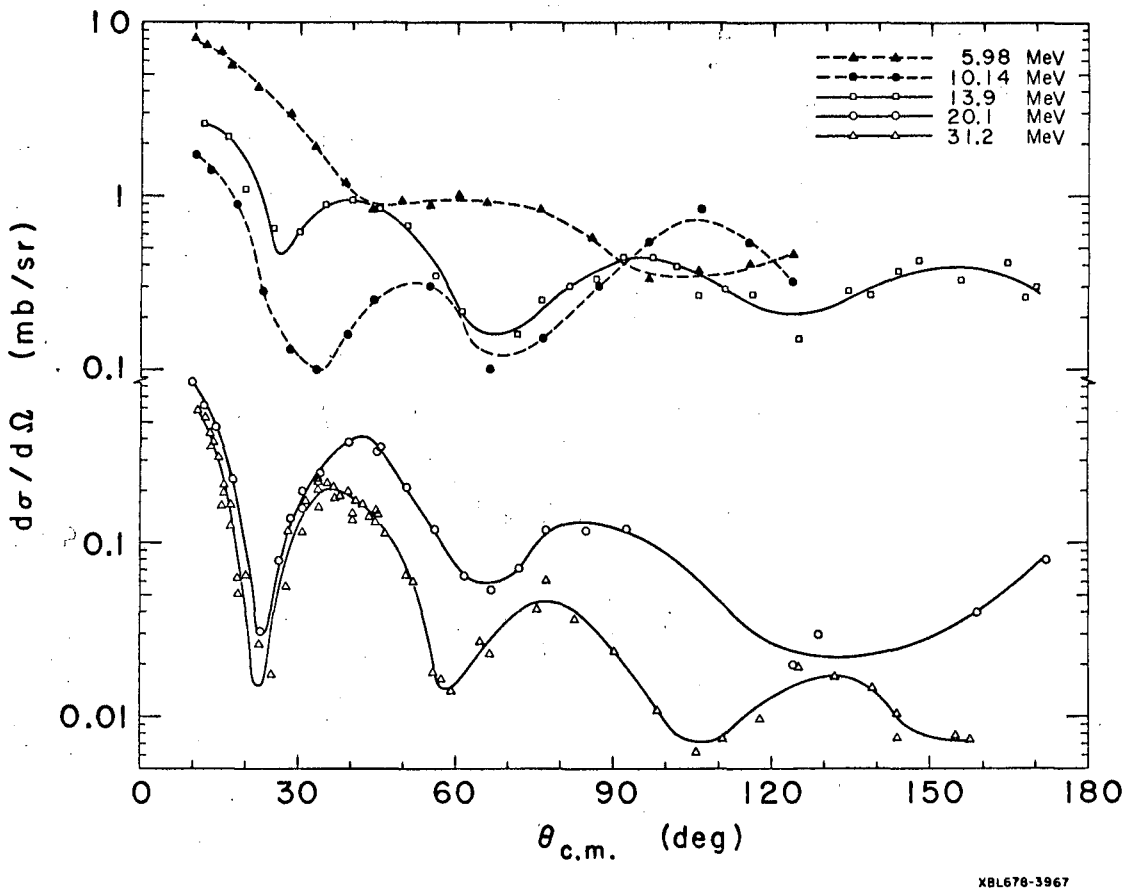

Fig. 10. Proton angular distributions for transitions to the ^{14}N 2.311-MeV state via a $^{12}C(^{3}He,p)^{14}N$ reaction. See caption of Fig. 9.

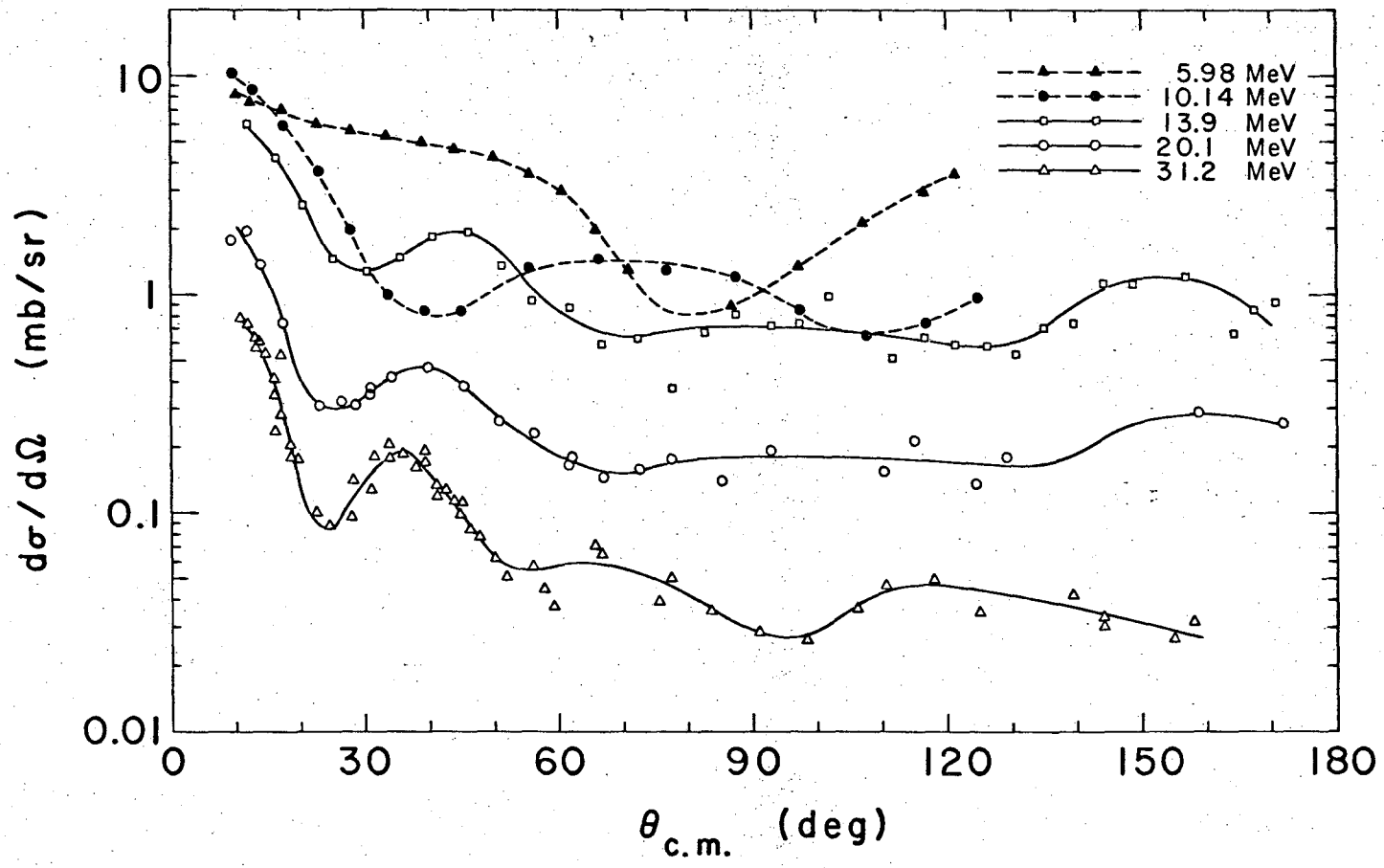

XBL678-3965

Fig. 11. Proton angular distributions for transitions to the ^{14}N 3.945-MeV state via a $^{12}C(^{3}He,p)^{14}N$ reaction. See caption of Fig. 9.

entirely to compound-nuclear effects, the cross section envelope might be expected to decrease with increasing angle for the reaction at higher ^{3}He energies. The fact that this trend is not observed suggests that effects other than compound-nuclear effects also influence the back-angle cross sections.

Fulbright et al.[74] have measured, simultaneously, excitation functions of the differential cross sections at 10° laboratory for the reactions $^{12}C(^3He,p)^{14}N$ and $^{12}C(^3He,n)^{14}O$ to the ground state of ^{14}O and the ^{14}N analog state at 2.311-MeV excitation energy. ^{3}He energies ranged from 65 MeV to 11 MeV. The excitation functions showed a strong energy dependence and neutron and proton angular distributions showed a forward peaking characteristic of direct reactions. Total and differential reaction cross sections for the reaction $^{12}C(^3He,n)^{14}O$ have also been measured by Osgood et al.[75] and by Deshpande et al.[76] for ^{3}He energies below 11 MeV. These workers also found strong energy dependence in the cross sections for this reaction in this energy region. These data suggest that $^{12}C(^3He,n \text{ or } p)$ reactions proceed in large measure by compound-nucleus mechanism below an energy of at least 12 MeV.

Manley[77] has obtained angular distributions for neutrons from the reaction $^{12}C(^3He,n)^{14}O$ to the ground state of ^{14}O at ^{3}He energies of 19, 22, and 25 MeV. The differential cross section at 0° and 19 MeV ^{3}He is about 3.4 mb/sr. This value is in good agreement with a value of $2 \times 1.8 = 3.6$ mb/sr obtained by extrapolating to 0° data reported herein for the reaction $^{12}C(^3He,p)^{14}N$ to the 2.311-MeV analog state. The factor of 2 is necessary to correct for the different value of b_{ST}^2 in the two reactions (see Sec. II-B). Bryant et al.[78] have measured the differential cross section at 0° for the $(^3He,n)$ reaction on ^{12}C at 25 MeV ^{3}He and obtained a value of 4.3 ± 0.6 mb/sr which is in reasonable agreement with these data and the 31 MeV data of Rivet.[4]

Eccleshall and Yates[79] have measured excitation functions of the differential cross section for the reaction $^{16}O(^3He,p)^{18}F$ to the ground state and first excited state of ^{18}F at angles of 15° and 60° between ^{3}He energies of 4 and 8.5 MeV. Resonant structure was observed in all four excitation functions. Hinds and Hinds[80] extended these excitation

functions to 11.4 MeV ^{3}He particles. No resonance structure was observed above 8.5 MeV. Hinds and Middleton[81] have measured the angular distribution to the ground state and four excited state of ^{18}F at E(^{3}He) = 5.9 and 9.16 MeV (see Fig. 12). Angular distributions are similar at both energies.

Hinds and Hinds[80] also studied the reaction ^{16}O(^{3}He,pγ)^{18}F at 10 MeV ^{3}He. They measured the angular correlation of the 0.937-MeV gamma rays from the first excited state of ^{18}F in coincidence with protons detected at angles of 36° and 71°. They concluded from their study that a direct, two-nucleon stripping process is the predominant reaction mechanism for this reaction at 10 MeV. These studies suggest that at a ^{3}He energy near 12 MeV a direct reaction mechanism contributes more to the (^{3}He,p) reaction on ^{16}O than on ^{12}C.

Aguilar et al.[82] have studied the ^{16}O(^{3}He,p)^{18}F reaction at E(^{3}He) = 29 MeV. Pühlhofer and Bock[5,83] have studied this reaction at 18 MeV ^{3}He energy. These latter workers obtain angular distributions to the ground state (Fig. 12) and nine excited states of ^{18}F. In general our values for the cross sections taken at E(^{3}He) = 20 MeV are 40% lower than the 18 MeV values. An error of 30% in the cross section magnitude is reported for the 18 MeV data. With this uncertainty in the cross section, the 20 MeV and 18 MeV data cannot be said to disagree.

Figure 12 shows that the shape of the proton angular distributions for the ^{16}O(^{3}He,p)^{18}F ground state transition at ^{3}He energies from 6 to 20 MeV are similar. This is in contrast to the observations on the ^{12}C-^{14}N system which showed a change in the proton angular-distribution character over this energy range.

Bryant et al.[78] have measured the differential cross section at 0° for the ^{16}O(^{3}He,n)^{18}Ne reaction at E(^{3}He) = 25 MeV and found a value of 2.0 ± 0.4 mb/sr. This is lower than might be expected in comparison to the data of Pühlhofer and Bock[5] and this work.

Manley and Stein[84] studied the (^{3}He,n) reaction at 19, 22 and 25 MeV ^{3}He on a number of nuclei from Be to Ag with oxygen included as one of the targets. These data together with data taken by Manley[77] on carbon at the same energies were analyzed to determine the proportion of direct mechanism and compound-nuclear mechanism contributing to the

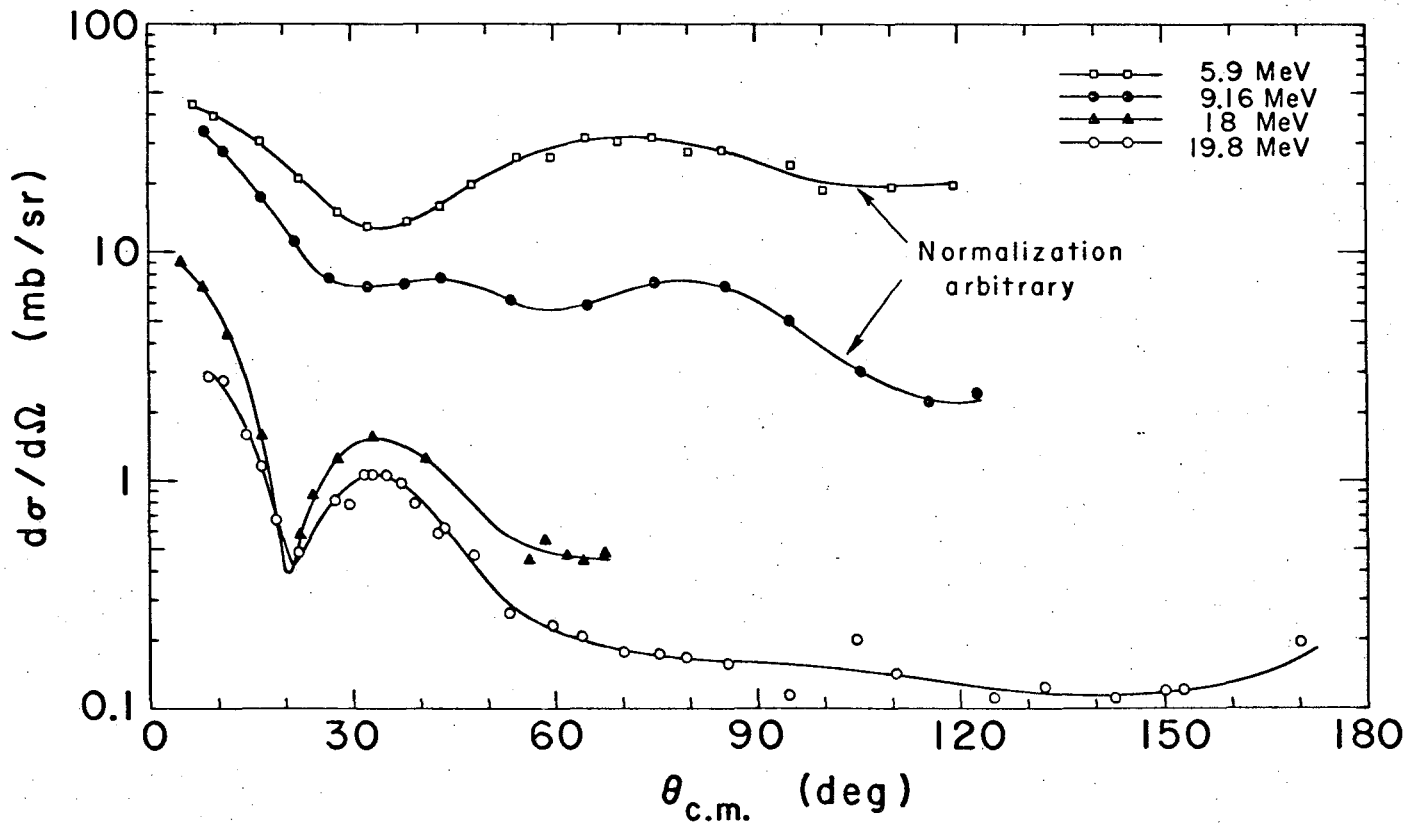

Fig. 12. Proton angular distributions for transitions to the ^{18}F ground state via an $^{16}O(^{3}He,p)^{18}F$ reaction at various energies: 5.9- and 9.16-MeV data by Hinds and Middleton;[81] 18-MeV data by Pühlhofer and Bock;[5,83] 19.8-MeV data by this work.

reactions at the energies studied. Data were taken such that a total neutron spectrum at a given angle was separated into three groups depending upon the neutron energy: ΔE_1 from 1 to 4.5 MeV, ΔE_2 from 4.5 to 12 MeV, and ΔE_3 from 12 MeV to the maximum energy neutron. Angular distributions for each of the three energy regions were obtained.

The cross sections expected for each energy region from a compound-nucleus mechanism, based upon a simple model giving isotropic, center-of-mass angular distributions, were calculated and arbitrarily normalized to the experimental angular distributions. The experimental angular distributions were similar to those calculated at angles larger than approximately 60° laboratory angle.

The 0° differential cross sections were also compared to the calculation. The cross section for energy groups ΔE_1 and $\Delta E_2 (E_n < 12$ MeV) agreed within a factor of two with the calculated values for compound-nucleus mechanism, but the high neutron energy group ΔE_3 was approximately a factor of ten greater than the calculation. Neutrons from group ΔE_3 correspond to formation of states near the g.s. while the other two groups correspond to higher excited states. The results of this work indicate, as is to be expected, that inasmuch as the emission of a neutron from a compound-nuclear system becomes less probable with increasing emission energy, a direct reaction mechanism will dominate for the formation of states with the highest energy scattered neutrons.

The work of Manley and Stein[84] then suggests that for the two-nucleon transfer reaction studied the excitation of low-lying states, particularly for small scattering angle, is predominantly by a direct reaction mechanism. It also suggests that back-angle cross sections include contributions from compound-nucleus mechanisms.

In summary the following can be noted. The model used by Manley and Stein[84] was very simple and their application of it gave only qualitative information. The excitation functions discussed were taken at energies about one half of that used in the experiments reported herein. Comparison of a few data in the energy region of these experiments suggests a smoothly varying excitation function. From these considerations a quantitative determination of the amount of compound-nuclear contribution

to reactions studied cannot be made. It is, however, safe to conclude that compound-nuclear contributions are significant in the differential cross sections at angles greater than about 90° center of mass. There is some suggestion that compound-nuclear effects are smaller in the ^{16}O system than in the ^{12}C system.

Possible multi-step mechanisms involving inelastic excitations in the entrance and exit channels of direct reactions were discussed in Sec. II-C. In ^{12}C the B(E2) for the quadrupole transition between the 0^+ ground state and the 2^+, 4.43-MeV excited state is 5 - 8 times the single-particle B(E2).[61,85] This strong coupling suggests the possibility of a two-step mechanism in the (^{3}He,p) reaction under consideration. The spectroscopic factors for two-nucleon transfer between the ^{12}C 2^+ state and states of ^{14}N must, however, be compared to spectroscopic factors for the direct, single-step process before an estimate of the magnitude of multi-step processes can be made.

For ^{16}O the B(E2) between the ground state and the first 2^+ level is 2 - 3 times the single-particle value. This would suggest less multi-step contribution to reaction cross sections than through the 2^+ level in the case of a ^{12}C target. The first 3^- level of ^{16}O may be more strongly excited than the 2^+ level[61] and, therefore, may make a contribution to a multi-step process. As stated above, however, the spectroscopic factors for transfer between states of ^{18}F and ^{16}O must be known before an estimate of multi-step contributions can be made.

The $^{16}O(\alpha,d)^{18}F$ reaction has previously been studied by Harvey et al.[2,3] at alpha particle energies of 47 MeV and 52 MeV. A comparison of these data to the data reported in this work taken at an alpha energy of 40 MeV shows that general characteristics of the data are the same at all three energies. Compound-nuclear effects are expected to be negligible at these alpha particle energies.

B. Spectroscopy of Nitrogen 14

Table I contains a listing of all the known levels of ^{14}N below an excitation energy of 13.2 MeV and a few additional levels above this energy which are applicable to the two-nucleon transfer reaction under discussion. The energies listed in column one and the spin, parity and isospin assignments are those in the compilation of Ajzenberg-Selove and Lauritsen[86] or are taken from the references listed. The third column contains the experimentally determined excitation energies and errors obtained in this work.

The fourth column contains the integrated cross sections between 10° and 70° center of mass from the present experiment. These limits were chosen to give a constant range of integration for all levels and in addition, this is the region of best agreement between the experimental and theoretical angular distributions. The dominant configurations of the energy levels are given in cases where they have been assigned. The mixing coefficients given are taken from the calculations of True[87] and Cohen and Kurath.[88]

Selection rules for $(^3He,p)$ reactions have been discussed in Sec. II-A and II-B. For this reaction on a target of spin zero, the spin J_2 and isospin T_2 of the final state are just equal to the transferred quantities J and T. For final states of isospin one, the intrinsic spin S transferred must be zero; therefore, the final state spin J_2 equals L, the transferred angular momentum. Inasmuch as the parity of the final state is odd or even as L is odd or even, $T = 1$ states of unnatural parity are forbidden in the reaction.

For final states of isospin zero the intrinisic spin transfer is one. In this case

$$J_2 + 1 \geq L \geq |J_2 - 1| \tag{47}$$

and L must be odd or even as the parity of the final state is odd or even. All $T = 0$ natural-parity states are, therefore, restricted to a single value of L transferred as in the case of $T = 1$ states; however, for $T = 0$ unnatural-parity states, two values of L are allowed by the selection rules. The proper mixing of the two allowed L values

in a transition can be a sensitive measure of the correctness of a theoretical calculation as will be seen in Sec. VI.

By the selection rules, as just discussed, transitions to a number of levels in ^{14}N via the $^{12}C(^{3}He,p)^{14}N$ reaction are restricted to a single L value. These restricted transitions were used to identify the angular distribution shape peculiar to a given L transfer. Figures 15 to 17 contain angular distributions for transitions proceeding via L = 0, 1 and 2 respectively. Figure 18 contains L = 3 angular distributions.

Note that the 8.71- and 9.508-MeV levels are unnatural-parity states of T = 1 and are, therefore, not allowed. Neither of these levels is observed above the tail of the neighbor level peak.

The 8.489-MeV level has been assigned $J = 4^-$ by Detenbeck et al.[89] who suggest a $(p3/2)^{-1}(p1/2)^{2}(d5/2)$ configuration for this state. The observation[90,91] of this level in the reaction $^{12}C(\alpha,d)^{14}N$ confirms the T = 0 assignment. By spin selection rules both L = 3 and 5 transitions are allowed for this state. The above proposed configuration would, however, restrict the L to a value of 3 only. As can be seen in Fig. 18, this transition does proceed by an L = 3 transition which confirms the negative-parity assignment and is consistent with the suggested configuration.

All of the known energy levels of ^{14}N below 8.7 MeV excitation energy are resolved by this work. Three levels near 9 MeV are, however, not resolved. The level of lowest energy in this group is a known 3^-, T = 1 level. The next level is the giant level seen by Harvey et al.[2] in the $^{12}C(\alpha,d)^{14}N$ reaction, and assigned by them to be $J = 5^+$. Dentenbeck et al.[89] have also measured the excitation energy of this level and confirmed the 5^+ assignment.

The third level of the group has been studied by Latorre and Armstrong.[92] They have assigned a spin and parity of 2^+ and a configuration of (2s,1d) to this level. In the calculations by True[87] for levels of ^{14}N a 2^+ T = 0 state of (2s,1d) configuration is predicted at an excitation energy of 8.8 MeV. This level was associated with the known level of ^{14}N at 10.09 MeV. Kashy et al.[93] have shown a preference for a 1^+ assignment for the 10.09 MeV level although the 2^+

value could not be eliminated as a possibility. On the basis of these data, the 2^+ T = 0 level predicted by True[87] to be at 8.8 MeV is assigned to the known 2^+ T = 0 level of ^{14}N at 8.979 MeV.

The 9.388-MeV level has also been studied by Latorre and Armstrong[92] and they restrict the spin and parity assignment of this level to 2^- or 3^-. By the spin and parity selection rules only an L = 3 transition is possible for a 3^- spin and parity assignment. Both L = 1 and 3 are allowed for a 2^- assignment. A comparison of the angular distribution of this level with other L = 1 transitions (Fig. 16) indicates that the transition to the 9.388-MeV level of ^{14}N is predominantly L = 1 which restricts the spin and parity of this level to a value of 2^-.

Rose et. al.[101] have shown the 10.213-MeV level to be of spin and parity 1^+ and, further, that the level is most likely T = 0. This level is not observed by Pehl et al.[91] and Zafiratos et al.[90] in the $^{12}C(\alpha,d)^{14}N$ reaction. As indicated in Table I this level was not observed in the $(^3He,p)$ reaction either. (In Fig. 6 the position of this level is indicated and a small peak is apparent at this excitation energy; however, this is the only spectrum, among all those taken, which has a peak at this excitation energy.)

A 1^+ T = 0 level predicted by True[87] at a calculated energy of 9.3 MeV was associated by him with the 9.702-MeV 1^+ T = 0 level of ^{14}N. This level is observed in both the (α,d) and $(^3He,p)$ reactions. It will be shown in Sec. VI that True's 1^+ T = 0 level is not expected to be observed. For this reason the predicted level is tentatively reassigned to the 10.213-MeV level of ^{14}N, which, as is mentioned above, was not observed.

The 10.85-MeV level of ^{14}N is strongly excited in the $^{12}C(\alpha,d)^{14}N$ reactions.[90,91] This suggests that the level has a high spin and T = 0. The angular distribution of protons from the $^{12}C(^3He,p)^{14}N$ reaction exciting this level, as shown in Fig. 18, indicates a transition of L = 3 or greater. The calculations by True[87] indicate that transitions in this region should involve L = 4 or less. The spin and parity of this level are then restricted to values of 2^-, $3^\pm$, $4^\pm$, 5^+. The strong population of this level suggest that it has a simple, 2-particle

Table I. Nitrogen 14: energy levels and cross sections for $^{12}C(^{3}He,p)^{14}N$ at $E(^{3}He)$ = 20 MeV.

Experimental			This Work			Dominant Configurations	References[b]
Energy (MeV)	J^{π}	T	Energy (MeV ± keV)		σ^{a} (mb)		
0.0	1^{+}	0	0.0	19	0.96	$0.975(p1/2)^{2} - 0.208(p3/2,p1/2)^{-1}$	88,90,91,94-96
						$-0.951(p1/2)^{2} - 0.217(d5/2)^{2}$	87
2.311	0^{+}	1	2.31	22	0.77	$0.914(p1/2)^{2} - 0.405(p3/2)^{-2}$	71,83,88,90,91,94-100
						$-0.931(p1/2)^{2} + 0.298(d5/2)^{2}$	87
3.945	1^{+}	0	3.94	32	1.41	$0.932(p3/2,p1/2)^{-1} - 0.318(p3/2)^{-2}$	71,88,90,91,94-96,98,100
4.910	0^{-}	0	4.93	33	1.34	1.00 (p1/2,s1/2)	71,87,90,91,94,95,98,100-102
5.104	2^{-}	0	5.12	36	3.35	0.960(p1/2,d5/2) - 0.220(d3/2,f7/2)	71,87,90,91,94,95,98,100-102
5.685	1^{-}	0	5.65	30	1.84	0.985(p1/2,s1/2) + 0.140(p1/2,d3/2)	71,87,90,91,94,95,98,100,101
5.832	3^{-}	0	5.84	30	1.58	0.989(p1/2,d5/2) - 0.120(d3/2,f7/2)	71,87,90,91,94,95,98,100,101
6.21	1^{+}	0	6.21	20	2.83	$0.834(s1/2)^{2} + 0.365(d3/2,d5/2) + 0.348(d5/2)^{2}$	87,90,91,94,95,98
6.44	3^{+}	0	6.46	18	10.80	$0.810(s1/2,d5/2) + 0.440(d5/2)^{2}$	87,90,91,94,98
7.029	2^{+}	0	7.01	42	0.84	$1.000(p3/2,p1/2)^{-1}$	88,90,91,94-96,98,103,104
7.97	2^{-}	0	7.95	26	0.91	$-0.980(p1/2,d3/2) - 0.160(d5/2,f7/2)$	87,90,91,94
8.060	1^{-}	1	8.05	35	0.70	$-0.987(p1/2,s1/2) + 0.132(p1/2,d3/2)$	87,90-92,94,95,99,105,106

Table I. (continued)

Experimental		This Work			Dominant Configurations	References[b]
Energy (MeV)	J^π T	Energy (MeV ± keV)		σ^a (mb)		
8.489	4^- 0	8.47	30	1.82	$(p3/2)^{-1}(p1/2)^2(d5/2)$	89-91,94,107
8.617	0^+ 1	8.61	34	0.68	$-0.907(s1/2)^2 - 0.308(d5/2)^2$	87,90,92,94,95,99,105
8.71	0^- 1				1.000(p1/2,s1/2)	87,92,94,95,99,105,106,108
8.906	3^- 1				$-0.994(p1/2,d5/2) - 0.086(d5/2,f7/2)$	87,92,94,95,99,105,106
8.963	5^+ 0	8.96	19	15.88	$-0.995(d5/2)^2 + 0.098(f7/2)^2$	2,3,87,89-91,107,109
8.979	2^+ 0				$-0.850(s1/2,d5/2) + 0.420(s1/2,d3/2)$	87,92,94
9.129	2^- 0	9.15	18	3.64	$(p3/2)^{-1}(p1/2)^2(s;d)$	89,90
9.17	2^+ 1				$\approx 0.7(s1/2,d5/2), \approx 0.7(p3/2,p1/2)^{-1}$	87,88,90,94,96,99,106,107,110
9.388	2^- 0[c]	9.39	26	2.71		90-92,94
9.508	2^- 1				$-0.999(p1/2,d5/2) + 0.026(p1/2,d3/2)$	87,90-92,94,95,99,105,106
9.702	1^+ 0	9.70	22	1.56		90-92,94
10.096	$(1^+)0$	10.08	18	1.63		90-94
10.213	$1^+(0)$[c]				$0.695(d5/2)^2 - 0.532(s1/2)^2$	87,92,94,101
10.431	2^+ 1	10.43	20	2.76	$\approx 0.7(s1/2,d5/2), \approx 0.7(p3/2,p1/2)^{-1}$	87,88,90-92,94-96,99,106,110
10.55	(1^-)	10.56	28	0.56		90,93
10.85	$(4^+)0$[c]	10.81	23	1.01	$0.770(d3/2,d5/2) + 0.640(p1/2,f7/2)$	87,90,91

Table I. (continued)

Experimental		This Work			Dominant Configurations	References[b]
Energy (MeV)	J^{π} T	Energy (MeV ± keV)		σ^{a} (mb)		
11.06	1^{+} 0	11.06	50	0.98		90,91
11.23	$(3^{-})1$	11.27	50			90,93
11.299	2^{-} 0					90,92
11.39	$(1^{+})0$	11.39	40			93
11.51	3^{+} 0	11.51	30			90
11.66		11.66	40			
11.74	1^{+}	11.79	110			
11.80	(2^{+})					
11.97	(2^{+})	11.95	30			
12.05						
12.21	3^{-}					
12.29						
12.41	4^{-} 0	12.40	30	3.41		90,91
12.52		12.50	20	2.18		
12.61	3^{+}	12.63	25	1.51		
12.69	3^{-}					
12.80	4^{+}	12.74	30	8.90		
12.83	4^{-} 0					90,91,109
12.95	(4^{+})	12.90	25	5.74		
(13.05)	(0)					90

Table I. (continued)

Experimental		This Work			Dominant Configurations	References[b]
Energy (MeV)	J^{π} T	Energy (MeV ± keV)		σ^{a} (mb)		
13.17	$0^-,1^-0$	13.15	40			90
13.72	1^+ 1				$(p3/2,p1/2)^{-1}$	96
14.84	0	14.91	60			111
15.5	$(6^-)0$	15.8	200		(d5/2,f7/2)	87,91,109,111
16.3	0					111
17.3	0	17.4	200			91,109,111

[a] Total cross section integrated between 10° and 70° center of mass.

[b] References used other than 86.

[c] J^{π} and/or configuration proposed by this work.

configuration. All of the energy levels of ^{14}N predicted by True[87] below an excitation energy of 10 MeV have been uniquely associated with known levels of ^{14}N. It is, therefore, reasonable to attempt to associate a level predicted by True with this ^{14}N level. By the spin and parity restrictions discussed above only two predicted levels can be considered; a 3^+ T = 0 at 11.0 MeV and a 4^+ T = 0 at 10.8 MeV. As will be shown in Sec. VI a transition to the 3^+ would be very weak while a transition to the 4^+ would be very strong. On this basis the 10.85-MeV level of ^{14}N is tentatively assigned 4^+ T = 0. The configuration predicted by True is indicated in Table I.

A region of levels between 12.4 MeV and 13.2 MeV is strongly populated by the reaction under discussion. A strong population of levels in this region has also been observed[90,91] in the $^{12}C(\alpha,d)^{14}N$ reaction and in the reaction $^{12}C(^{11}B,^{9}Be)^{14}N$ carried out by Sachs, Chasman and Bromley.[109]

A 4^+ T = 1 state of $(d5/2)^2$ configuration is predicted by True to be at an energy of 12.0 MeV. A comparison between the (α,d) reaction, which could not excite a T = 1 state, and the $(^3He,p)$ reaction, which could excite the T = 1 state, should allow identification of T = 1 levels in this region. Two levels in this region are proposed to be 4^+. One of these may be the T = 1 $(d5/2)^2$ level. As is shown in Table I, five levels can be individually resolved in the data from the $^{12}C(^3He,p)^{14}N$ reaction. A composite peak containing three levels is also observed.

The (α,d) data of Pehl et al.[91] has insufficient energy resolution for comparative purposes. The (α,d) data of Zafiratos et al.[90] has better energy resolution and should be useful for comparison. These workers report a very strong peak at an excitation energy of 13.05 MeV. An examination of Fig. 6 reveals that an excitation of 13.05 MeV in ^{14}N is in the region of a sharp minimum between the 12.95- and 13.17-MeV levels indicating very little excitation of a level at this excitation energy. It seems quite unreasonable to suppose a level so strongly populated in an (α,d) reaction would not be excited at all in a $(^3He,p)$ reaction. Data from both reactions have been carefully checked[90] in an effort to solve this apparent discrepance in excitation energy assignments, nevertheless the discrepancy still remains. It is, therefore, not possible to assign the 4^+ T = 1 state by a comparison of the results from the two reactions with these data.

Fig. 17 contains a group of L = 2 angular distributions. There is a distinct difference between the angular distributions for the ground state and the 7.029-MeV levels in comparison with that for the 6.44-MeV level. The two former levels are of $(p)^2$ configuration while the latter is of an $(s,d)^2$ configuration. These data suggest angular distributions may be dependent, to some degree, upon nuclear shell effects.

C. Spectroscopy of Fluorine 18

The low-lying energy levels of nuclei in the mass 18 isobar arise from three basic configurations. First positive-parity states are expected to arise from two particles in the (s,d) shell coupled to a closed ^{16}O core.[112,113] Second, as pointed out by Brown and Green,[114] three observations lead to the postulation of a two-hole-four-particle (2h4p) deformed configuration in mass 18 nuclei: (1) alpha scattering on ^{16}O excites levels which can be fit into a rotational band, (2) strong E2 transitions were observed in ^{16}O and ^{18}O, and (3) a 0^+ and 2^+ level in ^{18}O at excitation energies of about 5.5 MeV can not be explained by the simple shell model. There also exists in ^{18}F a 1^+ at 1.7 MeV excitation and a 2^+ at 2.5 MeV which are not accounted for by the shell model.

Engeland[115] and Federman and Talmi[116,117] have shown, that, indeed, the extra states of ^{18}O are described by mixing 2h4p deformed states with the shell model states. A deformed state with a $(p1/2)^{-2}(s,d)^4$ configuration is assumed by these workers. Their calculations suggest that the shell-model states contain 10% to 20% deformed character. Calculations by Brown and Green[118] indicate an even larger contribution of deformed character.

Arima et al.[119], on the basis of a weak-coupling model, have proposed a $(p1/2)^{-2}_{j=1}(s,d)^4_{J=0}$ configuration for the 1^+ level of ^{18}F at E_x = 1.7 MeV. Kuo and Brown[120] have shown that the 2h4p states in ^{18}F should lie at approximately 2.5 MeV excitation. This configuration would account for the positive-parity levels in this region.

The third type of levels to be found in these nuclei are negative-parity levels. Harvey[121] has proposed that these levels arise from a $(p)^{-1}(s,d)^3$, 1h3p configuration.

If ^{16}O is predominantly a closed shell it follows that only the simple $(s,d)^2$, shell-model states would be populated in a two-nucleon stripping reaction on an ^{16}O target. States with 1h3p or 2h4p character are expected to proceed through small components of ^{16}O or through more complicated mechanisms.

A comparison between known levels of ^{18}F and levels excited strongly enough for positive identification in the $^{16}O(\alpha,d)^{18}F$ and $^{16}O(^3He, p)^{18}F$ reactions is made in Table II. In accordance with the selection rules discussed in Sec. V-B the (α,d) reaction is expected to strongly excite only T = 0 states of ^{18}F. On this basis a number of states are definitely or tentatively assigned T = 0 as indicated in Table II. Other T = 0 assignments are confirmed by this work.

Ollerhead et al.[122] have made tentative assignments for ^{18}F levels corresponding to the T = 1 levels of ^{18}O. The levels at 1.042 and 3.060 MeV excitation energy are well established as indicated in the references of Table II. Note the 3.06-MeV level is not excited in the (α,d) reaction. It is, however, excited in the $(^3He,p)$ reaction and, although not resolved from the 3.134-MeV level is dominant over it as indicated by the excitation energy of the spectral peak corresponding to these two levels.

Assignment of the 4.651-, 4.741- and 4.964-MeV levels as 4^+, 0^+ and 2^+ T = 1 levels respectively is consistent with the decay-scheme work referred to in Table II. It is also consistent with the level spacing in ^{18}O as is shown in Fig. 20. The decay-scheme work, however, could not rule against the possibility that the 4.400-MeV state could be the 4^+ T = 1 state. As is shown in Table II, the 4.400-MeV level is excited in the (α,d) reaction and therefore must be assigned T = 0. On the other hand the 4.651-, 4.741-, and the 4.964-MeV levels are not excited by the (α,d) reaction and are excited by the $(^3He,p)$ reaction. These observations confirm the T = 1 assignments to the three levels under consideration.

Table II. Fluorine 18: energy levels and cross sections at $E(^3He) = 19.8$ MeV and $E(\alpha) = 40.3$ MeV.

Experimental		This Work						Dominant Configuration	References[a]
		$^{16}O(\alpha,d)^{18}F$			$^{16}O(^3He,p)^{18}F$				
Energy[a] (MeV)	J^π T[b]	Energy (MeV ± keV)		σ[c] (mb)	Energy (MeV ± keV)		σ[d] (mb)		
0.0	1^+ 0	0.0	17	0.85	0.0	7	2.42	$(s,d)^2$	79,123-126
0.9371	3^+ 0	0.934	14	1.89	0.937	8	6.10	$(s,d)^2$	79,123,125-127
1.0417	0^+ 1							$(s,d)^2$	79,123-128
1.0807	0^- 0							$(p)^{-1}(s,d)^3$	79,121,123,125-127,129-131
1.1310	5^+ 0	1.119	16	8.46	1.111	7	4.96	$(s,d)^2$	79,123,125-127
1.7005	1^+ 0	1.716	18	0.13	1.680	24	0.45	$(p)^{-2}(s,d)^4$	119,120,123,125-127,132
2.1008	2^- 0	2.100	11	0.27	2.096	13	1.05	$(p)^{-1}(s,d)^3$	121,125-127,129,130
2.5235	2^+ 0[e]	2.541	19	0.10	2.509	18	0.46	$(p)^{-2}(s,d)^4$	120,123,125-127,132
3.0603	2^+ 1				3.062	15	3.04	$(s,d)^2$	122-128,132
3.1339	1^- 0	3.122	14	0.13				$(p)^{-1}(s,d)^3$	121,123,125-127,132
3.3581	$2,(3)^+$ 0[e]	3.363	20	0.22	3.352	16	0.70	$(s,d)^2$	123,125-127,131,132
3.7248	1 0							$(s,d)^2$	126,127,131
3.790	$1,2,(3^-)$ 0							$(p)^{-1}(s,d)^3$	121,126,127,131
3.8385	2^+ 0[e]	3.808	12	0.89	3.830	12	6.41	$(s,d)^2$	126,127,131
4.108	$1,2,(3)$ 0[e]	4.140	12	0.44	4.134	11	1.02		131
4.218	1,(2)								126,131
4.350	2,3								126,131
4.400	≥ 2 0[e]	4.393	9	0.55	4.378	9	1.90		126,131
4.651	4^+ 1[e]				4.651	12	2.45	$(s,d)^2$	122,124-126,128,131
4.741	0^+ 1[e]							$(s,d)^2$	122,124,126,128,131

Table II. (continued)

Experimental		This Work						Dominant Configuration	References[a]
		$^{16}O(\alpha,d)^{18}F$			$^{16}O(^{3}He,p)^{18}F$				
Energy[a] (MeV)	J^{π} T[b]	Energy (MeV ± keV)		σ[c] (mb)	Energy (MeV ± keV)		σ[d] (mb)		
4.844	1^{-} 0[e]	4.852	10	0.55	4.843	12	1.36		131
4.964	2^{+} 1[e]				4.967	21	0.61	$(s,d)^2$	122,128,131
5.295	0[e]	5.266	34		5.297	25	0.48		131
5.502									
5.594	(4^{+})0[e]	5.590	27	0.37	5.601	12	2.71	$(s,d)^2$	
5.662	$(1,2^{-})(1)$								122
5.786	0[e]	5.785	31						
6.092					6.105	8	5.62		
6.139	0[e]	6.139	12	1.68					
6.233	$2^{(-)}(1)$								122
6.247	(1^{+})				6.265	13	3.38		
6.376									
6.472									
6.556	$(3,4,5^{+})0^{e}$	6.548	18	0.60					
6.634									
6.636	1^{-}								
6.765									
6.800	2^{-} 0[e]	6.807	10	1.17	6.779	7	7.67		
6.859									

Table II. (continued)

Experimental		This Work						Dominant Configuration	References[a]
		$^{16}O(\alpha,d)^{18}F$			$^{16}O(^{3}He,p)^{18}F$				
Energy[a] (MeV)	J^{π} T^{b}	Energy (MeV ± keV)		σ^{c} (mb)	Energy (MeV ± keV)		σ^{d} (mb)		
7.185	$(4^{+})0^{e}$	7.191	8	1.02	7.206	9	3.08		
7.26	(1^{+})								
7.315	$(3^{-})(1)$								122
7.493	$(3^{-})(0)^{e}$	7.434	13	0.51					
7.54									
7.60	$(0)^{e}$								
7.69	$(0)^{e}$	7.658	12	0.50	7.646	14	4.18		
7.72									
7.88	(2^{-}) 0^{e}	7.871	11	0.52	7.874	22	4.06		
7.92	(1^{+})								
8.07									
8.20									
8.22									
8.36									
	0^{e}	8.596	19	0.37					
8.98	$(0)^{e}$	8.861	190	0.43					
9.17					9.145	32	3.38		
9.35									

Table II. (continued)

Experimental		This Work						Dominant Configuration	References[a]
		$^{16}O(\alpha,d)^{18}F$			$^{16}O(^{3}He,p)^{18}F$				
Energy[a] (MeV)	J^{π} T^{b}	Energy (MeV ± keV)		σ^{c} (mb)	Energy (MeV ± keV)		σ^{d} (mb)		
9.42					9.404	31	5.69		
9.49	0^{e}	9.494	15	1.62					
9.60									
9.67	$2,3^{+}$								
9.79					9.82	40			
9.96	0^{e}	9.96	120	0.45					
10.11					10.06	45			
10.27		10.268	12	0.56					
10.38					10.352	25	3.58		
10.51	$(0)^{e}$	10.541	10	1.11					
(10.57)									
10.76									
(10.85)									
10.93					10.96	60	4.42		
11.02									
11.07	0^{e}	11.073	37	0.51					
11.16					11.13	50	4.96		
11.39	0^{e}	11.384	18	0.46					
11.78									
12.03	0^{e}	12.055	16	0.30					

Table II. (continued)

Experimental			This Work				Dominant Configuration	References[a]
			$^{16}O(\alpha,d)^{18}F$		$^{16}O(^{3}He,p)^{18}F$			
Energy (MeV)	J^{π}	T[b]	Energy (MeV ± keV)	σ[c] (mb)	Energy (MeV ± keV)	σ[d] (mb)		
12.51								
12.66	0^{e}		12.67	60				
12.94								

[a] References 86, 133 and 134 were used in addition to those in the reference column.

[b] A parenthesis ( ) indicates a preference or tentative assignment.

[c] Cross sections are integrated from approximately 12° to 80° center of mass.

[d] Cross sections are integrated from approximately 11° to 82° center of mass.

[e] Assignment of J^{π} and/or T and/or configuration made or confirmed by this work.

A $J = 1^-$ [135] level of ^{18}O at $E_x = 4.45$ MeV was proposed[122] as corresponding to one of two levels at 5.59- and 5.66-MeV excitation in ^{18}F. As is seen in Table II. the 5.59-MeV level is excited in both the (α,d) and $(^3He,p)$ reactions, which restricts this level to $T = 0$. The angular distribution of this level is characteristic of $L = 4$ as shown in Fig. 23. Arguments will be presented in Sec. VI for the assignment of this level as $J^\pi T = 4^+ 0$. The 5.66-MeV level is not resolved from the 5.59-MeV level just discussed and it is not certain that this level is excited in the (α,d) reaction. It may, therefore, be the $J^\pi = 1^-$, $T = 1$ level.

The $2(^-)$ level in ^{18}F at $E_x = 6.23$ MeV was proposed[122] as corresponding to the 5.09-MeV level of ^{18}O. The 5.09-MeV level is now known[136] to be a 3^- level which casts doubt on this proposed correspondence unless the 6.23-MeV level of ^{18}F has been assigned the wrong spin.

The 6.556-MeV level was also suggested[122] as a $T = 1$ level. The observation of this level in the (α,d) reaction indicates a $T = 0$ assignment. The ^{18}F energy levels in the region of 6.5 MeV are closely spaced and generally of unknown spins. The assignment of $T = 1$ levels in this region, therefore, seems unjustified.

Ollerhead et al.[122] also suggested that the 6.19-MeV level of ^{18}F (now known[137] to be $J^\pi = 2,3^-$) corresponds to either the 7.315- or the 7.499-MeV level in ^{18}F. Both are tentatively assigned 3^- spin and parity. The 7.499-MeV level is seen to be $T = 0$ by its observation in the (α,d) reaction. The 7.315-MeV level may, therefore, be the $T = 1$ level.

Angular distributions for $L = 0$, 2, and 4 transitions in the reaction $^{16}O(^3He,p)^{18}F$ are shown in Figs. 21 to 23. Angular distributions for the 2.101- and 2.524-MeV levels are shown in Fig. 24. As discussed above these two levels and the 1.700-MeV level are considered to be particle-hole states. The angular distributions to the two states first mentioned do not show a direct-stripping pattern. This observation helps to confirm their particle-hole character. All three states have a rather small cross section which is to be expected for states of strong collective character. The relative strengths of these states will be further examined in Sec. VI.

The L = 0 stripping-like angular distribution for the 1.700-MeV state is unexpected if the state is of predominantly particle-hole character, and if the angular distribution of the 2.524-MeV level is taken as typical for a state of particle-hole configuration. As was discussed in Sec. II-C, however, calculations suggest multi-step processes should be given angular distributions similar to those for single-step processes. Perhaps the two transitions proceed by different mechanisms, or the interference between contributing mechanisms is different in the two states. The 1.700-MeV state may also contain significant amounts of two particle configurations.

Pühlhofer and Bock,[5] in their study of the $^{16}O(^3He,p)^{18}F$ reaction at $E(^3He)$ = 18 MeV, were able to resolve the four levels of ^{18}F near 1 MeV excitation. Their work shows the 1.042- and 1.081-MeV levels to have cross sections about 1/4 and 1/20 that of the ground state respectively. In the work of this paper two distinct, but only partially resolved, peaks near 1 MeV were observed. It is assumed that the lowest-energy peak contains contributions from the 0.937-MeV level only and that the other peak contains contributions from the 1.042-, 1.081- and 1.131-MeV levels. A comparison of cross sections for the reaction at 18 and 20 MeV substantiates these assumptions.

In several cases an experimental peak in the spectrum is too broad to resolve individual levels but nevertheless a careful determination of the excitation energy of the peak shows the predominant contribution comes from only one level. If the $(^3He,p)$ reaction is considered, several such cases are observed. The 3.062-MeV peak has already been discussed. A peak at 3.830 MeV must arise predominantly from the proposed 2^+ T = 0 state at this energy. The 3^- T = 0 state nearby thus has a small cross section which is consistent with small cross sections to the other two negative parity levels discussed.

The observed peak at 4.651 MeV must arise predominantly from the known level at that energy. The cross section to the 0^+, T = 1 companion level must, therefore, be small. The 5.601-MeV peak has been discussed above.

A new ^{18}F level at an excitation energy of 8.596 ± 0.019 MeV was observed in the (α,d) reaction.

One further observation is of interest. Of the large number of known energy levels in ^{18}F below an excitation energy of 13 MeV only a relatively few are strongly or moderately excited in these two-nucleon stripping reactions. This observation points up one of the advantages of two-nucleon transfer reactions; that is the preferential population of specific types of states.

VI. THEORETICAL CALCULATIONS: COMPARISON WITH EXPERIMENT: DISCUSSION

Two computer programs were used for evaluation of the kinematic factors B^M_{NL} of Eq. (26). The program REACTION 6, written by Dr. Norman K. Glendenning, was used for most of the calculations. The program JULIE,[20,43] was used for a few model calculations as discussed in Sec. VI-D.

The program REACTION 6 employs the zero-range approximation and the local-potential approximation. The function $U^M_{NL}(\vec{R})$ describing the center-of-mass motion of the captured pair, is a harmonic oscillator with an exponential tail function matched as described in Sec. II-C-4. In the present calculations the harmonic-osciallator parameter defined by Eq. (48) was usually fixed at the value used in the nuclear structure calculations.

$$\nu = \frac{m_x \hbar\omega}{(c\hbar)^2} \tag{48}$$

The mass of the transferred pair m_x is in units of MeV.

The program carries out the coherent sum on N and the incoherent sum on M,L and J indicated in Eq. (26). This summing requires that the structure factors G_{NLSJT} be input parameters for the program. The program contains no spin-orbit coupling.

The program JULIE also employs the zero-range approximation and the local-potential approximation. It includes spin-orbit coupling. A Woods-Saxon function may be used for the bound-state function $U^M_{NL}(\vec{R})$. Calculations can be made for only one N value at a time.

Optical-model parameters were obtained from elastic scattering data by use of a modified version of the computer program SEEK.[138] The optical potential employed is defined as follows.

$$U(r) = V_c(r) - Vf(r) - iWf'(r) - iW_d g(r) \tag{49}$$

$$V_c(r) = \frac{ZZ'e^2}{2R_c}\left(3 - \frac{r^2}{R_c^2}\right) \quad , \quad r \leq R_c$$

$$= \frac{ZZ'e^2}{r} \quad , \quad r \geq R_c \tag{50}$$

$$f(r) = \left[1 + \exp \frac{r - R_o A^{1/3}}{A_o}\right]^{-1} \qquad (51)$$

$$f'(r) = \left[1 + \exp \frac{r - R_i A^{1/3}}{B}\right]^{-1} \qquad (52)$$

$$= 4 \left| \frac{d}{dr} f'(r) \right|$$

$$g(r) \quad \text{or} \qquad (53)$$

$$= \exp\left[-\left(\frac{r - R_i A^{1/3}}{B}\right)^2\right]$$

The program also includes a spin-orbit potential which was not used in this work. V_c, V, W and W_d are the Coulomb, real, imaginary-volume and imaginary-surface potentials respectively.

A. Optical-Model Parameters for $^{12}C(^3He,^3He)^{12}C$ Elastic Scattering

Several families of potentials were found in the optical-model analysis of ^3He scattering on ^{12}C at $E(^3He)$ = 20 MeV. Representative sets of parameters are given in Table III. The solid line curve in Fig. 13 is calculated using the optical potential with V = 220 MeV. It was found, as had been observed earlier,[139,140] that inclusion of spin-orbit parameters in the potential did not alter the angular distribution significantly.

Baugh et al.,[141] who studied ^{12}C and ^3He elastic scattering at 30 MeV ^3He, found that optical-model calculations did not fit experimental values at angles larger than 70°c.m. Kellogg and Zurmuhle[142] have studied ^3He elastic scattering on ^{12}C and on ^{13}C at 12, 15 and 18 MeV ^3He. The angular distributions at 15 and 18 MeV for ^{13}C are similar while angular distributions at these two energies for ^{12}C are not similar. The observations that ^3He elastic scattering from ^{12}C does not show the smooth trend with incident energy seen in ^3He elastic scattering on ^{13}C and differs from the optical-model predictions at large angles may be due to

Table III. Optical parameters for ^{3}He elastic scattering on ^{12}C at $E(^{3}He) = 20$ MeV.

V (MeV)	R_o (F)	A_o (F)	W (MeV)	R_i (F)	B (F)	R_c (F)	Chi^2 (F)
220	1.16	0.597	12.4	1.55	1.046	1.3	4.7
200	1.26	0.578	16.4	1.25	1.141	1.3	2.7
190	1.31	0.555	21.4	0.96	1.230	1.3	2.4
180	1.37	0.531	42.2	0.30	1.380	1.3	2.5
210	0.81	0.730	5.6	2.19	0.837	1.4	4.7
180	0.93	0.703	6.2	2.14	0.856	1.4	6.3
140	1.16	0.650	7.5	1.96	0.890	1.4	4.1
125	1.26	0.626	8.9	1.76	0.952	1.4	2.7
110	1.39	0.579	13.4	1.34	1.125	1.4	1.7
110	0.79	0.830	3.9	2.54	0.611	1.4	1.7
90	0.97	0.788	4.4	2.42	0.709	1.4	2.1
70	1.21	0.734	5.2	2.29	0.729	1.4	1.2
50	1.57	0.614	9.7	1.54	1.050	1.4	1.4

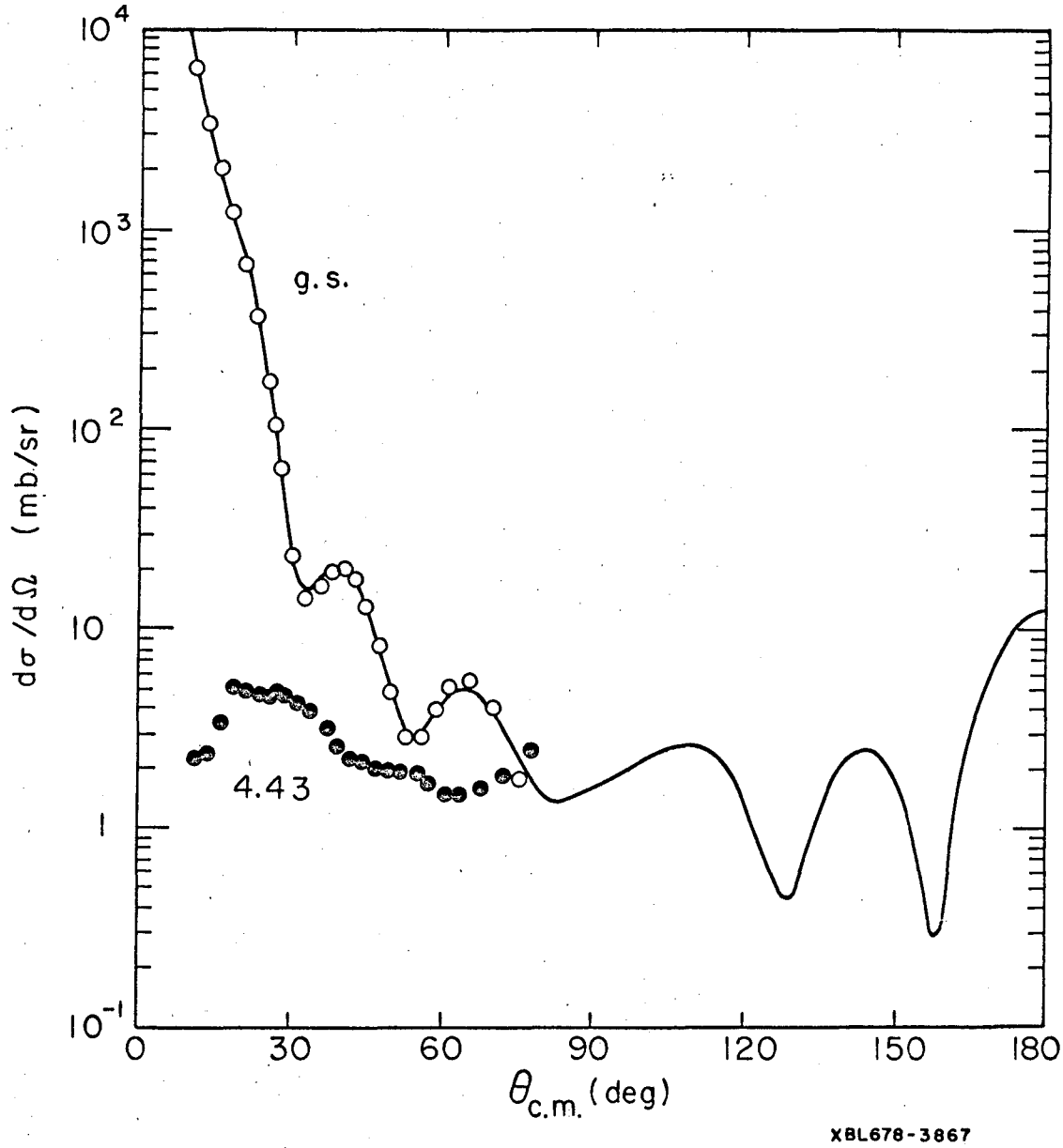

Fig. 13. ^{3}He angular distributions for the $^{12}C(^3He,^3He)^{12}C$ reaction at $E(^3He)$ = 20.1 MeV. The solid-line curve was calculated using the V = 220 MeV optical-model potential in Table III.

the strong coupling between the ^{12}C g.s. and first 2^+ state. Harvey et al.[61] obtained a value of 13 $e^2(fm^4)$ for the B(E2) in ^{12}C compared to a B(E2) of approximately 6 $e^2(fm^4)$ for a similar transition in ^{13}C.

B. Calculations for the Reaction $^{12}C(^3He,p)^{14}N$ at $E(^3He) = 20$ MeV

1. ^{12}C and ^{14}N Wave Functions and Calculation of Structure Factors

Energy levels of ^{14}N may be classified into three groups according to the major configuration of each level. The energy levels below 9 MeV excitation energy are shown in Fig. 14 and are grouped according to classification. One group of four positive-parity levels are predominantly of a $(p)^{-2}$ configuration. The ground state and 2.311-MeV state are predominantly $(p1/2)^{-2}$. The other two states of this group have a $(p3/2)^{-1}$ $(p1/2)^{-1}$ configuration (see Table I).

Another group of positive-parity levels arise from an $(s,d)^2$ configuration. Some mixing between these two types of positive-parity levels is expected.

A third group of levels are of negative parity and arise from a $(p)^{-3}$ (s,d) configuration.

Two sets of wave functions for ^{14}N states have been used in the calculations to be discussed. Cohen and Kurath[88] have made an intermidiate-coupling calculation for nuclei in the p shell. They therefore calculated wave functions only for the four $(p)^{-2}$ states of ^{14}N shown in Fig. 14. The ground-state wave function for ^{12}C is also taken from this calculation.

The $(p3/2)^{-n}$ character of the ^{12}C and ^{14}N wave functions will be shown by this work to be important. In addition to ^{14}N states with this major configuration, the ^{12}C ground state, in the Cohen and Kurath[88] calculations, has a 60% admixture of $(p3/2)^{-n}$ configuration (see Table VIII footnote). Of course the Cohen and Kurath calculation neglects any $(s,d)^2$ components in the wave functions.

True[87] has calculated the levels of ^{14}N based upon a model which assumed that ^{14}N consisted of a closed p3/2 core (i.e. ^{12}C as $(p1/2)^{-4}$) with two particles in the following single-particle states: p1/2, d5/2,

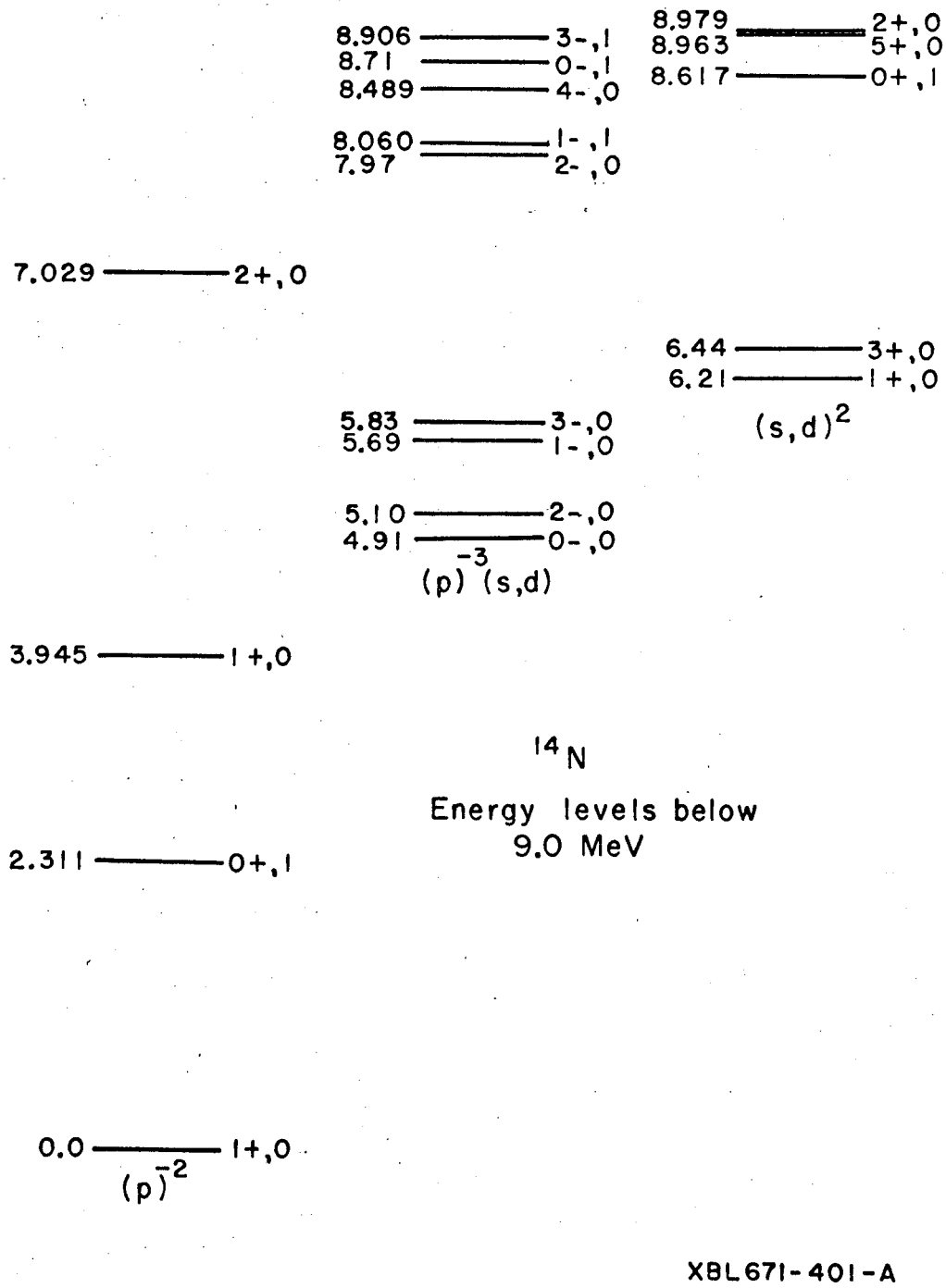

XBL671-401-A

Fig. 14. ^{14}N energy levels below 9-MeV excitation grouped according to major configuration. References are listed in Table I.

2s1/2, d3/2 and f7/2. True, therefore, does not describe states with major components of $(p3/2)^{-n}$ configurations, neither do these configurations mix into other states. The two lowest $(p)^{-2}$ states, the negative-parity states except for the 8.489-MeV level, and the $(s,d)^2$ states all below 9 MeV excitation energy in ^{14}N are some of the states predicted by True.

These two sets of wave functions have been found to predict physical quantities in agreement with experimental quantities. Both are in good agreement with the measured energies of energy levels described below 10 MeV of excitation energy. Cohen and Kurath[88] have calculated a number of magnetic dipole moments, Gamow-Teller beta decays and M1 gamma transitions. These show reasonable agreement with experiment. They point out that use of an ^{14}N wave function with 0.988 overlap with the calculated ^{14}N ground state would produce the observed log ft value for ^{14}C beta decay. Warburton[143] and co-workers have compared experimental gamma transitions for the positive-parity states of ^{14}N to calculated values obtained from the following ^{14}N wave functions. They have taken from True's[87] calculation the coefficients for configuration mixing and the $(s,d)^2$ configurations. They have replaced all $(p)^2$ components by the wave functions of Cohen and Kurath. These comparisons show excellent agreements.

Morrison et al.[144] have studied the (d,p) reaction at E(d) = 12 MeV on all stable targets from ^{6}Li to ^{14}N and have compared the experimentally determined spectroscopic factors with calculations based upon Cohen and Kurath[88] wave functions. Excellent agreement has been found except for the $^{12}C(d,p)^{13}C$ ground-state transition. Ball and Cerny[145] have studied the $(^3He,\alpha)$ reaction at $E(^3He) \approx 40$ MeV on a several p-shell nuclei. Relative spectroscopic factors extracted are in good agreement with Cohen and Kurath predictions; and specifically the $^{13}C(^3He,\alpha)^{12}C$ ground-state transition is in good agreement with the predicted strength relative to other transitions.

Holbrow, Middleton and Rosner[100] have studied the $^{13}C(^3He,d)^{14}N$ reaction at $E(^3He) = 15$ MeV. Relative spectroscopic factors for the four $(p)^{-2}$ states are in good agreement with predicted values from Cohen and Kurath[88] wave functions. Spectroscopic factors to the first four,

negative-parity levels of ^{14}N were also obtained. These factors were in good agreement with predicted values from the True[87] wave functions with the exception of the 5.83-MeV state which is only 60% as large as the predicted value.

Alburger et al.[105] have compared total radiative widths and branching ratios for five of the first six excited states of ^{14}C to predicted values for these quantities based upon True's,[87] ^{14}C wave functions. One radiative width is known and the predicted value is in agreement with this known value. Lower limits are placed on radiative widths for three other levels and the predictions are above these limits. One upper limit is placed on a radiative width and the prediction is just larger than the limit. Branching ratios from four levels are in good agreement, but the branching ratios from one level are very poor--the ground-state branch being predicted too strong. This failure is though to be due to the fact that True does not inlude the $(p3/2)^{-n}$ character of the ^{14}C ground state.

Lieb and Hartmann[146] have studied transitions from several negative-parity levels of ^{14}N and compared the transition strengths to the predicted values from True's[87] wave functions. Four predicted values are in essential agreement with the known data. One transition is about a factor of three larger than the experimental value.

In order to evaluate G_{NLSJT} (Eq. (20)) from the wave functions of Cohen and Kurath,[88] the two-particle c.f.p. values were needed. Kurath[88] kindly provided these coefficients in an LS coupling scheme. In the notation of Sec. II-A these coefficients may be designated by

$$\langle J_2T_2 | J_1T_1;\ JT\rangle$$

J_2T_2 indicate the state of ^{14}N, J_1T_1 indicate the ground state of ^{12}C and JT indicate the two transferred particles with their LS coupled to J. Inherent in the coefficient above is a sum over the various configurations in the ^{14}N state and the ^{12}C ground state. β_{NLSJT} is then equal to a statistical factor $\binom{10}{2}$ times the above coefficient. The factor indicates two particles taken from the ten p particles in ^{14}N.

The radial wave functions of the bound pair of transferrred particles were assumed to be harmonic oscillators which meant the P_{NLSJT} factor was just the Moshinsky[32] bracket for coupling two p particles to center-of-mass motion designated by N and L and relative motion designated by principle quantum number n and angular moment $\ell = 0$. Ω_n was evaluated according to the method of Glendenning[1] which assumes a Gaussian wave function for ^{3}He with a size parameter of 0.206. A harmonic-oscillator parameter = 0.32 was used. P_{NLSJT} and Ω_n were evaluated in this manner for all calculations to be performed and will not be further discussed in other sections.

Values of G_{NLSJT} calculated as outlined above are listed in Table IV. The structure factor for the 8.489-MeV state was calculated using the Cohen and Kurath ^{12}C ground state and a $(p3/2)^{-1}(p1/2)^2(d5/2)$ configuration[89] for this ^{14}N state.

The wave functions of True[87] are two-particle wave functions and, therefore, the two-particle c.f.p. is identically one. In this case

$$B_{NLSJT} = C_\gamma \begin{bmatrix} \ell_1 & 1/2 & j_1 \\ \ell_2 & 1/2 & j_2 \\ L & S & J \end{bmatrix} \delta_{JJ_2} \delta_{TT_2} \qquad (54)$$

C_γ is the mixing coefficient for the configuration $[j_1 j_2]_{J_2}$ in a mixed configuration wave function for the state of ^{14}N. The bracket is a jj to LS transformation bracket. Structure factors calculated from True's wave functions using a harmonic-oscillator parameter ν equal to 0.32 are shown in Table IV.

Both Cohen and Kurath[88] and True[87] predict a $2^+ T = 1$ state near 9.5 MeV excitation with a $(p)^{-2}$ and an $(s,d)^2$ configuration respectively. As discussed in the references of Table I, the 9.17- and 10.431-MeV states are proposed each to contain approximately a 50% admixture of these two configurations. Assuming the wave function shown in Table I for these two states, structure factors have been calculated.

As was mentioned in Sec. V-B a 1^+ $T = 0$ state predicted by True had been associated with the 9.702-MeV level of this spin parity assignment.

Table IV. Structure factors G_{NLSJT} for the $^{12}C(^{3}He,p)^{14}N$ reaction.[a]

Level[b]				True[c]				Cohen and Kurath[c]	
(MeV)	J^{π}	Tx	L	N=1	N=2	N=3	N=4	N=1	N=2
0.0	1^+	0a	0	0.016	0.112	-0.113	0.007	-0.012	-0.085
			2	-0.560	0.112	-0.004		0.417	
2.311	0^+	1a	0	-0.049	-0.348	0.189	-0.013	0.075	0.541
3.945	1^+	0b	0					0.057	0.410
			2					0.017	
4.91	0^-	0a	1	-0.023	0.639				
5.10	2^-	0a	1	0.065	0.349	-0.077			
			3	0.216	-0.001				
5.69	1^-	0a	1	-0.013	0.542	-0.017			
5.83	3^-	0a	3	0.557	-0.048				
6.21	1^+	0b	0	0.014	0.057	0.574	-0.011		
			2	-0.113	0.013	0.006			
6.44	3^+	0a	2	0.060	0.653	-0.009			
			4	0.022	0.005				
7.029	2^+	0a	2					0.218	
7.97	2^-	0b	1	0.018	0.097	-0.032			
			3	-0.712	0.014				
8.060	1^-	1a	1	-0.006	0.401	-0.021			
8.489	4^-	0[d]	3					-0.381	
8.617	0^+	1b	0	-0.024	-0.115	-0.525	0.012		
8.71	0^-	1a		forbidden					
8.906	3^-	1a	3	0.488	-0.030				
8.963	5^+	0a	4	-0.599	0.016				
			6	-0.006					
8.979	2^+	0a	2	0.033	0.550				
9.17	2^+	1[e]	2	-0.104	0.388	-0.004			
9.508	2^-	1a		forbidden					
10.213	1^+	0c	0	0.004	0.109	0.056	-0.011		
			2	-0.102	-0.069	0.006			
10.431	2^+	1[e]	2	0.117	0.388	-0.004			
10.85	4^+	0a	4	0.756					

Table IV. (continued)

Level[b]				True[c]				Cohen and Kurath[c]	
(MeV)	J^π	Tx	L	N=1	N=2	N=3	N=4	N=1	N=2
11.00[f]	3^+	0b	2	-0.047	0.031	0.006			
			4	0.047	-0.003				

[a] A ^{3}He size parameter of 0.206 was used.[1] A harmonic-oscillator parameter ν of 0.32 was used.

[b] The a,b, etc. refer to the first, second, etc. theoretical level of J^π given in the relevant calculation. The ^{14}N energy level associated with a J^πTx theoretical level is given.

[c] References for the wave functions used are as follows: True,[87] and Cohen and Kurath.[88]

[d] Wave functions were the ^{12}C g.s. by Cohen and Kurath and the ^{14}N configuration of $(p3/2)^{-1}(p1/2)^2(d5/2)$.

[e] The 2^+ T = 1 states in this region from both calculations were mixed as discussed in the text.

[f] This is the energy value predicted by True.[87]

The 10.096- and 10.213-MeV levels have also been tentatively assigned 1^+ T = 0. The structure factors for the state in question (listed in Table IV under the 10.213-MeV state) are much smaller than those for other $(s,d)^2$ states and on this basis it is not expected that the state should be observed. Of the three levels under discussion only the 10.213-MeV level is not observed and the predicted state is tentatively assigned to this level.

The 10.85-MeV level was also discussed in Sec. V-B. Two states predicted by True[87] may possibly be assigned to this level; a 4^+ T = 0 and a 3^+ T = 0. The spectroscopic factors for these two states are the last two entries in Table IV. The factors are vanishingly small for the 3^+ state leaving only the 4^+ state for tentative assignment to the 10.85-MeV level of ^{14}N. The spectroscopic factor for the 4^+ state is larger than the factor for the 5^+ T = 0 giant state seen in (α,d) reactions.[90,91] If the 10.85-MeV level is to be associated with the 4^+ state predicted by True the strength of this configuration must be mixed into other 4^+ states. Two states near 12.5 MeV excitation are tentatively assigned 4^+. If one of these is a T = 1 state, as discussed in Sec. V-B, the other could contain part of the strength of the 4^+ state under consideration.

2. Optical-Model Parameters

Optical-model parameters used in distorted wave (DW) calculations for the $^{12}C(^3He,p)^{14}N$ reaction are shown in Table V. Several sets of parameters obtained from the elastic scattering of ^3He on ^{12}C were used, without success, in DW calculations. Parameter set 2 yielded a fit to positive-parity states up to about 7.5 MeV excitation energy. It did not, however, yield a fit for odd-parity states.

Potential set 1 was constructed by summing the potentials of single nucleons and was found to give reasonable fits to the data. Bjorklund and Fernbach[147] obtained a single set of optical potentials for the scattering of 7 MeV neutrons on targets of mass 27 to 209. Perey[148] has obtained a systematic set of parameters for proton scattering at energies of 9 to 22 MeV and for targets of mass 27 to 197. It was assumed these systematics would extend to mass 12 and 7 MeV energy.

Table V. Optical-model parameters for the $^{12}C(^{3}He,p)^{14}N$ reaction.

Particle	Target	Set	V (MeV)	R_o (F)	A_o (F)	W (MeV)	W_d (MeV)	R_i (F)	B (F)	R_c (F)
^{3}He(20 MeV)	^{12}C	1	146.5	1.25	.65		36.5	1.25	.47	1.25
"	"	2	220.0	1.16	.597	12.4		1.55	1.046	1.3
p(30 MeV)	^{14}N	3	42.0	1.25	.65		6.0	1.25	.50	1.25
p(20 MeV)	"	4	47.0	1.25	.65		6.0	1.25	.50	1.25

These proton and neutron potentials both used the same radius and diffusness parameters and were, therefore, used in set 1. The potential well depths of set 1 were obtained by summing the single-nucleon potential depths discussed above.

Proton parameters for the exit channel were obtained by fitting data for proton elastic scattering on ^{14}N. Proton data at 31 MeV taken by Kim et al.[149] and at 20 MeV taken by Chow and Wright[150] were fitted using a fixed set of parameters as shown in Table V. Only the real well depth was adjusted as a function of energy. A straight-line interpolation or extrapolation from these two potentials was taken to obtain a potential set for the energy of the outgoing proton. The systematic proton potentials of Perey[148] were also used in a few calculations and were found to give a 1% to 4% change in cross section magnetidue and no observable change in calculated angular distribution in comparison to the use of potentials 3 and 4 as discussed.

3. Distorted-Wave Calculation

A DW calculation for the reaction $^{12}C(t,p)^{14}C$ at E(t) = 10 MeV has been made by Glover and Jones[36] for the ground state and first three excited states of ^{14}C. The general character of the experimental angular distributions are reproduced. However, the theoretical curves begin to deviate from experiment for center-of-mass angles of 50° and greater. Relative total cross sections were not reproduced without using a radial cutoff of 4f.

Henley and Yu[10] have made DW calculations for the $^{12}C(^{3}He,n)^{14}O$ reaction at $E(^{3}He)$ = 20 MeV. Their calculation for the ^{14}O ground-state angular distribution fits our data for the analog state at 2.311 MeV in ^{14}N. Their predicted relative cross sections for other T = 1 states are much too large. This may be due to the fact that they used an unrealistically small harmonic-oscillator parameter in order to fit the ^{14}O g.s. transition. This was necessary because they used a pure harmonic oscillator without correcting for the exponential decay in the nuclear surface region.

Cohen and Kurath[88] evaluated nuclear interaction matrix elements and did not employ single-particle wave functions in their nuclear-structure calculation. For this reason no harmonic-oscillator parameter is suggested for the reaction calculation.

True,[87] however, did nuse harmonic-oscillator functions in his calculations with an oscillator parameter of 0.32 for p1/2 particles and of 0.27 for other particles. The value of $\nu = 0.32$ for $(p)^{-2}$ states was used in calculations of both True and Cohen and Kurath $(p)^{-2}$ states. The value of $\nu = 0.27$ was used for True $(s,d)^2$ states and an average value of $\nu = 0.295$ was used for negative-parity states. Structure factors calculated using the respective values of ν were used in the calculations. The dominant factors for each level given in Table IV are very nearly equal to the factors actually used.

The curves in Figs. 15 to 19 were obtained by using the optical-model parameter set 1 for the incident ^{3}He and sets 3 and 4, as discussed above, for the scattered proton; curves were individually normalized to the data. The calculations did not involve a cutoff radius. Several attempts were made to use a cutoff radius but fits obtained in such attempts were inferior to those shown in the figures. Calculated angular distributions are shown for ^{14}N energy levels up to an excitation energy of 9 MeV. The wave functions of levels at higher excitation energy are uncertain as discussed above, and the binding energy is so small that calculated angular distributions are not meaningful.

Data and calculations for several L = 0 transitions are shown in Fig. 15. The general features of the transitions are reproduced although the first maximum beyond zero degrees is at too large an angle in general. The fit to the 8.617-MeV level is the worst obtained. In this case the first experimental maximum is entirely out of phase with the calculated curve.

A group of L = 1 transitions is shown in Fig. 16. These transitions are reasonably well fit to an angle of about 70° center of mass, beyond which the calculations fall below the experimental values.

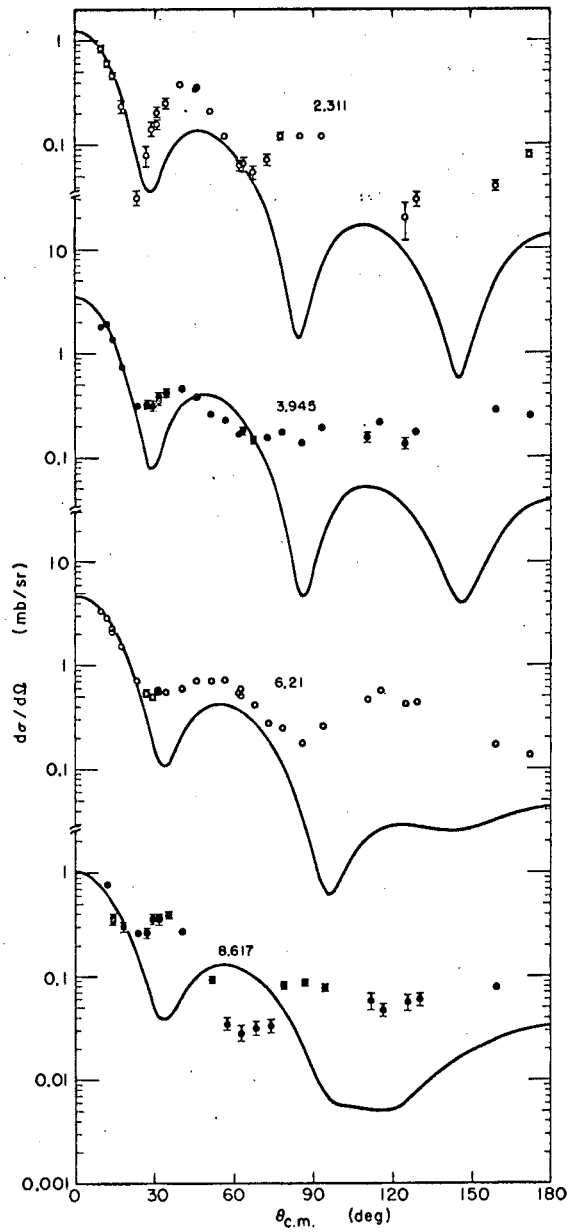

Fig. 15. Proton angular distributions for the $^{12}C(^{3}He,p)^{14}N$ reaction at $E(^{3}He)$ = 20.1 MeV; transitions of predominant L = 0 character. The solid-line curves are DW calculations. Statistical errors are indicated by error bars or are smaller than the point symbols.

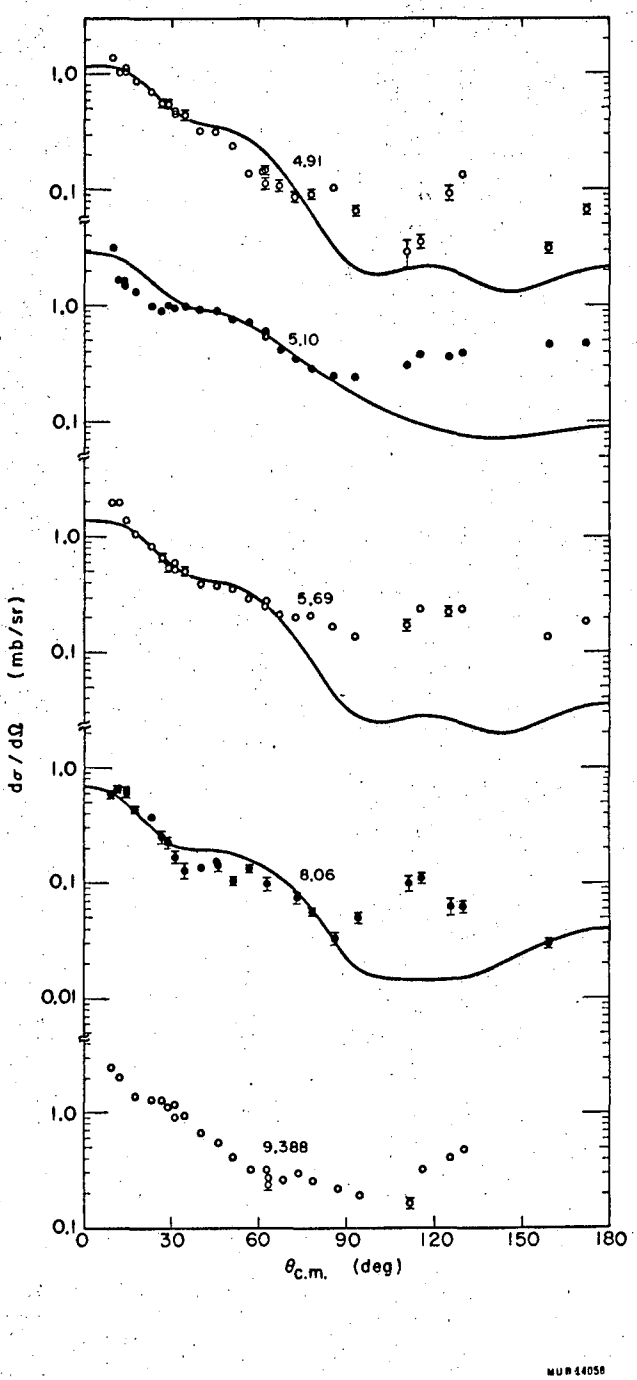

Fig. 16. Proton angular distributions for transitions of predominant L = 1 character. See caption of Fig. 15.

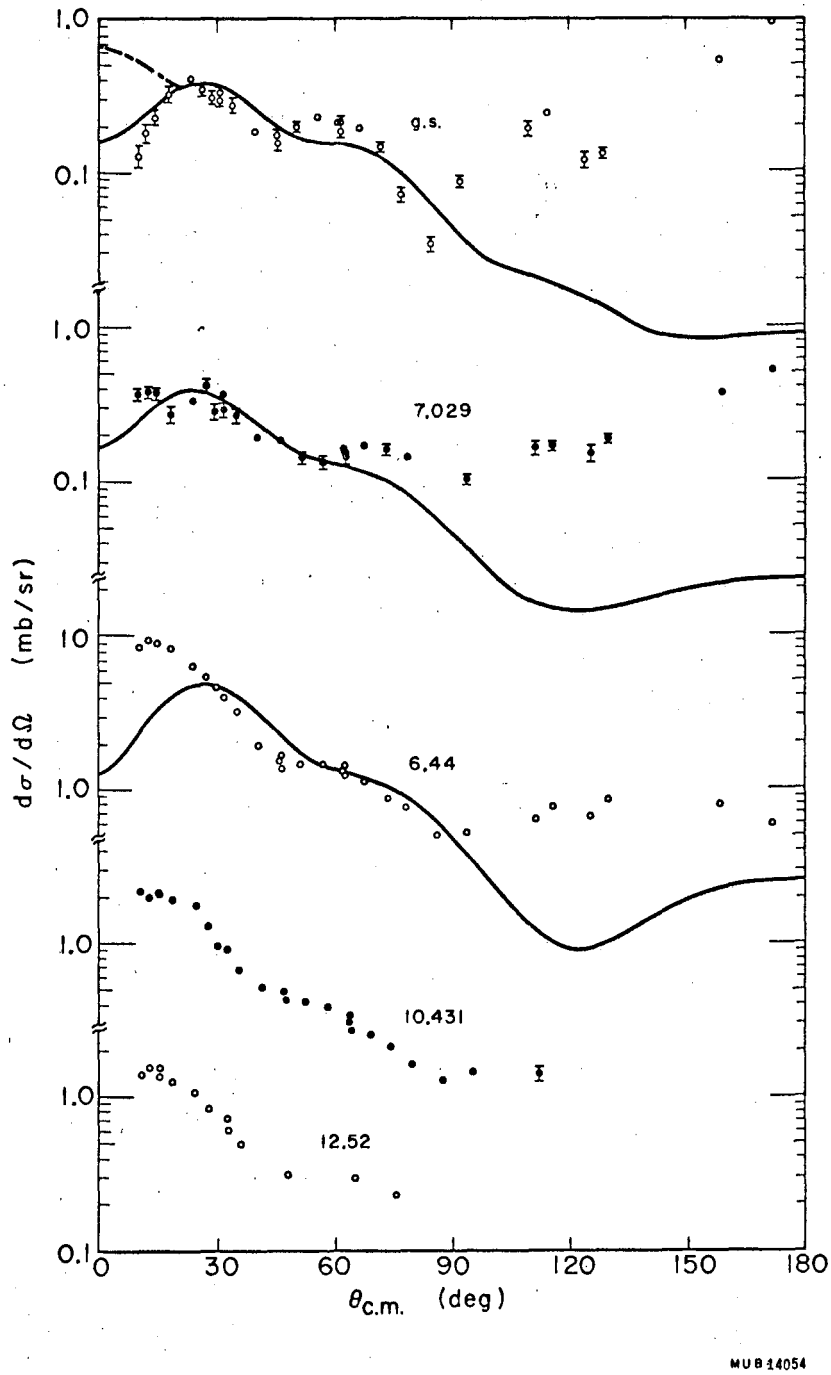

Fig. 17. Proton angular distributions for transitions of predominant L = 2 character. The solid-line curve of the g.s. transition is calculated using the Cohen and Kurath[88] wave functions--the broken-line segment is calculated using True[87] wave functions. See caption of Fig. 15.

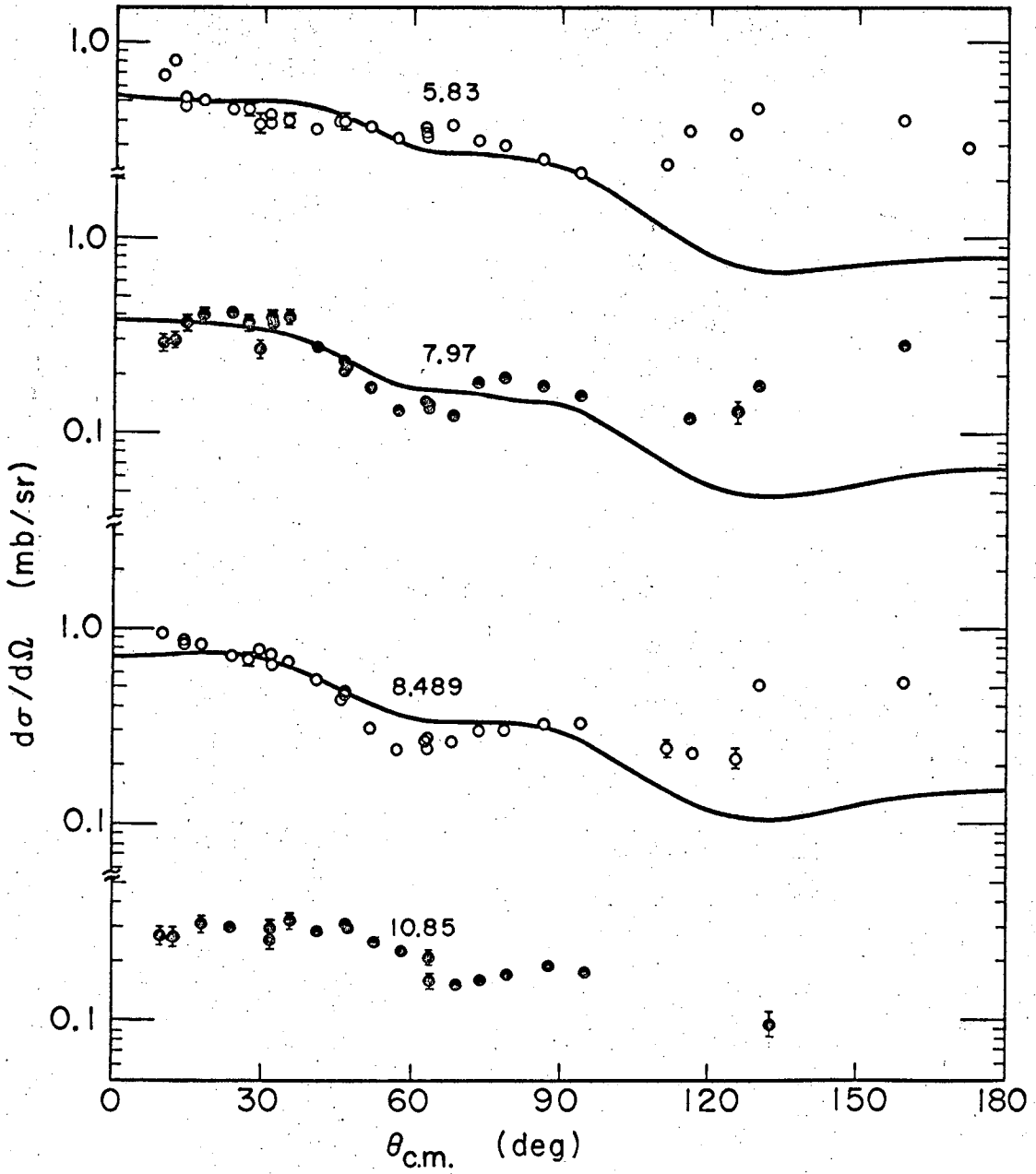

Fig. 18. Proton angular distributions. The first three distributions are of predominant L = 3 character. The fourth distribution may be an L = 4 transition. See caption of Fig. 15.

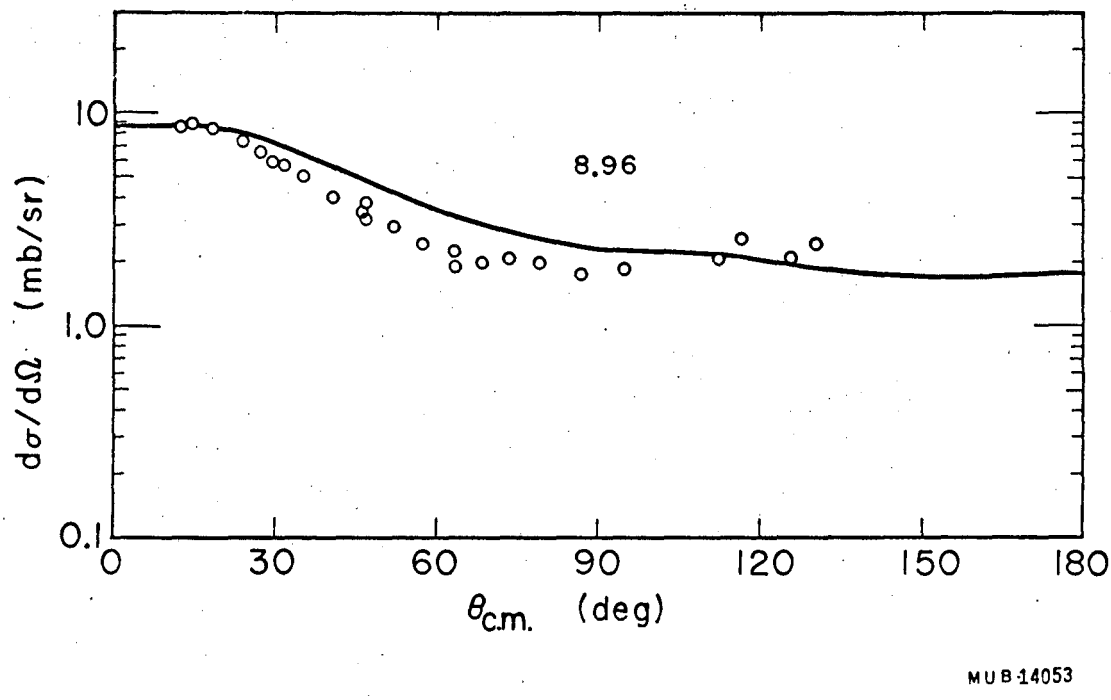

Fig. 19. Proton angular distribution for a composite peak containing transitions to the 8.906-, 8.963- and 8.979-MeV levels of ^{14}N. See caption of Fig. 15.

A group of L = 2 transitions is shown in Fig. 17. Note again the contrast between the transitions to two $(p)^{-2}$ type states and the 6.44-MeV state. The calculated curves agree quite well with the g.s. and 7.019-MeV state angular distributions but the calculation for the 6.44-MeV state does not reproduce its more forward peaking. This may suggest that corrections must be made in the calculations for shell effects.

The ground-state transition is allowed, by selection rules, to have both an L = 0 and an L = 2 component; however, an examination of the angular distribution indicates that very little L = 0 component is present. The solid-line curve is a calculation based upon the wave functions of Cohen and Durath.[88] This calculation reproduces the data very well. The dashed line segment is a calculation based upon the wave functions of True.[87] The forward-rising nature of this latter calculation indicates too large an L = 0 component in the True wave function. The source of this error will be further discussed in connection with other calculations.

A group of L = 3 transitions is shown with DW calculations in Fig. 18. Note the 8.489-MeV level is well fit with an L = 3 type angular-distribution which helps to confirm its assigned configuration.

The angular distribution of Fig. 19 arises from three unresolved levels near 9 MeV excitation in ^{14}N. Calculations for all three of these levels have been made, the contributions of each level have been weighted by $(2J_2 + 1)$ as indicated by Eq. (24), and the values summed to give the DW fit to the data. The 3^- level gave the smallest contribution.

Before a comparison of the relative cross sections can be made, each transition must be properly weighted by factors not considered. The calculation cross section for a level must be multiplied by its $(2J_2 + 1)$ value as indicated in Eq. (24). The factor C_{ST} of Eq. (18) must also be evaluated. The value of the coupling coefficient, as written in Eq. (18), has a value of one for all states in reactions reported in this work. Likewise the value of b_{ST} is $1/\sqrt{2}$ for all transitions. A value of unity for D(S) was found to be necessary. Further discussion of D(S) will follow in Sec. VI-D-1.

Experimental and theoretical relative cross sections integrated between 10° and 70° center of mass are shown in Table VI. The factor F at the bottom of Table VI is a measure of the goodness of fit and is defined as the average value of the greater ratio between experimental relative cross section and calculated relative cross section minus one. For a perfect fit F would be zero.

The calculated relative cross section for four states predicted by Cohen and Kurath[88] and the four values for $(s,d)^2$ states predicted by True[87] are in good agreement with experiment.

Those states in the True[87] calculation which have p character are not in good relative agreement with the experiment. Two cases of disagreement are particularly striking. The experimental ratio of the first excited state to the ground state is 0.8. This ratio is predicted to be 0.7 by the wave functions of Cohen and Kurath.[88] The wave functions of True,[87] on the other hand, predict a ratio 0.2. The disagreement in the calculated relative cross section of the 4.91- and 5.10-MeV levels is also striking.

It seems reasonable to postualte that the failure of the calculations based upon True wave functions of p character is due to the fact that these functions do not account for the $(p3/2)^{-n}$ character of these levels. To test this idea further, several model calculations were carried out for the ground state and the 2.311-MeV state of ^{14}N. Structure factors for these calculations are listed in Table VII. The results of the calculations are shown in Table VIII.

Two experimentally-observable quantities were examined in the model calculations. One is the ratio between the cross sections to the two states and the other is the ratio of the L = 0 to L = 2 amplitudes in the ground-state transition. The ground-state angular distribution is sharply falling at small angles. As seen in the case of the 2.311 MeV transition, an L = 0 angular distribution is strongly forward peaked. From these two observations it is concluded that the L = 0 conttribution to the ground-state transition is small.

It is noted that the Cohen and Kurath wave functions properly account for both of these observables. The calculation in the jj limit gives a poor value for the relative strength of the states. It is

Table VI. Cross section ratios for the reaction $^{12}C(^{3}He,p)^{14}N$ at $E(^{3}He) = 20$ MeV: experiment and theory compared.

Level (MeV)	Major L	Relative Level Cross Sections[a] Experiment	Cohen & Kurath[b]	True[b] (Relative to 6.44 MeV State)	
			(p^2)	(s,d)	$(p^2)+(p)(s,d)$
0.0	2	1.0	1.0		0.7
2.311	0	0.8	0.7		0.2
3.945	0	1.5	1.2		
4.91	1	1.4			0.5
5.10	1	3.5			0.5
5.69	1	1.9			1.1
5.83	3	1.6			1.8
6.21	0	3.0		2.5	
6.44	2	11.3		11.3	
7.029	2	0.9	0.5		
7.97	3	1.0			1.6
8.06	1	0.7			0.5
8.489	3	1.9			0.7[d]
8.617	0	0.7		0.5	
8.71	forbidden				
8.906	3 [c]				
8.963	4 [c]	16.6		10.5	
8.979	2 [c]				
			$F^e = 0.3$	0.3	1.8

[a] Cross sections integrated from 10° to 70° center of mass.

[b] References for wave functions used are as follows: True[87] and Cohen and Kurath.[88]

[c] These three states are unresolved by the experiment.

[d] This level was assumed to be $(p3/2^{-1}, d5/2)_{4-}$ coupled to Cohen and Kurath wave function for ^{12}C.

[e] Goodness of fit parameter defined in the text.

Table VII. Structure factors G_{NLSJT} for the $^{12}C(^{3}He,p)^{14}N$ model calculations.[a]

Wave Function[b]			^{14}N g.s. Level				^{14}N 2.311-MeV Level			
^{14}N	^{12}C	L	N=1	N=2	N=3	N=4	N=1	N=2	N=3	N=4
C & K	C & K	0	-0.012	-0.085			0.075	0.541		
		2	0.417							
True	$(p1/2)^0$	0	0.016	0.112	-0.113	0.007	-0.049	-0.348	0.189	-0.013
		2	-0.560	0.112	-0.004					
$(p1/2)^2$	$(p1/2)^0$	0	-0.019	-0.135			0.056	0.404		
		2	0.602							
$(p1/2)^2$	C & K	0	-0.019	-0.147			0.063	0.453		
		2	0.397							
True	C & K	0	0.016	0.123	-0.113	0.007	-0.056	-0.394	0.189	-0.013
		2	-0.365	0.112	-0.004					
Combined[c]	C & K	0	0.009	0.065	-0.113	0.007	-0.066	-0.475	0.189	-0.013
		2	-0.384	0.112	-0.004					

[a] A ^{3}He size parameter of 0.206 was used.[1] A harmonic-oscillator parameter of 0.32 was used.

[b] C & K designates Cohen and Kurath.[88] True designates True.[87]

[c] True wave function with the C & K wave function replacing the $(p1/2)^2$ configuration.

Table VIII. Model calculations for g.s. $(1^+,0)$ and 2.311-MeV $(0^+,1)$ states of ^{14}N.

^{14}N Wave Function[a] / ^{12}C Wave Function	Experiment	C & K / C & K	True $(p1/2)^0$	$(p1/2)^2$ $(p1/2)^0$	$(p1/2)^2$ C & K	True C & K	Combined[c] C & K
Cross Section (2.311) / Cross Section (g.s.) [b]	0.8	0.7	0.2	0.2	0.5	0.4	0.6
Cross Section (L=0,g.s.) / Cross Section (L=2,g.s.)	small	0.06	0.3	0.07	0.2	0.4	0.3
Cross Section (Relative,g.s.)	-	7.2	32.0	14.8	7.1	22.6	18.8

[a] $\Psi(14,\text{g.s.}) = -0.951\ (p1/2)^2 - 0.217\ (d5/2)^2 + \text{-----}$ (True)[87]

$= 0.975\ (p1/2)^2 - 0.208\ (p1/2)^3 - 0.076\ (p1/2)^4$ (Cohen & Kurath)[88]

$\Psi(14,2.311) = -0.931\ (p1/2)^2 + 0.299\ (d5/2)^2 + \text{-----}$ (True)

$= 0.914\ (p1/2)^2 - 0.405\ (p1/2)^4$ (Cohen & Kurath)

$\Psi(12,\text{g.s.}) = 0.612\ (p1/2)^0 + 0.261\ (p1/2)^2_A + 0.625\ (p1/2)^2_B + 0.255\ (p1/2)^3 + 0.319\ (p1/2)^4$ (Cohen & Kurath)

[b] Cross sections integrated over 10° to 70°.

[c] True wave functions with the C & K wave functions replacing the $(p1/2)^2$ configurations.

important to note that the introduction of the Cohen and Kurath ^{12}C wave function makes a big improvement in the relative strengths of the two states although agreement with experiment is still poor. This improvement is not too surprising when it is noted that the intermediate-coupling wave function[88] of ^{12}C is only 40% closed p3/2 core.

It is seen in Table VIII that only 10% of the g.s. and 15% of the first excited state are of components other than $(p1/2)^2$ and yet the consideration of this small admixture makes the pronounced change seen between using the Cohen and Kurath $(p1/2)^2$ wave functions for ^{14}N with the Cohen and Kurath wave function for ^{12}C. These calculations entirely within the p shell are to be considered quite reliable. This is a case where the coherent and enhancing effects of two-nucleon transfer make the transitions sensitive to the minor components of the wave function.

In all cases were the True wave functions are introduced no agreement with experiment is found. It will be shown in Sec. VI-D that in this particular instance, calculations in two different shells are not properly treated. It cannot, therefore, be concluded that the $(s,d)^2$ admixtures predicted by True are too large. It can be said that the p3/2 hole character in these wave functions is very important and may account for some of the failure in the case of True's p-type states.

Two other important observations should be made concerning the groups of levels which are in good relative agreement. First, as the excitation energy increases the relative agreement becomes poorer in both groups. Second, there is a large discrepancy in the relative cross section between the group of states calculated by Cohen and Kurath[88] and the group of $(s,d)^2$ states calculated by True.[87] The ratio of the 6.44-MeV state to the ground state is 77.2 nearly a factor 7 too high. These problems are most interesting and will be treated in Sec. VI-D-2.

C. Calculations for the Reaction $^{16}O(^3He,p)^{18}F$ at $E(^3He) = 20$ MeV

1. ^{18}F Wave Functions and Calculation of Structure Factors

Four sets of wave functions for the energy levels of ^{18}F were used for calculations and compared to the experiment. All four sets assume a closed ^{16}O core with two particles in shell-model states. One set was calculated by Kuo and Brown.[120] These workers used the Hamada-Johnston (HJ)[151] potential to construct an effective two-nucleon interaction. This potential has been used successfully to fit free nucleon-nucleon scattering up to about 350 MeV and the deuteron properties. The effective interaction was constructed by allowing the two particles to interact via the HJ potential and by adding an additional interaction of one particle upon the other through polarization of the core. Only single-particle states of the (s,d) shell were included in the calculation.

Arima et al.[152,153] have constructed an effective interaction which includes central, tensor and spin-orbit potentials. Their calculation includes (s,d) shell, single-particle states only.

Redlich[154] has kindly made available two sets of calculations based upon a simple, central potential. The methods used for the calculation are similar to those reported[155] for ^{210}Pb calculations. One set of calculations (Redlich), using a triplet-even force 1.5 times the singlet-even force, included only (s,d) shell, single-particle states. The other set (Redlich (E)), using a triplet-even force 1.25 times the singlet-even force, included all possible delta-two excitations from the (s,d) shell as well (A delta-two excitation is the excitation of one particle by $2\hbar\omega$ energy units or the excitation of two particles, each by $1\hbar\omega$ energy unit).

Each of these calculations employed harmonic-oscillator radial wave functions. The oscillator parameters used in these nuclear structure calculations were also used in the reaction calculations under discussion. The respective oscillator parameters are indicated in Table IX.

The energy levels of ^{18}F and ^{18}O together with the four sets of calculated energy levels are shown in Fig. 20. The ground state of ^{18}O has been normalized to the 0^+ $T = 1$ state of ^{18}F and the ground state of the two Redlich calculations have been normalized to the ^{18}F ground state.

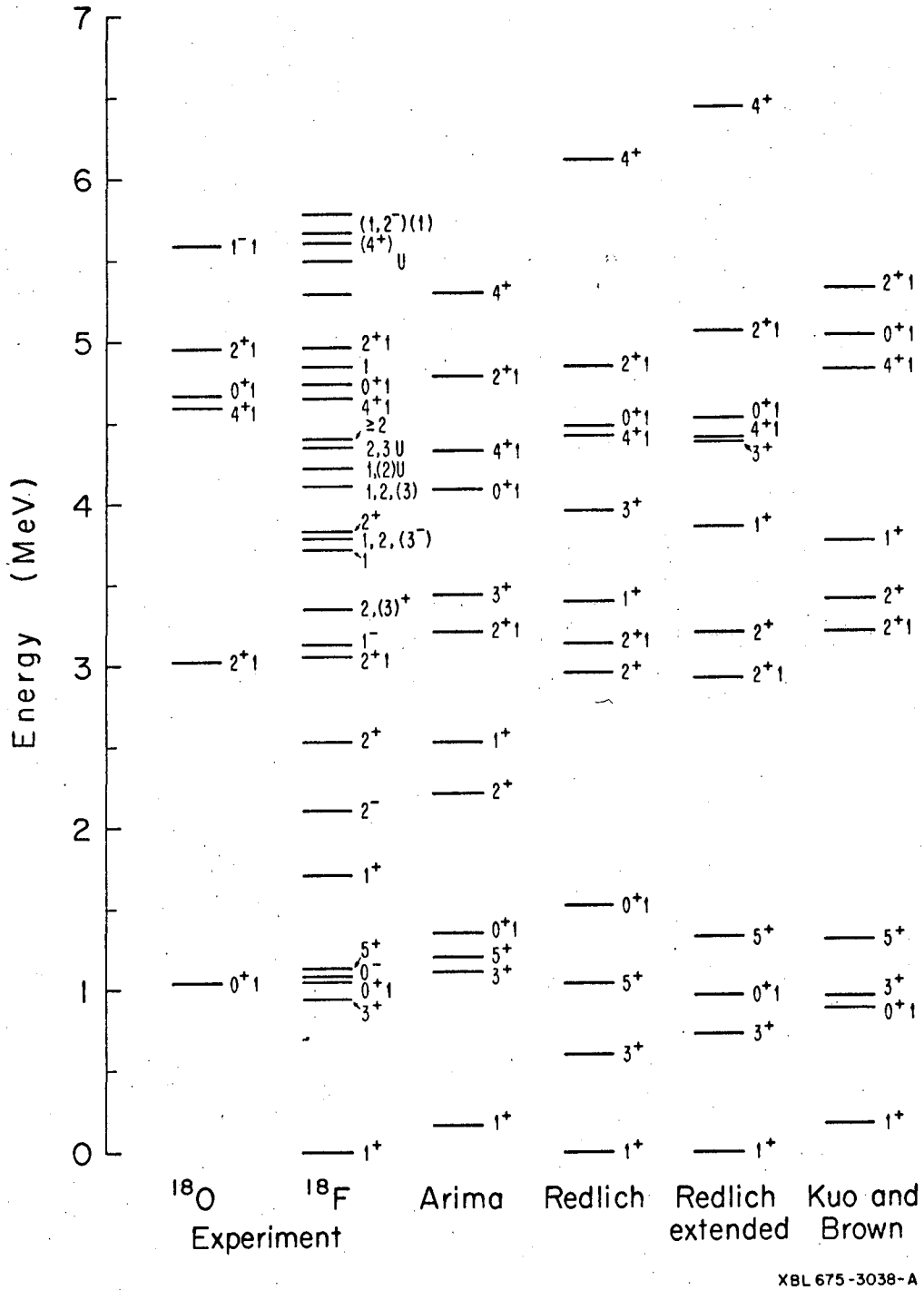

Fig. 20. Energy level diagram of ^{18}F with a comparison to levels of ^{18}O and to calculations by Arima,[152,153] and Kuo and Brown.[120] See also references of Table II.

The positions of the ground states for the other two calculations, relative to the ^{18}F ground state, reflect their calculated binding energy relative to the experimental binding energy of ^{18}F.

Note that for three of the sets no predicted levels fall between 1.5 to 2.5 MeV excitation. Arima,[152] by means of the tensor force, has lowered a 2^+ and a 1^+ level into this region.

Zamick,[156] using matrix elements evaluated with the HJ potential, has been able to account for the very long life time of ^{14}C. Using the Kuo and Brown[120] matrix elements and wave functions for ^{18}Ne and ^{18}F he has also accounted for the fast beta transition between ^{18}Ne and ^{18}F. Brown and Green[118] have been able to predict the known transitions in ^{18}O by using the HJ potential for mixing deformed states with the Kuo and Brown[120] single-particle states. It is pleasing to see that a free nucleon-nucleon potential can be so successfully used for calculations in finite nuclei.

The four sets of calculations discussed above provide two-particle wave functions. The calculation of two-nucleon transfer structure factors for such wave functions was discussed in connection with True[87] wave functions for ^{14}N and need not be further discussed here. Table IX contains structure factors for a number of the states of ^{18}F.

An examination of the factors of Table IX reveals several interesting facts. For each ^{18}F level one value of G_{NLSJT} is much larger than the rest. In cases where there are two states of the same $J^\pi T$, the dominant structure factor of the second state is considerably smaller than the factor of the state of lowest excitation. These phenomena arise from the correlations introduced in configuration mixing by the residual interaction. It is further noted that although these sets of wave functions have been calculated using very different interaction potentials, the dominant structure factors are nearly identical. Redlich[154] has pointed out that this similarity in the wave functions is to be expected when working entirely within the (s,d) shell. He further states, however, that admixtures of higher order components into the wave functions may be quite different for different potentials and that these admixtures may be important in obtaining calculated quantities that are in agreement with experimental quantities.

Table IX. Structure factors G_{NLSJT} for the $^{16}O(^{3}He,p)^{18}F$ reaction.[a]

Level[b] J^{π} Tx	L	Arima[c] ν = 0.362			Kuo and Brown[c] ν = 0.339		
		N=1	N=2	N=3	N=1	N=2	N=3
1^{+} 0a	0	-0.023	-0.108	-0.556	0.015	0.090	0.556
	2	-0.000	-0.020		0.008	0.097	
b	0	-0.008	0.087	-0.199	-0.005	0.081	-0.179
	2	-0.024	-0.012		-0.018	-0.119	
2^{+} 0a	2	0.066	0.560		0.056	0.563	
3^{+} 0a	2	0.072	0.583		0.058	0.592	
	4	0.005			0.016		
b	2	-0.052	0.108				
	4	0.004					
4^{+} 0a	4	0.598					
5^{+} 0a	4	0.598			0.603		
0^{+} 1a	0	0.023	0.113	0.544	0.014	0.103	0.499
b	0	0.009	-0.099	0.218	0.009	-0.063	0.310
2^{+} 1a	2	0.076	0.518	0.060	0.484		
b	2	-0.030	0.219	-0.019	0.238		
4^{+} 1a	4	-0.444		0.419			

Table IX. (continued)

Level[b] J^π Tx	L	Redlich[c] $\nu = 0.350$			Redlich(E)[c] $\nu = 0.339$				
		N=1	N=2	N=3	N=1	N=2	N=3	N=4	N=5
1^+ 0a	0	-0.019	-0.095	-0.548	-0.014	-0.081	-0.502	0.068	-0.010
	2	0.012	0.056		0.009	0.045	-0.006	-0.001	
b	0	-0.008	0.074	-0.225	-0.006	0.062	-0.217	0.015	-0.000
	2	-0.027	-0.157		-0.025	-0.160	0.022	-0.001	
2^+ 0a	2	0.050	0.548		-0.043	-0.511	0.078	-0.008	
3^+ 0a	2	-0.066	-0.583		0.055	0.535	-0.086	0.015	
	4	0.027			-0.024	0.004	0.000		
b	2	-0.043	0.127		0.037	-0.127	0.014	-0.003	
	4	0.090			0.086	0.007	-0.000		
4^+ 0a	4	0.601			0.564	-0.086	0.010		
5^+ 0a	4	0.601			-0.563	0.082	-0.016		
0^+ 1a	0	0.017	0.105	0.499	-0.013	-0.089	-0.480	0.050	-0.005
b	0	-0.010	0.073	-0.292	0.007	-0.067	0.266	-0.017	0.000
2^+ 1a	2	-0.065	-0.508		0.056	0.493	-0.057	0.007	
b	2	-0.028	0.190		0.027	-0.166	0.015	-0.002	
4^+ 1a	4	-0.410			0.413	-0.039	0.005		

[a] A ^{3}He size parameter of 0.206 was used.[1]

[b] a,b refer to first and second $J^\pi T$ theoretical level respectively.

[c] References for the wave functions used are as follows: Arima,[152,153] Kuo and Brown,[120] Redlich.[154,155]

2. Optical-Model Parameters

Optical-model parameters used in calculations for the $^{16}O(^{3}He,p)^{18}F$ reaction are shown in Table X. Sets 5 and 7 were taken from the paper of Hiebert et al.[33] who used them successfully for (d,^{3}He) calculations. Set 6 is an average of these two. Sets 8 and 10 were obtained by fitting the data of Artemov et al.[157] Set 9 was obtained by taking the average of sets 8 and 10.

Potential set 11 for proton scattering on mass 18 was calculated from the systematic potentials of Perey[148] and is typical of potentials used in the exit channel.

A potential constructed from single-nucleon potentials as was done for the ^{12}C system discussed was used unsuccessfully in an attempt to fit the data of the $^{16}O(^{3}He,p)^{18}F$ reaction.

3. Distorted-Wave Calculation

Distorted-wave calculations for the reaction $^{16}O(t,p)^{18}O$ have been made by Glover et al.[37,158] at E(t) = 10 MeV. Angular distributions for the ground state and first two excited states were calculated. Total cross sections for the ground state and the first excited state were in good relative agreement with experimental values. Henley and Yu[10] have made calculations for the $^{16}O(^{3}He,n)^{18}Ne$ reaction at E(^{3}He) = 20 MeV for the ground state and two excited states of ^{18}Ne. These calculations are not in agreement with experimental values.

Pühlhofer and Bock[5,83] have made calculations for the $^{16}O(^{3}He,p)^{18}F$ reaction at E(^{3}He) = 18 MeV. They calculated angular distributions and total relative cross sections to the ground state and six excited states of ^{18}F below 4 MeV excitation. They used the wave functions of Inoue et al.[159] and Arima.[152,153] Their results are in agreement with those reported here.

The curves in Figs. 21-23 are DW fits to the $^{16}O(^{3}He,p)^{18}F$ data for E(^{3}He) = 20 MeV; curves are individually normalized to the data. The solid curves use optical potential set 9 for the ^{3}He particle and the dashed curves use set 6. As can be observed the angular distributions are best fit by using parameter set 9.

Table X. Optical-model parameters for the $^{16}O(^{3}He,p)^{18}F$ reaction.

Particle	Target	Set	V (MeV)	R_o (F)	A_o (F)	W (MeV)	W_d (MeV)	R_i (F)	B (F)	R_c (F)
^{3}He(10.5 MeV)	^{16}O	5	170	1.03	0.893	20.0		2.06	0.510	1.40
^{3}He(20 MeV)	(average)	6	180	1.08	0.784	15.6		2.12	0.468	1.40
^{3}He(29 MeV)	^{16}O	7	190	1.14	0.675	11.2		2.17	0.426	1.40
^{3}He(16.6 MeV)	^{16}O	8	220	1.01	0.663	5.3		2.21	0.803	1.40
^{3}He(20 MeV)	(average)	9	220	1.11	0.653	7.1		2.11	0.815	1.40
^{3}He(25.8 MeV)	^{16}O	10	220	1.29	0.633	10.4		1.93	0.837	1.40
p (22 MeV)	^{18}X	11	42.6	1.25	0.65		8.4	1.25	0.47	1.25

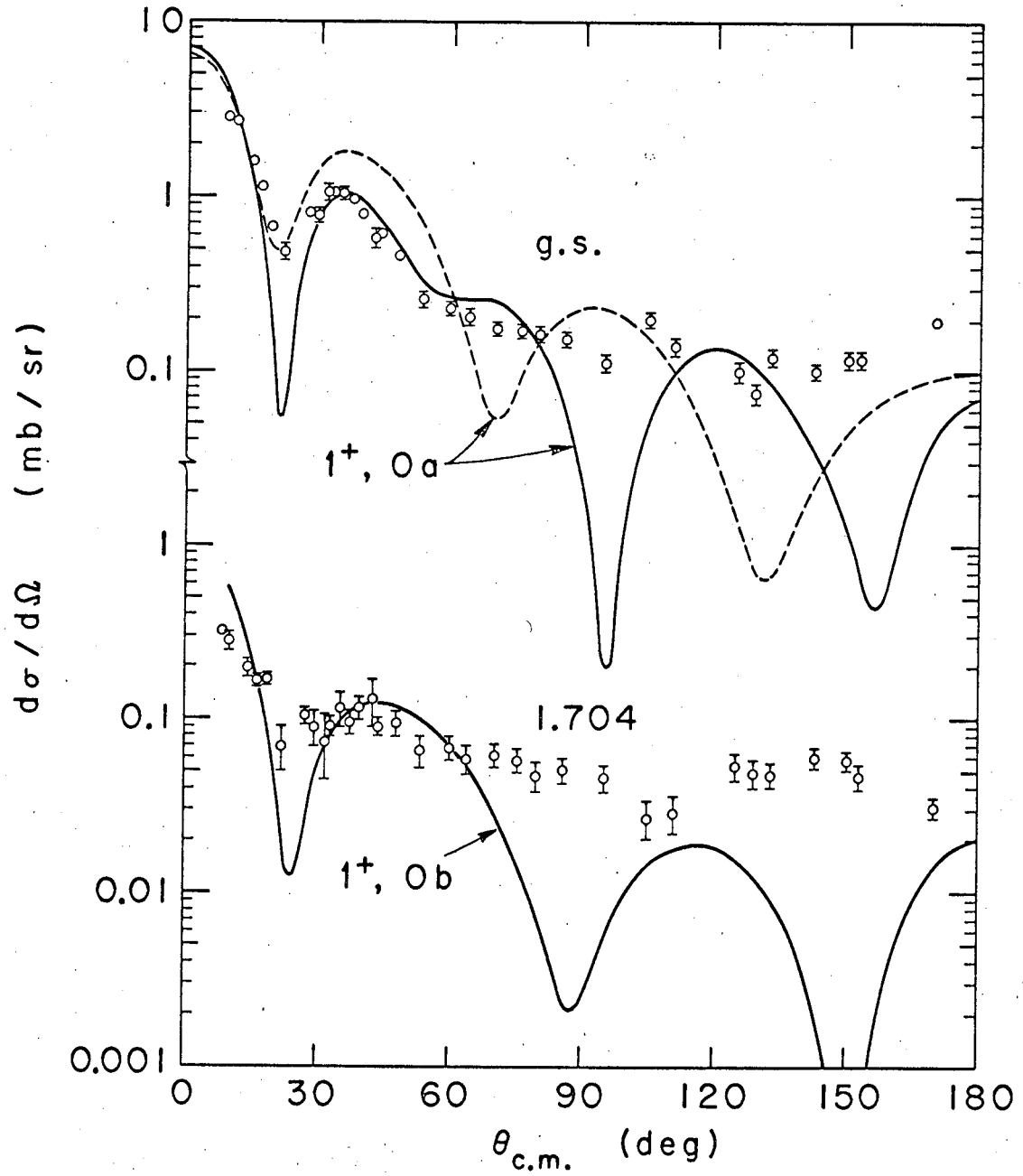

XBL675-3041

Fig. 21. Proton angular distributions for the $^{16}O(^{3}He,p)^{18}F$ reaction at $E(^{3}He)$ = 19.8 MeV. The g.s. transition is of predominant L = 0 character and the 1.704 transition may have L = 0 character. The solid-line curves are DW calculations using ^{3}He optical-model potential set 9 and the dashed-line curve is a DW calculation using set 6. Statistical errors are indicated by error bars or are smaller than the point symbols.

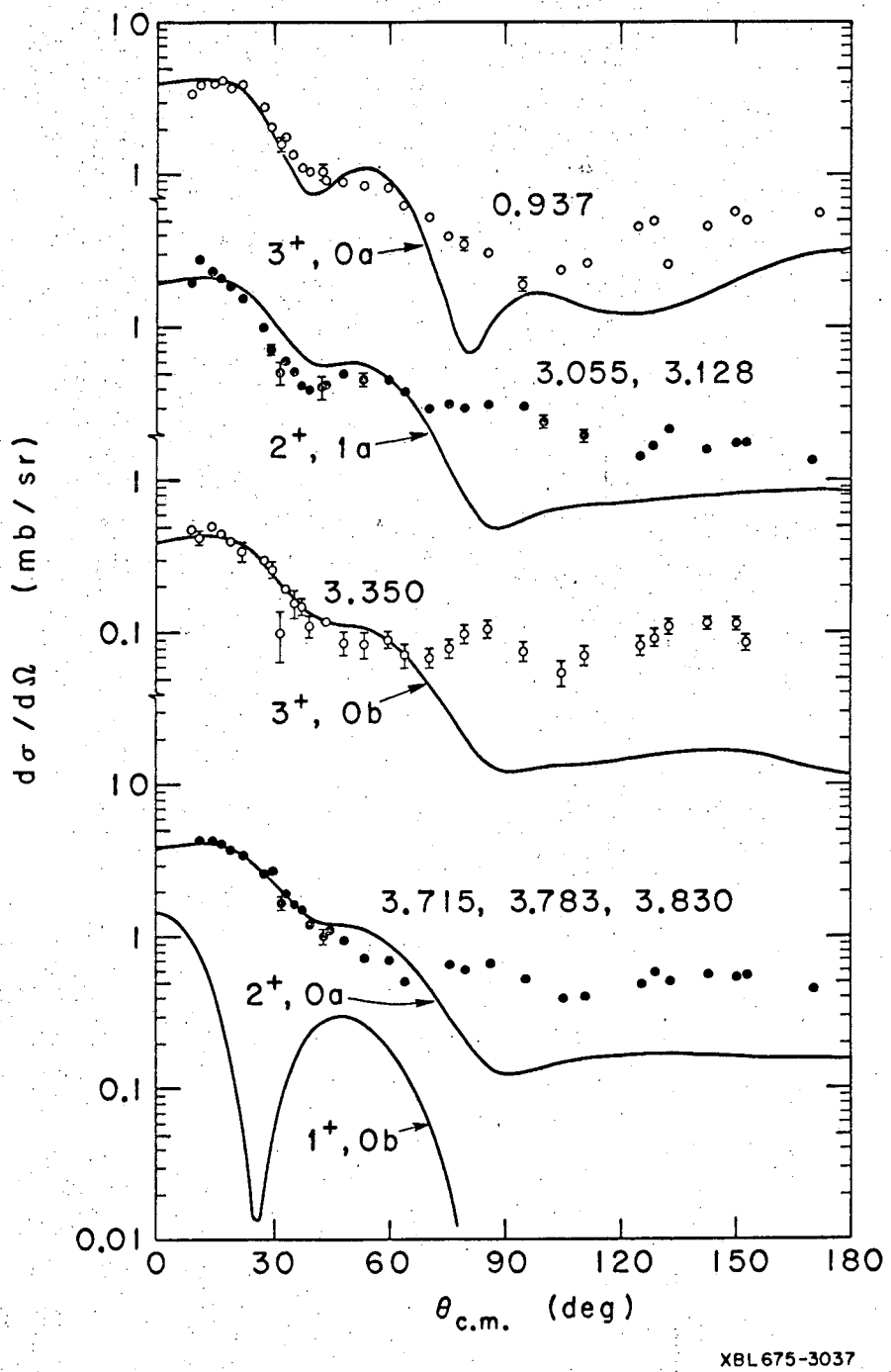

Fig. 22. Proton angular distributions for transitions of predominant L = 2 character. The curves labeled 2^+,0a and 1^+,0b are in proper relative proportion to each other. See caption of Fig. 21.

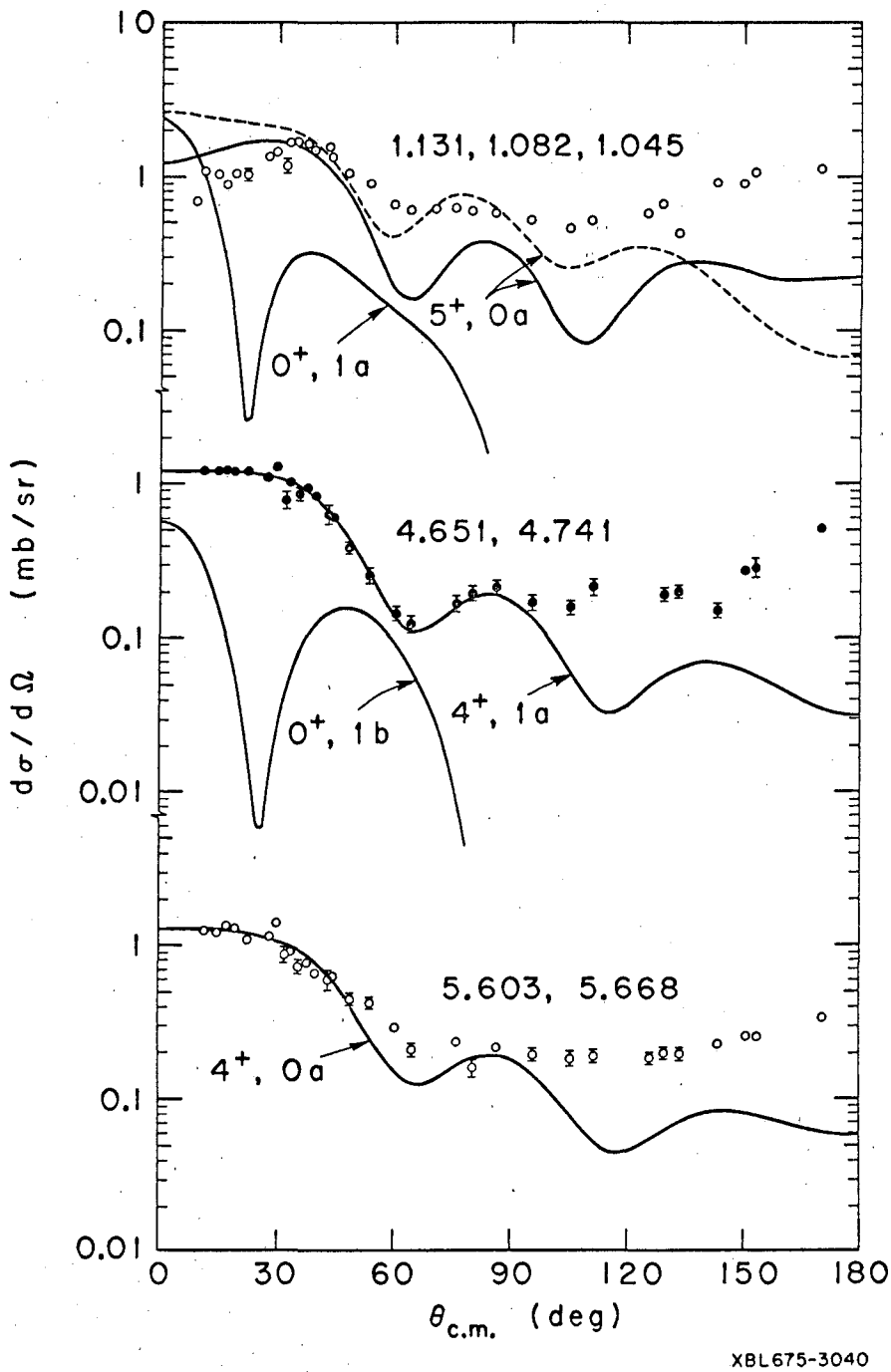

Fig. 23. Proton angular distributions for transitions of predominant L = 4 character. The pairs of curves for the first two transitions are in proper relative proportion to each other. See caption of Fig. 21.

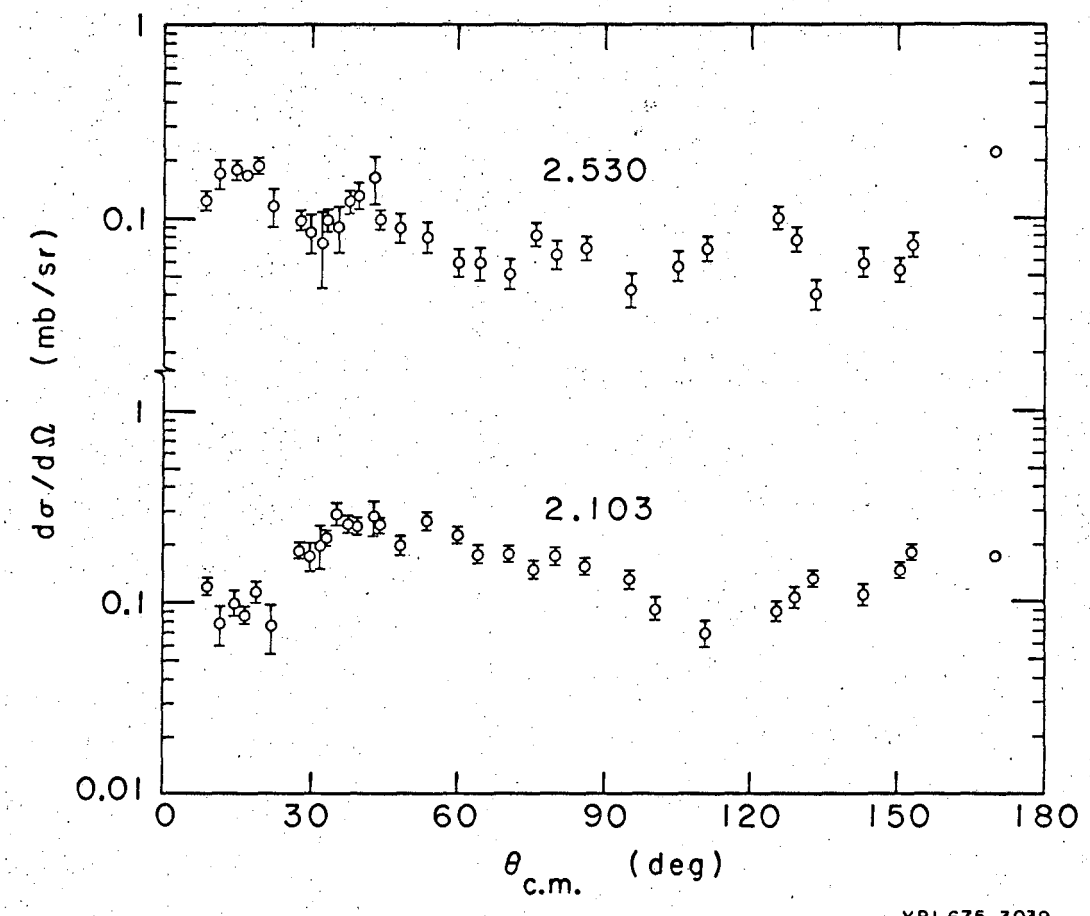

Fig. 24. Proton angular distributions for transitions of predominant particle-hole character. See caption of Fig. 21.

Experimental and calculated relative cross sections are listed in Table XI. In general, good agreement with experiment is found. If the level 1^+0b is assumed to be the 1.7-MeV level the calculated cross section and angular distribution both appear to be in agreement. However, it should be noted that the cross section is small and this is also to be expected for a particle-hole configuration. In Sec. V it was suggested that the level could be mixed in configuration with both particle-hole and $(s,d)^2$ character. The 1^+0b level could also be associated with the 3.725-MeV state. A small cross section for this state is in agreement with the experiment. This excitation energy is in better agreement with the predicted energy of the 1^+0b state.

For purposes of comparison, calculations were made for the 2^+0a state at both 2.524- and 3.838-MeV excitation. The 2^+0a must be asigned to the 3.838-MeV level on the basis of relative cross section and on the basis of angular distribution.

The relative cross section and L = 2 angular distribution of the 3^+0b agree well with experimental observations for the 3.358-MeV state. The 4.108-MeV state is also a possible choice for the 3^+0b assignment even though its cross section is nearly twice the predicted value, as the 4.218-MeV may be making a contribution to the cross section reported. The 4.108-MeV level does not have an L = 2 angular distribution, but this may also be affected by the 4.218-MeV level.

The excellent agreement in the relative cross sections of the 4^+a, 0^+b, and 2^+b T = 1 states and the agreement in the angular distribution for the 4^+a and 0^+b states confirms the suggested assignment[122] of these levels.

The predicted cross section to the 5.594-MeV state is not in as good agreement with experiment as predictions to other levels, nevertheless, a relatively strong level is predicted which agrees qualitatively with the observation. This fact, together with the very characteristic L-4 angular distribution, make an argument for a 4^+ T = 0 assignment to this level.

The relative cross sections of two levels seem to deviate from the experimental values by more than would be expected on the basis of the relative errors in the experimental cross sections. The composite

Table XI. Comparison of relative cross sections for the reaction $^{16}O(^{3}He,p)^{18}F$ at $E(^{3}He)$ = 20 MeV.

Levels				Relative Level Cross Sections[a]				
Experiment		Theory[b]	Experiment	Arima[d]	Arima[d]	Kuo & Brown[d]	Redlich[d]	Redlich(E)[d]
(MeV)	J^{π} T	J^{π} Tx		V^{c} = 180	220	220	220	220
0.0	1^{+} 0	1^{+} 0a	1.0	1.0	0.8	0.8	0.8	0.8
0.9371	3^{+} 0	3^{+} 0a	2.5	2.5	2.5	2.5	2.5	3.2
1.0417	0^{+} 1	0^{+} 1a						
1.0807	0^{-} 0		2.0	1.4	1.6	1.4	1.5	2.0
1.1310	5^{+} 0	5^{+} 0a						
1.7005	1^{+} 0	1^{+} 0b	0.2	0.2	0.2	0.2	0.3	0.3
2.1008	2^{-} 0		0.4					
2.5235	2^{+} 0	2^{+} 0a	0.2	1.9	2.0	1.9	2.0	2.1
3.0603	2^{+} 1	2^{+} 1a	1.3	1.7	1.9	1.5	1.8	1.7
3.1339	1^{-} 0							
3.3581	$2(3)^{+}$ 0	3^{+} 0b	0.3	0.2	0.2		0.2	0.2
3.7248	1 0	1^{+} 0b						
3.790	$1,2,(3^{-})$ 0		2.6	2.5	2.8	2.6	2.8	2.6
3.8385	2^{+} 0	2^{+} 0a						
4.108	1,2,(3) 0		0.4					
4.218	1,(2)							
4.350	2,3		0.8					
4.400	≥ 2 0							
4.651	4^{+} 1	4^{+} 1a	1.0	0.9	1.0	0.9	0.9	0.9
4.741	0^{+} 1	0^{+} 1b						

Table XI. (continued)

Levels				Relative Level Cross Sections[a]				
Experiment		Theory[b]	Experiment	Arima[d]	Arima[d]	Kuo & Brown[d]	Redlich[d]	Redlich(E)[d]
(MeV)	J^π T	J^π Tx		V^c = 180	220	220	220	220
4.844	1 0		≈ 0.6					
4.964	2^+ 1	2^+ 1b	≈ 0.3	0.4	0.5	0.5	0.4	0.2
5.295	0		0.2					
5.502								
5.594	$(4^+)0$	4^+ 0a	1.1	1.6	1.8		1.8	2.0
5.662	$(1,2^-)(1)$							
				F^e = 0.32	0.36	0.27	0.32	0.25

[a] Cross sections integrated from 10° to 82° center of mass. The theoretical cross sections in each column are in proper relative proportion to each other, but have been arbitrarily normalized.

[b] a,b refer to the 1st and 2nd J^πt theoretical level respectively.

[c] V = real well depth of the ^{3}He optical model potential.

[d] Wave function references are as follows: Arima[152,153] Kuo and Brown[120] and Redlich.[154,155]

[e] Goodness of fit parameter defined in text. Calculations for 2.524-MeV level not included.

peak at about 1 MeV excitation energy has a low predicted value for three of the wave function sets. The predicted cross section of the 3.060-MeV level is too large in all four cases.

A possible explanation for these observed errors may be that no account has been taken of the particle-hole character of either ^{16}O or ^{18}O. In the case of the ^{12}C - ^{14}N system such configurations were found to be very important. In Sec. V-C it was pointed out that the states of mass 18 nuclei have significant amounts of particle-hole components. Brown and Green[114] have predicted 22% 2h-2p and 2% 4h-4p character in the ^{16}O ground state. The $^{16}O(d,^3He)^{15}N$ data of Hiebert et al.[33] is in agreement with these predictions.

A few comments concerning the wave functions used in these calculations are in order. It appears that the calculations of Arima et al.[152,153] predict the 2^+a T = 0 level at too low an excitation energy. Arima[152] has suggested that this may mean the tensor force, which lowers this state, is too strong or that a stronger spin-orbit force may be needed to raise the state to higher excitation. In this connection, it is interesting to note that the potential used by Kuo and Brown also included tensor and spin-orbit forces but gives a better excitation energy for the 2^+a T = 0 level.

The higher configurations included in the wave functions of the Redlich(E) calculation do not improve the fit in general. This may indicate that such higher configurations do not contribute to low-lying levels of ^{18}F, or as Redlich[154] has suggested, that the simple potential used does not properly mix these configurations.

It appears significant that the Kuo and Brown[120] calculations, using the HJ free-nucleon potential, compare so favorably with other shell model calculations.

It should also be pointed out that the relative cross sections do not show an increasing disagreement with increasing excitation energy as was seen in the ^{12}C - ^{14}N system.

D. Spin-Dependent Two-Nucleon Force and Model Calculations

1. Spin-Dependent Two-Nucleon Force

If the interaction potential $V_{bx}(\rho)$ (Eq. (8)) is a central force a factor D(S) (Eq. (17)), which accounts for the difference in the singlet and triplet nucleon-nucleon interaction, appears in the cross section expression. If the singlet and triplet interactions are assumed equal, D(S) is unity for both S = 0 and S = 1 (S is the intrinsic spin transferred by the pair of nucleons). Consideration of the free nucleon-nucleon interaction and of effective interactions used in nuclear structure calculations, however, shows that the singlet and triplet forces are not the same. It is to be expected, then, that a spin dependent interaction should be used in reaction calculations

Fleming et al.[15] have made calculations for the (p,t) and ($p,^3He$) reactions on ^{15}N and on ^{16}O. They have found that a spin dependent force can be used to obtain an improvement in calculated relative cross sections in comparison to experimental relative cross sections. Let R(S) be defined as follows:

$$R(S) = |D(1)/D(0)|^2 \qquad (54)$$

If these workers use an $R(S) \approx 0.33$ they obtain agreement for the relative cross sections in the reactions on ^{16}O and an improved agreement in the reactions on ^{15}N. In the latter case, however, some large discrepancies still exist.

As mentioned in Sec. II-B, Hardy and Towner[16] have evaluated R(S) for several potentials used as effective interactions in nuclear-structure calculations. They obtain values ranging from 0.4 to 0.6.

Furthermore, they evaluate R(S) experimentally for the reaction $^{12}C(^3He,p)^{14}N$ using the ground state and first two excited states of ^{14}N. The cross section data shown in Table I were used in their evaluation. They assumed that only one value of B^M_{NL} contributed to the cross section for each L value. They assumed the ^{12}C ground state to be a pure wave function in the L-S limit, that is a $^{11}S[44]$ state. They used ^{14}N wave functions from four different calculations and found R(S) to vary from 0.38 to 0.56. In particular, they used the Cohen and Kurath[88] ^{14}N wave functions and found R(S) to be 0.52.

Using the method of Hardy and Towner[16] for finding R(S) and using the Cohen and Kurath[88] structure factors of Table IV R(S) was found to be 1.14. The only difference between this and the calculation above was in the ^{12}C ground state wave function. This determination used the Cohen and Kurath[88] wave function for ^{12}C. Using the data of Rivet[4] at $E(^3He)$ = 30 MeV the value of R(S) was found to be 0.78.

It should further be noted that no spin-dependent force was found necessary in the $^{16}O(^3He,p)^{18}F$ calculations. Pühlhofer and Bock[5] independently made calculations for this same system and likewise found no need for a spin-dependent force.

Several observations may be made concerning the above calculations. Consideration of the calculations of Hardy and Towner[16] and of those of this work show that a determination of the strength of the spin-dependent force is dependent upon the assumed wave functions for the states involved. Since invoking a spin-dependent force is not able to bring complete agreement in the $^{15}N(p,t)$ and ^3He) work of Fleming et al.[15] other effects that they enumerate must also be significant and must be considered in order to evaluate the strength of the spin-dependent force.

Glendenning[48] has pointed out that the variation in R(S) between the calculations for $^{12}C(^3He,p)^{14}N$ at 20 MeV and 30 MeV ^3He may be due to the use of improper nuclear wave functions or to the use of an improper bound-state wave function. This latter effect may be due to the method of calculation which neglects the contributions of the B^M_{12} terms.

In summary, although a spin-depdnent force is to be expected the contribution of the force cannot be determined with certainty until wave functions, known to be correct, are used and until other contributing effects are understood.

2. Model Calculations

Model calculations in this section will demonstrate a strong relationship between the optical-model distorted waves and the bound-state wave function and will show the total cross-section trends for the calcultions used in this work.

In their calculations on the $^{16}O(^{3}He,p)^{18}F$ reaction. Pühlhofer and Bock[5,83] used a WS potential well for the bound-state wave function with parameters of R_o = 1.25F and A = 0.65F which are the real-well, single-nucleon parameters of Perey.[148] They use the following set of optical-model parameters for generation of the ^{3}He distorted wave: V = 140.9 MeV, W_d = 6.5 MeV, R_o = 1.22F, A = 0.731F, R_1 = 1.24 F, B = 0.814F, and R_C = 1.3F where W_d is the potential for the surface derivative term (see Eqs. (49) to (53)). As mentioned before, calculations in this work were made using HO (with matched tail) wave functions for the bound state.

Three bound-state radial wave functions are compared in Fig. 25. A quantity proportional to $|u(r)|$ is plotted vs. radius. Each function is arbitrarily normalized. The two functions just discussed are shown. A WS function with R_o = 0.9F and A = 0.9F is also shown. These values are the real well geometry parameters obtained by Satchler[160] for deuteron elastic scattering on ^{12}C. It is interesting to note that this latter function is nearly identical to the HO inside the nucleus and to the other WS outside the nucleus. The decay of the WS and the HO beyond the nuclear surface differ in relative magnitude but are equal in slope. Broglia and Riedel[46] found that the WS function decayed faster than the HO function in a Pb nucleus and criticized the WS for this behavior.

Model calculations were made for an L = 0 transition at E_x = 0 using the ^{3}He potential of Pühlhofer and Bock given above. Their proton potential was also used but the calculations were not significantly changed if the Perey[148] potential was used. Calculations were made for the three bound-state wave functions discussed. The results are shown in Fig. 26. The calculation using the R_o = 1.25F WS well gives a reasonable fit to the ^{18}F ground state angular distribution at both 18 and 20 MeV ^{3}He. The other two calculations give no fit at all. These calculations demonstrate the sensitive relationship which can exist between the distorted waves and the bound-state wave function..

Model calculations for L = 0 and L = 2 transitions to ^{18}F at E_x = 0, made with potentials 9 and 11 from Table X, are shown in Fig. 27. The R_o = 0.9F WS function was used in the calculations but it was found that very little change was made if the R_o = 1.25F WS function was used.

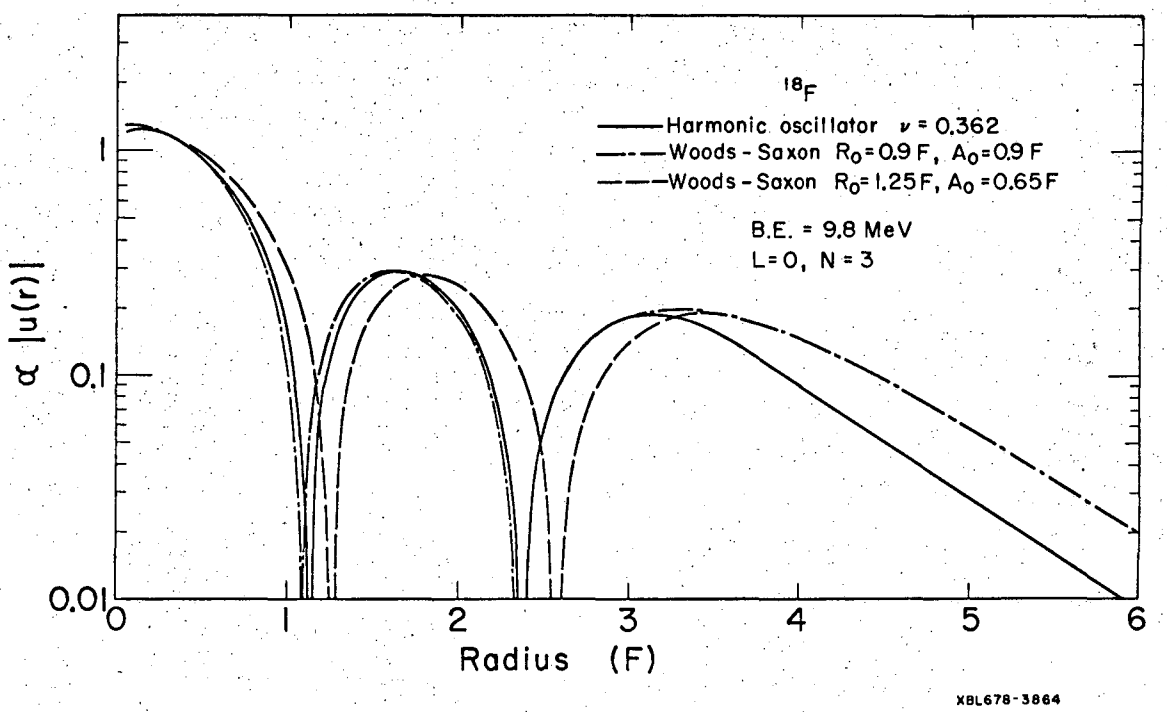

Fig. 25. Bound-state radial wave functions.

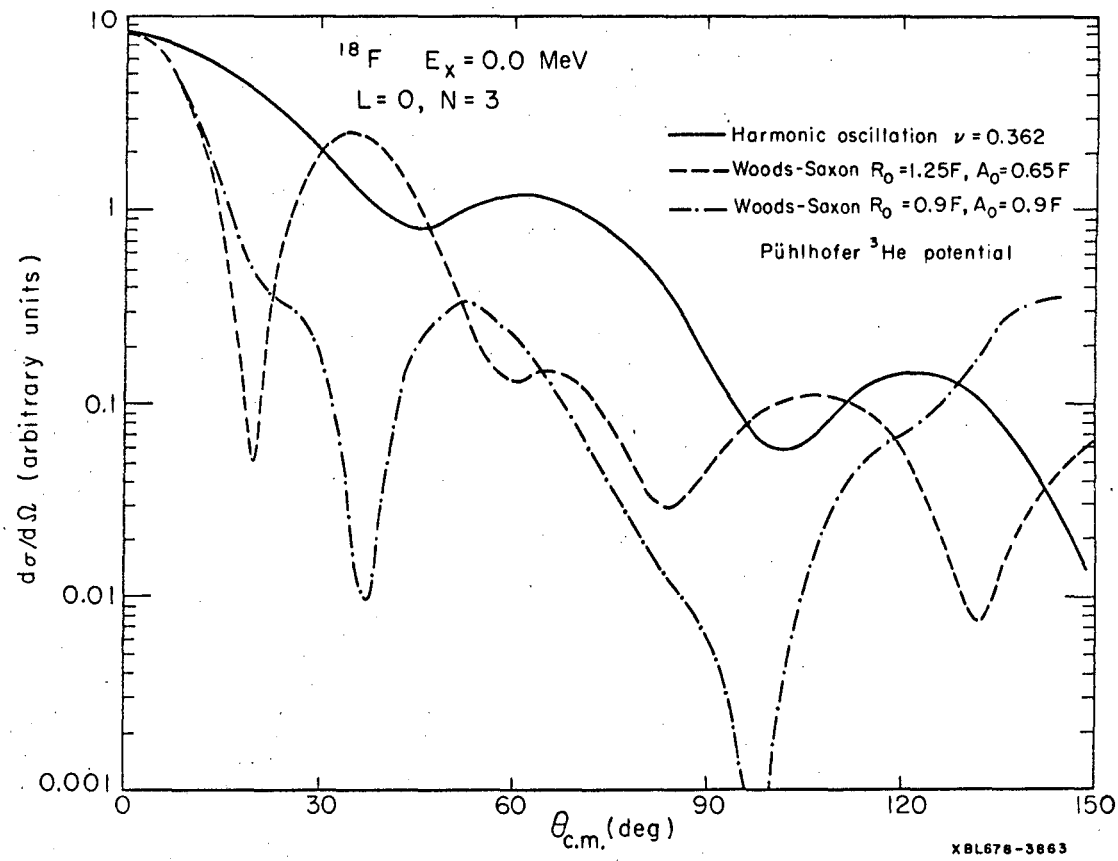

Fig. 26. Proton angular distributions from L = 0 DW calculations of the $^{16}O(^3He,p)^{18}F$ reaction at $E(^3He)$ = 20 MeV for E_x = 0. The ^{3}He optical-model potential of Pühlhofer[81] was used.

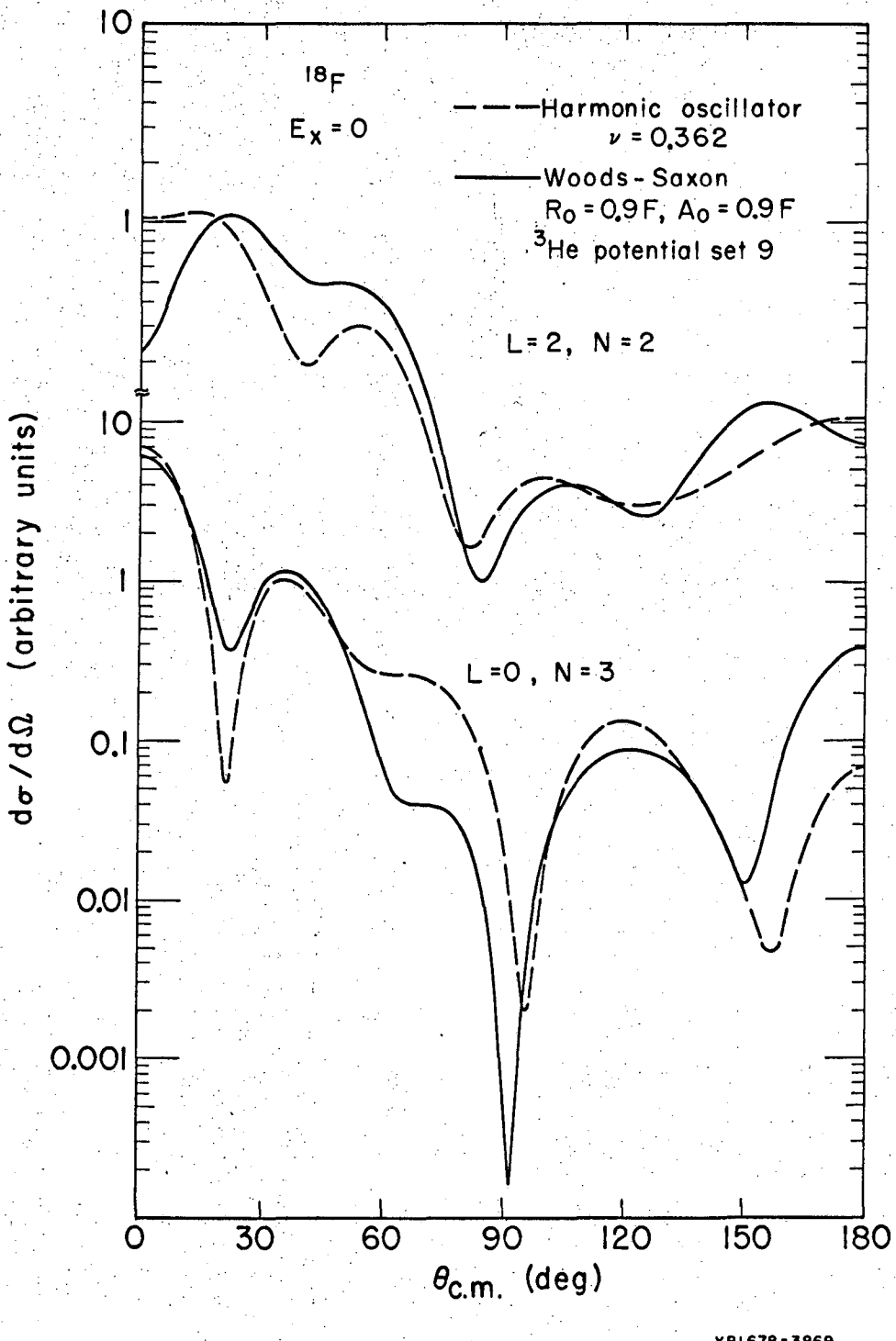

Fig. 27. Proton angular distributions from L = 0 and L = 2 DW calculations of the $^{16}O(^3He,p)^{18}F$ reaction at $E(^3He)$ = 20 MeV for E_x = 0. The ^3He optical-model potential set 9 was used.

The set of functions used for the HO calculations were those used to fit the ^{18}F data in Figs. 21-23. It is seen that potential 9 is much less sensitive to the bound-state wave function than the Pühlhofer potential. Nevertheless, the L = 2 WS calculation could not be considered as a fit to the data.

Several calculations, using unit spectroscopic factors, were made to compare the change of total cross section with excitation energy (or binding energy of the transferred pair) for several sets of functions. The results of these calculations are shown in Fig. 28. The cross section for L = 0 and L = 2 are nearly equal and are increasing with excitation energy. The trends are nearly the same for three sets of functions. The calculation using the Pühlhofer ^{3}He distorted wave appears to deviate from the trend, perhaps because of the hypersensitivity seen earlier. It should be noted that the relative cross sections in the $^{16}O(^{3}He,p)^{18}F$ reaction are well accounted for over the range of excitation studied which suggest that the trends seen for the calculated total cross section are correct.

Calculations for $^{12}C(^{3}He,p)^{14}N$ were made. Results for L = 2 and L = 0 transitions at E_x = 0 are shown in Fig. 29. In this case the results for WS and HO are nearly equal. The agreement for the L = 0 transition becomes even better with increasing excitation energy.

Model calculations, using unit spectroscopic factors, were made for a number of sets of functions in the ^{14}N system to show the trends of total cross section vs. excitation energy and shell-model state. Results of these calculations are shown in Figs. 30 and 31.

Configurations of $(p)^2$ require L,N combinations of 0,2 and 2,1 while $(s,d)^2$ configurations require 0,3 and 2,2 combinations. The $(p)^{-3}$ (s,d) configurations require 1,2 and 3,1 bound-state wave functions. In Fig. 30(a) are seen the trends for function sets used in the ^{14}N calculations.

In Sec. VI-B-3 it was pointed out that ^{14}N calculated cross sections became relatively smaller with increasing excitation energy and that a factor of 7 discrepancy existed between the $(p)^2$ type transitions and $(s,d)^2$ type transitions.

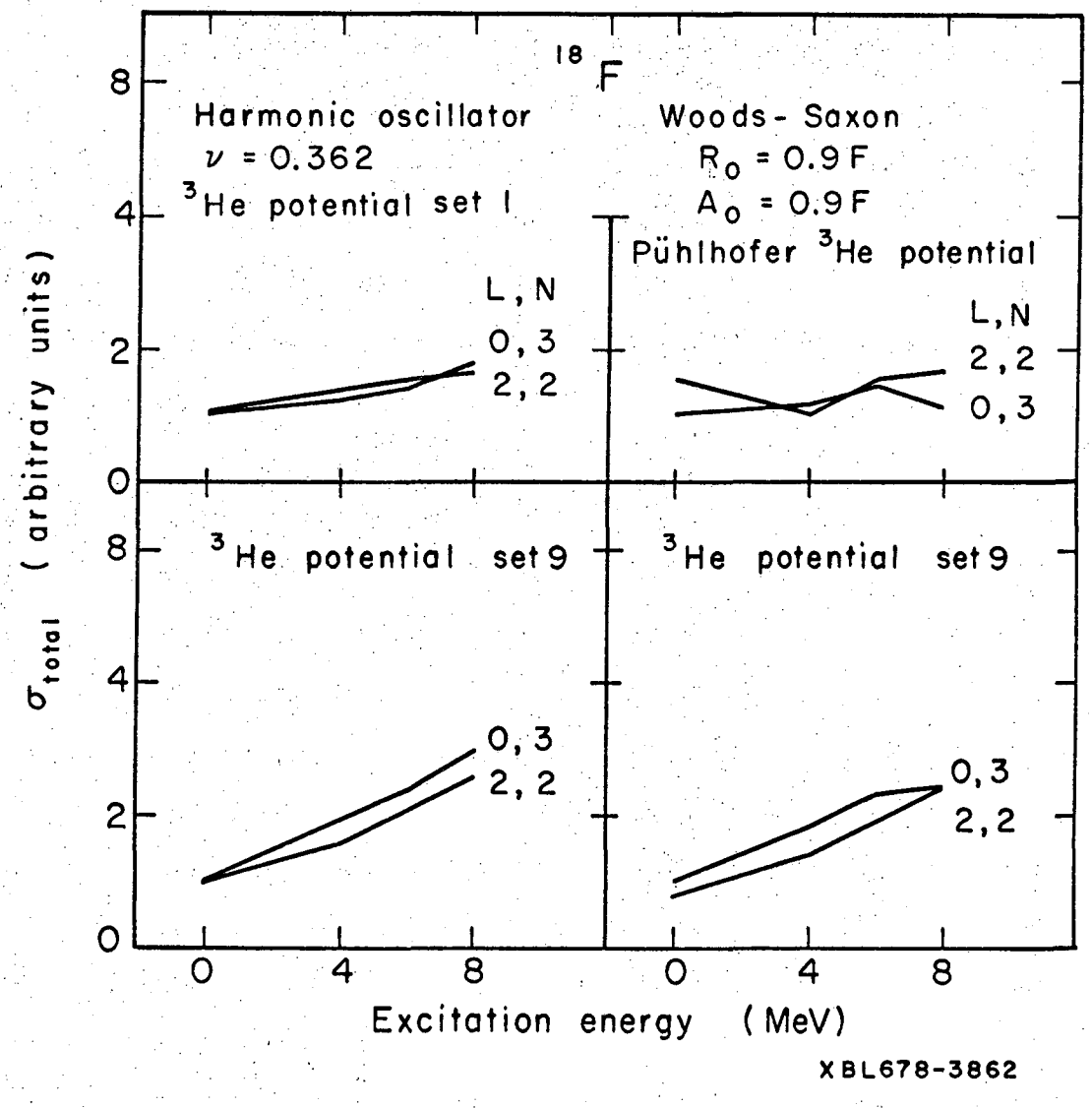

Fig. 28. Relation between total cross section and excitation energy given by DW calculations for the $^{16}O(^{3}He,p)^{18}F$ reaction at $E(^{3}He)$ = 20 MeV for several sets of functions.

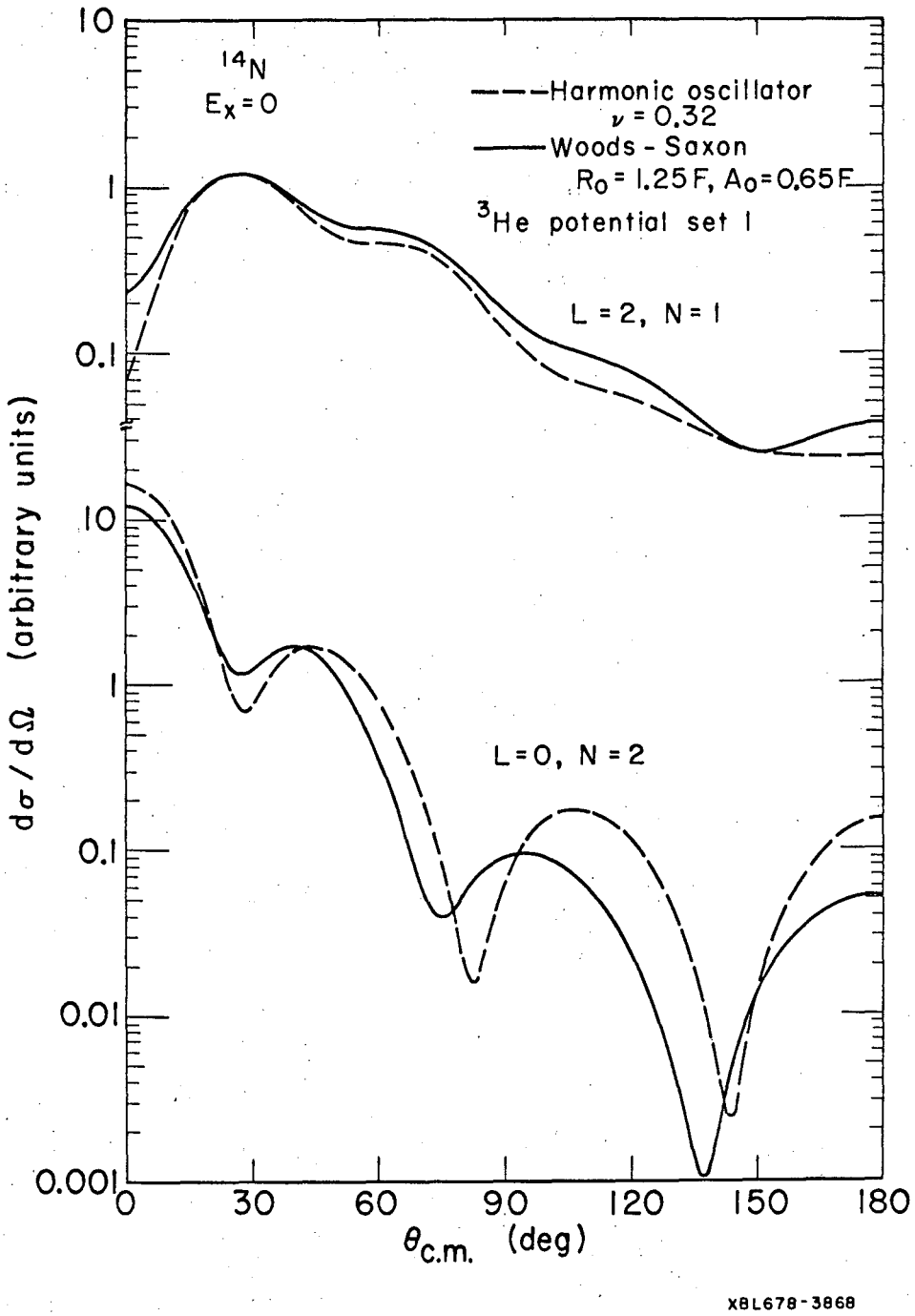

Fig. 29. Proton angular distributions from L = 0 and L = 2 DW calculations of the $^{12}C(^3He,p)^{14}N$ reaction at $E(^3He)$ = 20 MeV for E_x = 0. The ^{3}He optical-model potential set 1 was used.

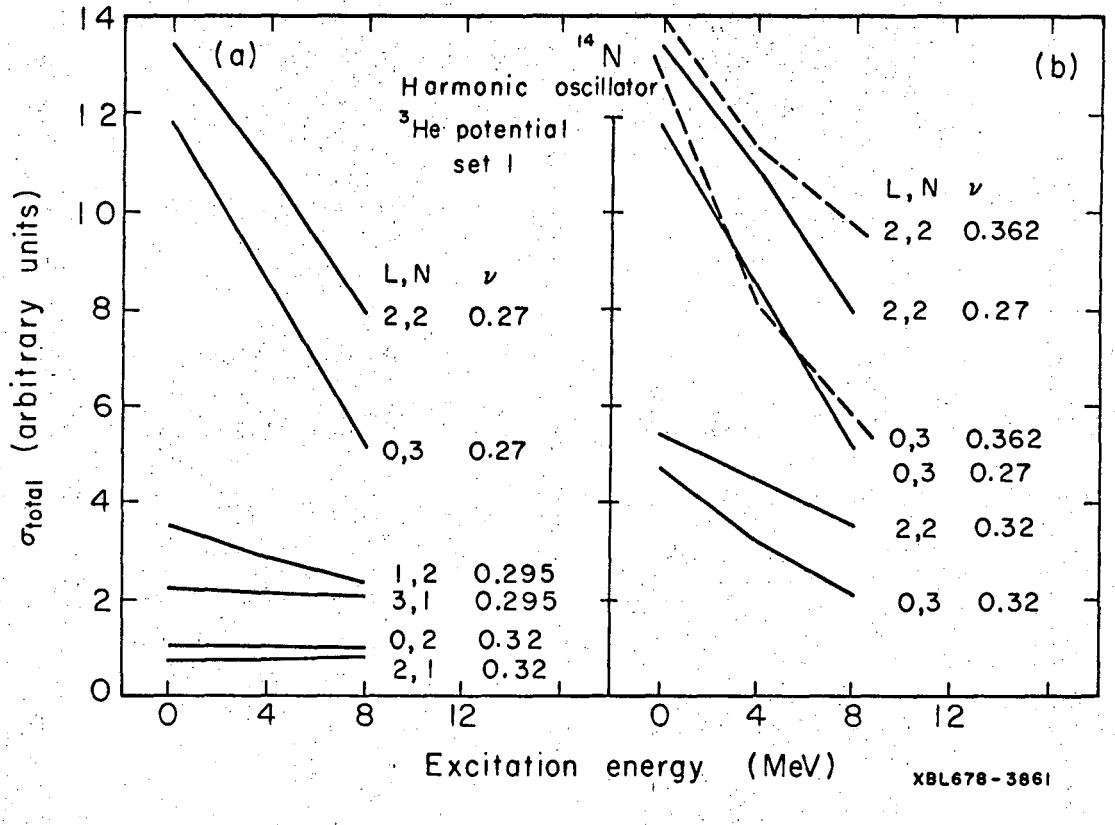

Fig. 30. Relation between total cross section and excitation energy given by DW calculations for the $^{12}C(^3He,p)^{14}N$ reaction at $E(^3He)$ = 20 MeV for several sets of functions using a truncated HO bound-state wave function.

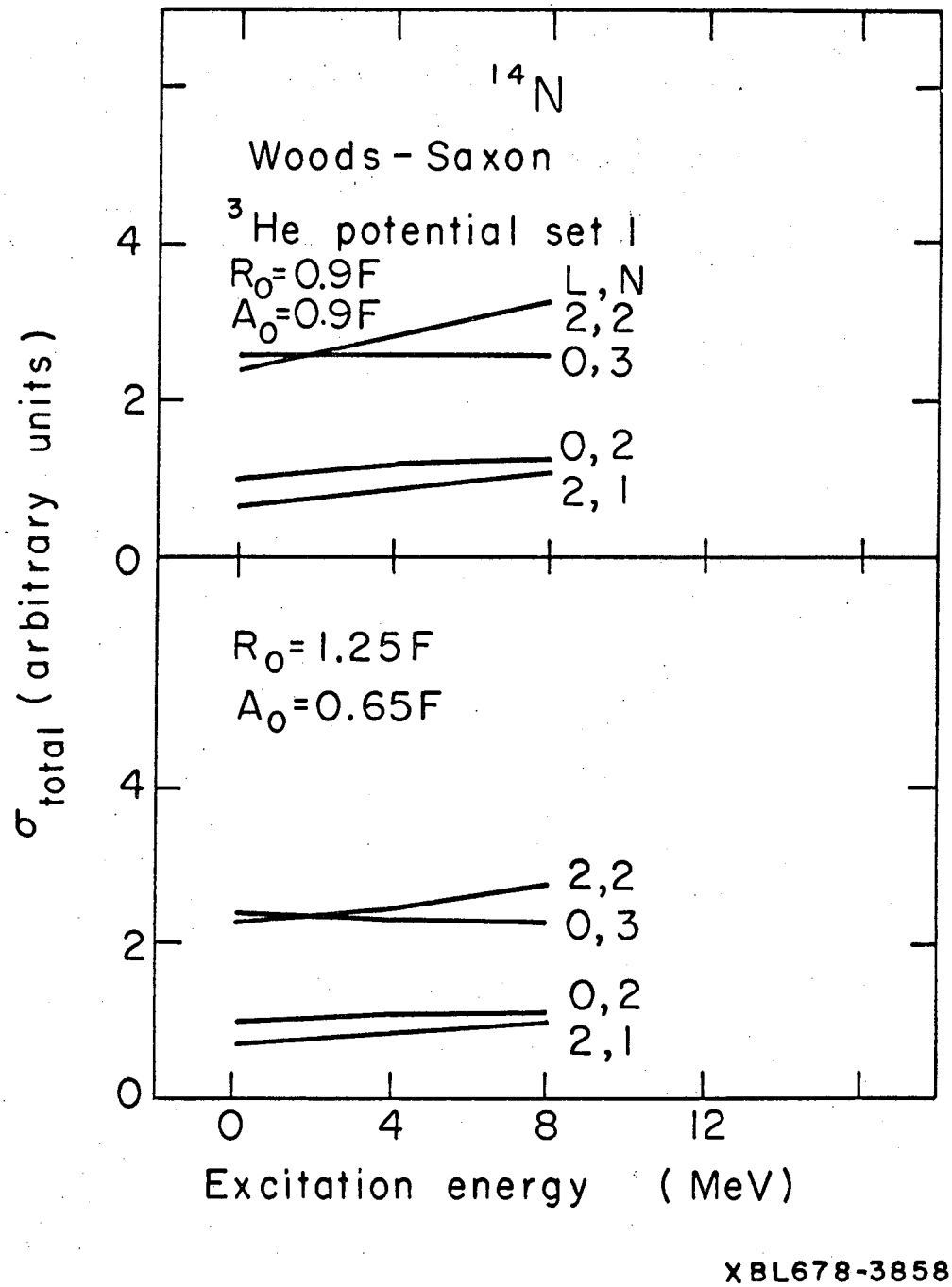

Fig. 31. Relation between total cross section and excitation energy given by DW calculations for the $^{12}C(^{3}He,p)^{14}N$ reaction at $E(^{3}He)$ = 20 MeV for several sets of functions using a Woods-Saxon bound-state wave function.

The cause of both of these discrepancies is easily seen by comparison of Fig. 30(a) and Fig. 28. Cross sections for the $(s,d)^2$ type transitions are much larger than for $(p)^2$ type which would account for the discrepancy mentioned. The cross section is sharply dropping as a function of excitation energy for $(s,d)^2$ transitions and remains constant for $(p)^2$ transitions, which is in contrast to an increasing cross section in the calculations for ^{18}F.

Calculations using a WS function are shown in Fig. 31. The $(p)^2$ type transitions show a small increase in cross section vs. excitation energy. This small increase is the amount needed to give good agreement in the reaction calculations. The $(s,d)^2$ type transitions are much nearer the $(p)^2$ type in magnitude and have constant or slightly increasing cross section vs. excitation energy. This behavior would bring down the discrepancy between the $(p)^2$ and $(s,d)^2$ transitions by a factor of 2 and would give better relative agreement within the $(s,d)^2$ transitions.

Figure 30(b) shows the change in cross section trends for a change in the HO bound-state function.

In this section the interddpendence[7,40] of nuclear structure, through the bound-state wave function, with the reaction mechanism, through the distorted waves, has been strikingly illustrated. The problem of properly choosing the bound-state wave function and the potential for distorting the scattering waves remains important and challenging.

VII. SUMMARY

Information in three categories has been obtained from this work: (1) spectroscopy of ^{14}N and ^{18}F, (2) wave functions of ^{14}N and ^{18}F and (3) stripping reaction mechanism in light nuclei.

The following spectroscopic information has been obtained for levels of ^{14}N. An L = 3 angular distribution has been observed for the transition to the 8.489-MeV level which was consistent with its 4^+0 spectroscopic assignment and suggested $(p3/2)^{-1}(p1/2)^2(d5/2)$ configuration.[89] The 2^+0, 8.979-MeV level[92] was associated with the 2^+0a state calculated by True[87] and the observed cross section was consistent with this assignment. The 9.388-MeV level was restricted to a unique spin and parity of 2^-. The 10.213-MeV level was associated with the 1^+0c state calculated by True[87] on the basis of its suggested spin and parity and the fact that the level was not observed in either the (α,d)[90,91] or the $(^3He,p)$ reaction. The 10.85-MeV level[90] was tentatively assigned 4^+0 with a partial amplitude of the 4^+0a state predicted by True.[87] This suggestion was made on the basis of its observed angular distribution in the $(^3He,p)$ reaction and its large cross section in the (α,d) reaction.[90,91]

The following spectroscopic information for ^{18}F was obtained in this work. The 2.524-MeV 2^+0 level[126] was shown to have little $(s,d)^2$ configuration. This conclusion was based on the nature of its angular distribution and the magnitude of its cross section. On similar evidence the 3.838-MeV 2^+0 level[126] was associated with the 2^+0a $(s,d)^2$ state. Although a particle-hole configuration has been suggested for the 1.700-MeV state,[119] these experiments were unable to eliminate an $(s,d)^2$ configuration for this state. The 3.358-MeV level[126] was tentatively associated with the 3^+0b $(s,d)^2$ state. These conclusions are supported by the recent work of Pühlhofer and Bock.[5]

By comparison of the reactions (α,d) and $(^3He,p)$ and by use of a pure ^{16}O target the following observations, not made by the above mentioned workers, were made in this work. The 4.400-MeV level[126] was excited in the (α,d) reaction and is, therefore, a T = 0 level. A comparison of the two reactions indicated that the 4.651-, 4.741- and 4.964-MeV levels[122] are not T = 0. These levels were confirmed as the 4^+a, 0^+b and 2^+b T = 1 levels respectively by the agreement of their

relative cross sections to predicted values. The 5.594-MeV level was associated with the 4^+0a $(s,d)^2$ state. It was excited in both reactions and had an L = 4 angular distribution. Its cross section was in qualitative agreement with calculated values. In addition to these levels, 22 other levels were either assigned or confirmed as T = 0 states. A new ^{18}F level at an excitation energy of 8.596 MeV was identified.

The above spectroscopic assignments were based in part upon reaction calculations for the $(^3He,p)$ reactions which employed two sets of wave functions for ^{14}N and four sets of wave functions for ^{18}F. The ^{14}N wave functions and the necessary ^{12}C ground state wave function were taken from the work of Cohen and Kurath[88] and of True.[87] Using these wave functions, relative cross sections to predicted levels were calculated and compared to experimental, relative cross sections. Such comparisons were satisfactory for the four $(p)^{-2}$ states predicted by Cohen and Kurath[88] and for the states of dominant $(s,d)^2$ configuration predicted by True.[87]

Calculated cross sections for states with p character predicted by True[87] did not agree with experimental values. This last observation, together with model calculations for the ground state and 2.311-MeV state of ^{14}N indicated that the p3/2 hole character of wave functions with p character must be included.

The model calculations just noted were sensitive to 10 or 15 per cent admixtures in the wave functions which demonstrated that the two-nucleon transfer reaction can be sensitive to the details of the wave function.

Calculations for the ^{18}F system were based on ^{18}F wave functions of Arima et al.,[152,153] Redlich,[154,155] and Kuo and Brown.[120] Relative cross sections calculated using four sets of wave functions from these workers are all in good agreement with the data. Arima et al.[152,153] predict the 2^+0a at about 2.5 MeV excitation. As mentioned above, this shell model level is found experimentall at 3.838 MeV excitation, It must, therefore, be concluded that in the limited, shell-model space of the (s,d) shell, Arima et al.[152,153] have chosen the wrong effective interaction. A comparison of the two Redlich[154,155] calculations, one based on $(s,d)^2$ configurations and the other including, in addition,

higher configurations, indicates, that for the simple effective interaction used, the higher configurations make no significant changes in the wave functions. It is most satisfying to note that the calculations of Kuo and Brown,[120] which are based on a free nucleon-nucleon interaction potential, are good as calculations based on an impirical effective interaction.

In the system involving ^{14}N, it was shown that the particle-hole character of the wave functions had a significant effect upon the reaction calculations. It is, therefore, to be expected that accounting for the particle-hole character of ^{16}O and ^{18}F would further improve calculations in this system.

This work has indicated that the two-nucleon transfer mechanism is basically understood and applicable in the region of light nuclei. In general, calculated differential and total cross sections are in satisfactory agreement with experimental values. It has been possible, on the basis of calculations, to make some spectroscopic assignments and to confirm a number of other suggested assignments.

Two problems concerning the reaction mechanism have been emphasized by the results of this work. It has been found necessary to use a spin-independent potential for the interaction in the distorted-wave theory which is responsible for the nuclear rearrangement. Other data[15] suggest the need for a spin-dependent potential and indeed from basic considerations[16] one expects it. This important problem, therefore, remains for future solution.

The interdependence between the bound-state wave function of the transferred pair and the distorted waves as generated from the optical-model potential was seen in the cross-section calculations. It was observed that a set of these functions which account of the experimental cross sections is not unique. A more complete understanding of the bound-state wave function and of the distorted waves, is therefore, still to be sought.

ACKNOWLEDGMENTS

This work marks the completion of the formal education of the author. Numerous and subtle are the contributions made by many people who have helped and aided the author in his progress. It is impossible at this time to adequately express appreciation to these many people.

Deep appreciation is due to Dr. Bernard G. Harvey under whose able guidance this work was performed. His insight into the problems of physics and his understanding of the needs of his co-workers are equally commendable.

Appreciation is due Professor Joseph Cerny for his continued interest in this work and for many hours spent in discussing it.

Dr. Norman K. Glendenning has given excellent guidance and direction in the theoretical aspects of this work. He has also made available several computer codes which made possible the computations here reported.

Dr. David L. Hendrie and Dr. John R. Meriwether have given much guidance in the operation of equipment, in the analysis of data and in the calculations here reported.

Dr. Martin G. Redlich has discussed this work with the author on several occasions and has made available ^{18}F theoretical wave functions.

Dr. Hans H. Duhm, Dr. O. Neil Jarvis, Dr. Richard H. Pehl, Dr. Ernest J. Rivet, Mr. Roy F. Burton, Miss Jeannette Mahoney, and others of the research staff have contributed much in both technical and scientific help.

The opportunity to work with Dr. Fay Ajzenberg-Selove and to enjoy her encouragement and guidance was appreciated.

The associations with a relatively large group of peers have been most valuable. Dr. Arthur Springer introduced the author to the experimental equaipment and techniques and gave valuable suggestions in that initial period. He also made available several valuable computer codes. Mr. Chi Chang Lu has been closely associated with this work and has given much help, particularly during the course of experiments. Mr. Donald G. Fleming and Mr. Gordon C. Ball, through discussion and comparison of data, have contributed much to this work. Mr. Creve Maples has made available several computer codes of invaluable utility. Mr. Gilber W. Butler,

Miss Mary Reed, Mr. Joel M. Moss, Mr. Heinz Brunnader and others have aided during the acquisition of data and in ways too numerous to mention.

Dr. Fred Goulding and Dr. Donald A. Landis were irreplaceable in the help they gave, both in supplying detectors and in providing the necessary electronic equipment.

Mr. Claude E. Ellsworth provided foil targets for the experiments. This service was sincerely appreciated.

Those of the cyclotron crew and support groups who have been of significant aid are too numerous to list. These qualified people were always ready and able to aid with any problem. For this willing service they are due a debt of gratitude.

The author is deeply grateful to his family. First, for training as a young student to strive and attain worth while goals. During the years in Berkeley he is grateful for three little faces that often took the gloom from the foggiest days. Above all, he is grateful to his wife, Marian, for encouragement and for preparing the manuscript for final typing.

To three other friends are due special appreciation for their encouragement. These are James E. Sabine, LL.B., Dr. W. Gordon Rose and Dr. D. Emerton Williams.

This work was performed under the auspices of the U. S. Atomic Energy Commission.

APPENDIX

Tables of center-of-mass differential cross sections are given in this section. Errors listed are the standard deviation arising from statistics only. The tables are labeled by reaction and excitation (E_x) of the product nucleus. Tables A1 and A2 are for the reaction $^{12}C(^3He,^3He)^{12}C$ at $E(^3He)$ = 20.1 MeV. Tables A3 to A25 are for the reaction $^{12}C(^3He,p)^{14}N$ at $E(^3He)$ = 20.1 MeV. Tables A26 to A49 are for the reaction $^{16}O(^3He,p)^{18}F$ at $E(^3He)$ = 19.8 MeV. Tables A^{50} to A^{70} are for the reaction $^{16}O(\alpha,d)^{18}F$ at $E(\alpha)$ = 40.3 MeV.

Table A1. $^{12}C(^{3}He,^{3}He)^{12}C$
E_x = 0.00 MeV

θcm. (deg)	dσ/dΩ (mb/sr)	Error (mb/sr)
10.6	6387	12
13.1	3453	8
15.6	2050	5
18.1	1272	4
20.6	681	2
23.1	368	1
25.3	174	0.5
26.8	104	0.5
26.8	108	0.7
28.0	64.1	0.3
30.5	23.4	0.2
33.0	14.5	0.1
35.4	16.6	0.1
37.9	19.5	0.1
40.3	19.9	0.1
42.8	17.4	0.1
45.1	12.9	0.1
47.6	8.26	0.08
49.9	4.95	0.05
52.9	2.85	0.06
55.9	2.84	0.05
58.8	3.95	0.05
61.7	5.09	0.06
65.8	5.47	0.05
70.4	3.99	0.05
75.4	1.80	0.03

Table A2. $^{12}C(^{3}He,^{3}He)^{12}C$
E_x = 4.433 MeV

θcm. (deg)	dσ/dΩ (mb/sr)	Error (mb/sr)
11.0	2.3	0.2
13.6	2.4	0.2
16.2	3.4	0.2
18.8	5.1	0.2
21.3	5.0	0.1
23.9	4.7	0.1
26.2	4.6	0.1
27.7	4.7	0.1
27.7	4.9	0.1
29.0	4.7	0.1
31.6	4.3	0.05
34.1	3.9	0.05
36.6	3.2	0.05
39.2	2.6	0.05
41.7	2.2	0.05
44.2	2.2	0.05
46.7	2.0	0.05
49.1	2.0	0.05
51.6	2.0	0.05
54.7	1.9	0.01
57.7	1.7	0.01
60.7	1.5	0.05
63.7	1.5	0.05
67.9	1.6	0.05
72.6	1.8	0.05
77.8	2.5	0.05

Table A3. $^{12}C(^{3}He,p)^{14}N$
E_x = 0.00 MeV

$\theta_{cm.}$ (deg)	$d\sigma/d\Omega$ (mb/sr)	Error (mb/sr)
9.4	0.13	0.021
11.6	0.18	0.025
13.9	0.23	0.024
17.2	0.32	0.032
22.8	0.41	0.019
26.1	0.35	0.033
28.3	0.31	0.032
30.5	0.29	0.026
30.5	0.33	0.034
33.9	0.27	0.029
39.4	0.18	0.012
44.8	0.17	0.015
45.3	0.15	0.017
45.3	0.17	0.010
50.3	0.26	0.017
55.7	0.23	0.018
61.0	0.21	0.017
61.4	0.18	0.019
61.4	0.21	0.011
66.3	0.20	0.016
71.6	0.14	0.014
76.8	0.07	0.008
84.5	0.03	0.005
92.1	0.08	0.009
109.5	0.19	0.026
114.3	0.24	0.017
123.8	0.12	0.020
128.5	0.13	0.012
158.6	0.54	0.018
171.9	0.92	0.023

Table A4. $^{12}C(^{3}He,p)^{14}N$
E_x = 2.31 ± 0.022 MeV

$\theta_{cm.}$ (deg)	$d\sigma/d\Omega$ (mb/sr)	Error (mb/sr)
9.5	0.85	0.054
11.7	0.62	0.046
14.0	0.48	0.034
14.0	0.46	0.041
17.3	0.24	0.027
22.9	0.03	0.005
26.3	0.08	0.016
28.5	0.14	0.021
30.7	0.16	0.019
30.7	0.20	0.026
34.1	0.25	0.027
39.6	0.38	0.018
45.1	0.34	0.021
45.5	0.36	0.027
45.5	0.36	0.014
50.6	0.21	0.017
56.0	0.12	0.013
61.4	0.06	0.009
61.8	0.06	0.011
61.8	0.07	0.006
66.7	0.05	0.009
72.0	0.07	0.010
77.2	0.12	0.010
84.9	0.12	0.009
92.5	0.12	0.010
124.2	0.02	0.010
128.9	0.03	0.006
158.8	0.04	0.005
172.0	0.08	0.007

Table A5. $^{12}C(^{3}He,p)^{14}N$
E_x = 3.94 ± 0.032 MeV

θcm. (deg)	dσ/dΩ (mb/sr)	Error (mb/sr)
9.5	1.79	0.077
11.8	1.93	0.080
14.0	1.37	0.057
17.4	0.74	0.048
23.0	0.31	0.016
26.4	0.32	0.032
28.6	0.31	0.031
30.9	0.38	0.029
30.9	0.35	0.035
34.2	0.42	0.035
39.8	0.46	0.019
45.3	0.38	0.023
50.8	0.26	0.019
56.2	0.23	0.018
61.6	0.16	0.015
62.1	0.18	0.019
62.1	0.18	0.010
67.0	0.15	0.014
72.3	0.16	0.015
77.5	0.18	0.013
85.2	0.14	0.010
92.8	0.19	0.013
110.2	0.15	0.023
115.0	0.21	0.016
124.5	0.14	0.022
129.2	0.18	0.014
158.9	0.29	0.013
172.0	0.26	0.012

Table A6. $^{12}C(^{3}He,p)^{14}N$
E_x = 4.93 ± 0.033 MeV

θcm. (deg)	dσ/dΩ (mb/sr)	Error (mb/sr)
9.5	1.38	0.068
11.8	1.03	0.058
14.1	1.05	0.050
14.1	1.11	0.035
17.5	0.87	0.052
23.1	0.71	0.024
26.5	0.57	0.042
28.7	0.55	0.042
31.0	0.47	0.033
31.0	0.46	0.040
34.3	0.45	0.036
39.9	0.32	0.016
45.5	0.31	0.021
51.0	0.24	0.018
56.4	0.14	0.014
61.8	0.14	0.014
62.3	0.11	0.015
62.3	0.15	0.009
67.2	0.11	0.013
72.5	0.09	0.011
77.8	0.09	0.010
85.4	0.10	0.008
93.1	0.06	0.008
110.4	0.03	0.010
115.2	0.04	0.006
124.7	0.09	0.018
129.4	0.13	0.012
159.0	0.03	0.004
172.0	0.07	0.006

Table A7. $^{12}C(^{3}He,p)^{14}N$
E_x = 5.12 ± 0.036 MeV

θcm. (deg)	dσ/dΩ (mb/sr)	Error (mb/sr)
9.5	3.19	0.103
11.8	1.70	0.075
14.1	1.46	0.059
14.1	1.61	0.070
17.5	1.35	0.065
23.1	0.98	0.029
26.5	0.91	0.053
28.8	1.01	0.056
31.0	0.98	0.047
31.0	0.94	0.057
34.4	0.99	0.054
39.9	0.95	0.027
45.5	0.92	0.035
51.0	0.78	0.032
56.4	0.73	0.032
61.9	0.54	0.026
62.3	0.56	0.033
62.3	0.61	0.018
67.2	0.42	0.023
72.5	0.35	0.022
77.8	0.29	0.017
85.5	0.25	0.013
93.2	0.24	0.016
110.5	0.31	0.033
115.3	0.38	0.021
124.7	0.37	0.036
129.4	0.40	0.022
159.0	0.46	0.017
172.1	0.48	0.017

Table A8. $^{12}C(^{3}He,p)^{14}N$
E_x = 5.65 ± 0.030 MeV

θcm. (deg)	dσ/dΩ (mb/sr)	Error (mb/sr)
9.6	1.99	0.083
11.8	1.97	0.081
14.1	1.43	0.058
14.1	1.40	0.062
17.5	1.08	0.057
23.2	0.85	0.027
26.6	0.67	0.046
28.8	0.55	0.041
31.1	0.52	0.035
31.1	0.59	0.045
34.4	0.50	0.041
40.0	0.39	0.018
45.6	0.38	0.020
51.1	0.35	0.025
56.6	0.29	0.020
62.0	0.25	0.018
62.4	0.28	0.023
67.4	0.21	0.017
72.7	0.20	0.017
77.9	0.21	0.015
85.6	0.17	0.011
93.3	0.14	0.012
110.6	0.17	0.025
115.4	0.24	0.017
124.9	0.22	0.028
129.5	0.24	0.017
159.1	0.14	0.009
172.1	0.18	0.010

Table A9. $^{12}C(^{3}He,p)^{14}N$
E_x = 5.84 ± 0.030 MeV

$\theta_{cm.}$ (deg)	$d\sigma/d\Omega$ (mb/sr)	Error (mb/sr)
9.6	0.68	0.047
11.8	0.81	0.052
14.1	0.52	0.035
14.1	0.47	0.041
17.5	0.50	0.039
23.2	0.45	0.019
26.6	0.46	0.042
28.8	0.38	0.038
31.1	0.42	0.031
31.1	0.38	0.036
34.5	0.40	0.034
40.1	0.36	0.017
45.6	0.40	0.024
46.0	0.40	0.023
51.1	0.38	0.021
56.6	0.32	0.021
62.0	0.37	0.022
62.4	0.34	0.025
62.4	0.33	0.013
67.4	0.38	0.023
72.7	0.32	0.021
78.0	0.30	0.017
85.7	0.25	0.013
93.3	0.22	0.015
110.6	0.24	0.029
115.5	0.35	0.020
124.9	0.33	0.034
129.5	0.46	0.023
159.1	0.40	0.016
172.1	0.29	0.013

Table A10. $^{12}C(^{3}He,p)^{14}N$
E_x = 6.21 ± 0.020 MeV

$\theta_{cm.}$ (deg)	$d\sigma/d\Omega$ (mb/sr)	Error (mb/sr)
9.6	3.38	0.106
11.9	2.92	0.097
14.1	2.26	0.073
14.1	2.17	0.089
17.6	1.51	0.068
23.2	0.71	0.024
26.6	0.54	0.041
28.9	0.50	0.039
31.1	0.55	0.034
31.1	0.59	0.045
34.5	0.55	0.040
40.1	0.61	0.022
45.7	0.71	0.031
51.2	0.71	0.031
56.7	0.63	0.029
62.1	0.53	0.026
62.5	0.51	0.031
62.5	0.59	0.018
67.5	0.42	0.023
72.8	0.28	0.020
78.1	0.25	0.016
85.8	0.18	0.011
93.4	0.26	0.016
110.7	0.46	0.040
115.6	0.57	0.026
125.0	0.42	0.038
129.6	0.44	0.023
159.1	0.17	0.010
172.1	0.14	0.009

Table A11. $^{12}C(^{3}He,p)^{14}N$
E_x = 6.46 ± 0.018 MeV

θcm. (deg)	dσ/dΩ (mb/sr)	Error (mb/sr)
9.6	8.51	0.169
11.9	9.35	0.177
14.2	9.03	0.146
14.2	8.71	0.178
17.6	8.28	0.160
23.3	6.45	0.073
26.7	5.37	0.128
28.9	4.59	0.114
31.2	4.00	0.094
31.2	3.90	0.115
34.5	3.17	0.094
40.1	1.95	0.039
45.7	1.52	0.045
46.2	1.36	0.051
46.2	1.64	0.030
51.2	1.44	0.044
56.7	1.43	0.045
62.2	1.29	0.041
62.6	1.23	0.048
62.6	1.43	0.034
67.5	1.12	0.038
72.9	0.88	0.035
78.1	0.76	0.028
85.8	0.50	0.018
93.5	0.51	0.023
110.8	0.64	0.047
115.6	0.77	0.030
125.1	0.66	0.048
129.7	0.85	0.032
159.2	0.80	0.022
172.1	0.60	0.019

Table A12. $^{12}C(^{3}He,p)^{14}N$
E_x = 7.01 ± 0.042 MeV

θcm. (deg)	dσ/dΩ (mb/sr)	Error (mb/sr)
9.6	0.37	0.035
11.9	0.38	0.035
14.2	0.37	0.035
17.6	0.27	0.030
23.3	0.34	0.017
26.7	0.41	0.040
29.0	0.28	0.030
31.2	0.29	0.030
31.2	0.37	0.025
34.6	0.26	0.025
40.2	0.19	0.012
45.8	0.18	0.010
51.4	0.14	0.014
56.9	0.13	0.014
62.3	0.16	0.011
62.7	0.15	0.017
62.7	0.14	0.009
67.7	0.17	0.015
73.0	0.16	0.015
78.3	0.14	0.012
93.7	0.10	0.010
111.0	0.16	0.024
115.8	0.16	0.014
125.2	0.15	0.023
129.8	0.18	0.015
159.2	0.37	0.015
172.1	0.51	0.017

Table A13. $^{12}C(^{3}He,p)^{14}N$
$E_x = 7.95 \pm 0.026$ MeV

$\theta_{cm.}$ (deg)	$d\sigma/d\Omega$ (mb/sr)	Error (mb/sr)
9.7	0.29	0.031
12.0	0.30	0.031
14.3	0.37	0.029
14.3	0.37	0.037
17.7	0.40	0.035
23.4	0.42	0.019
26.8	0.37	0.033
29.1	0.27	0.029
31.4	0.39	0.029
31.4	0.36	0.035
34.8	0.30	0.029
40.4	0.27	0.014
46.0	0.21	0.017
46.5	0.22	0.021
46.5	0.23	0.011
51.6	0.17	0.015
57.1	0.13	0.013
62.5	0.14	0.014
63.0	0.14	0.016
63.0	0.13	0.008
67.9	0.12	0.013
73.3	0.18	0.016
78.6	0.19	0.014
86.3	0.17	0.011
93.9	0.15	0.013
116.1	0.12	0.012
125.5	0.13	0.022
130.1	0.17	0.014
159.3	0.29	0.013

Table A14. $^{12}C(^{3}He,p)^{14}N$
$E_x = 8.05 \pm 0.035$ MeV

$\theta_{cm.}$ (deg)	$d\sigma/d\Omega$ (mb/sr)	Error (mb/sr)
9.7	0.60	0.044
12.0	0.66	0.046
14.3	0.63	0.038
14.3	0.61	0.047
17.7	0.44	0.036
23.4	0.38	0.018
26.9	0.25	0.028
29.1	0.22	0.026
31.4	0.17	0.019
34.8	0.13	0.019
40.4	0.14	0.010
46.0	0.15	0.014
46.5	0.14	0.016
51.6	0.10	0.012
57.1	0.13	0.013
63.0	0.10	0.013
63.0	0.10	0.007
73.3	0.08	0.010
78.6	0.06	0.008
86.3	0.03	0.005
94.0	0.05	0.007
111.3	0.10	0.019
116.1	0.11	0.012
125.5	0.06	0.015
130.1	0.06	0.009
159.3	0.03	0.004

Table A15. $^{12}C(^{3}He,p)^{14}N$
E_x = 8.47 ± 0.030 MeV

θcm. (deg)	dσ/dΩ (mb/sr)	Error (mb/sr)
12.0	0.95	0.055
14.3	0.82	0.044
14.3	0.85	0.055
17.7	0.82	0.049
23.5	0.73	0.024
26.9	0.69	0.046
29.2	0.78	0.049
31.5	0.73	0.040
31.5	0.65	0.046
34.9	0.68	0.044
40.5	0.55	0.021
46.1	0.44	0.024
46.6	0.46	0.030
46.6	0.48	0.016
51.7	0.31	0.020
57.2	0.24	0.018
62.7	0.26	0.018
63.1	0.24	0.021
63.1	0.28	0.012
68.1	0.26	0.018
73.5	0.30	0.020
78.7	0.30	0.017
86.5	0.33	0.015
94.1	0.33	0.019
111.4	0.25	0.030
116.2	0.33	0.020
125.6	0.32	0.034
130.2	0.51	0.025
159.4	0.54	0.019

Table A16. $^{12}C(^{3}He,p)^{14}N$
E_x = 8.61 ± 0.034 MeV

θcm. (deg)	dσ/dΩ (mb/sr)	Error (mb/sr)
12.0	0.77	0.050
14.3	0.37	0.029
14.3	0.35	0.035
17.8	0.30	0.030
23.5	0.26	0.015
26.9	0.26	0.028
29.2	0.37	0.033
31.5	0.34	0.027
31.5	0.37	0.035
34.9	0.39	0.033
40.6	0.27	0.014
46.2	0.18	0.016
46.6	0.15	0.017
51.7	0.09	0.011
57.3	0.03	0.007
62.7	0.03	0.006
68.1	0.03	0.006
73.5	0.03	0.007
78.8	0.08	0.009
86.5	0.09	0.008
94.2	0.08	0.009
111.5	0.06	0.014
116.3	0.05	0.008
125.7	0.06	0.014
130.3	0.06	0.009
159.4	0.08	0.007

Table A17. $^{12}C(^{3}He,p)^{14}N$
$E_x = 8.96 \pm 0.019$ MeV

θcm. (deg)	dσ/dΩ (mb/sr)	Error (mb/sr)
12.0	8.66	0.165
14.3	8.77	0.144
14.3	8.95	0.178
17.8	8.46	0.160
23.5	7.28	0.077
27.0	6.63	0.141
29.3	6.00	0.135
31.5	5.68	0.110
31.5	5.93	0.140
35.0	5.13	0.121
40.6	4.13	0.057
46.2	3.43	0.068
46.7	3.27	0.078
46.7	3.75	0.044
51.8	2.94	0.062
57.4	2.46	0.058
62.8	2.23	0.052
63.3	1.90	0.059
63.3	2.29	0.034
68.2	2.00	0.050
73.6	2.07	0.053
78.9	1.99	0.045
86.6	1.75	0.035
94.3	1.82	0.044
111.6	2.06	0.086
116.4	2.55	0.055
125.8	2.10	0.086
130.4	2.42	0.053

Table A18. $^{12}C(^{3}He,p)^{14}N$
$E_x = 9.15 \pm 0.018$ MeV

θcm. (deg)	dσ/dΩ (mb/sr)	Error (mb/sr)
9.7	4.79	0.124
17.8	2.58	0.088
23.6	1.97	0.040
27.0	1.77	0.073
29.3	1.54	0.068
31.6	1.18	0.050
31.6	1.34	0.067
35.0	1.01	0.053
40.7	0.64	0.022
46.3	0.54	0.027
46.7	0.55	0.032
51.9	0.43	0.024
57.4	0.43	0.024
62.9	0.38	0.022
63.3	0.33	0.025
63.3	0.40	0.014
68.3	0.34	0.021
73.7	0.27	0.019
79.0	0.27	0.016
86.7	0.23	0.013
94.4	0.29	0.017
111.7	0.28	0.032
116.5	0.37	0.021
125.9	0.26	0.030
130.5	0.30	0.019

Table A19. $^{12}C(^{3}He,p)^{14}N$
$E_x = 9.39 \pm 0.026$ MeV

θcm. (deg)	dσ/dΩ (mb/sr)	Error (mb/sr)
9.7	2.50	0.089
12.1	2.03	0.080
17.8	1.41	0.065
23.6	1.31	0.033
27.0	1.27	0.062
29.3	1.13	0.058
31.6	0.91	0.044
31.6	1.19	0.063
35.0	0.93	0.051
40.7	0.68	0.023
46.4	0.56	0.027
51.9	0.41	0.023
57.5	0.32	0.021
63.0	0.32	0.020
63.4	0.27	0.022
63.4	0.23	0.011
68.4	0.26	0.018
73.8	0.30	0.020
79.1	0.26	0.016
86.8	0.22	0.012
94.5	0.19	0.014
111.8	0.16	0.024
116.6	0.32	0.020
125.9	0.41	0.038
130.5	0.48	0.024

Table A20. $^{12}C(^{3}He,p)^{14}N$
$E_x = 9.70 \pm 0.022$ MeV

θcm. (deg)	dσ/dΩ (mb/sr)	Error (mb/sr)
9.8	1.16	0.061
12.1	1.17	0.061
14.4	1.11	0.050
14.4	1.04	0.061
23.6	0.82	0.026
27.1	0.74	0.047
29.4	0.66	0.045
31.7	0.50	0.033
31.7	0.59	0.044
35.1	0.59	0.041
40.8	0.45	0.019
46.4	0.37	0.022
52.0	0.30	0.020
57.6	0.26	0.019
63.1	0.21	0.016
63.5	0.18	0.018
63.5	0.24	0.011
68.5	0.17	0.015
73.9	0.14	0.014
79.2	0.13	0.012
86.9	0.14	0.010
94.6	0.18	0.014
111.9	0.18	0.025
116.7	0.32	0.020

Table A21. $^{12}C(^{3}He,p)^{14}N$
E_x = 10.08 ± 0.018 MeV

θcm. (deg)	dσ/dΩ (mb/sr)	Error (mb/sr)
9.8	1.02	0.057
12.1	0.76	0.049
14.4	0.85	0.044
14.4	0.85	0.054
17.9	0.61	0.042
27.2	0.53	0.040
29.5	0.44	0.036
31.8	0.38	0.028
31.8	0.43	0.037
35.2	0.44	0.035
40.9	0.38	0.017
46.5	0.40	0.023
52.1	0.38	0.022
57.7	0.34	0.021
63.2	0.30	0.019
63.7	0.31	0.013
68.6	0.24	0.018
74.0	0.26	0.019
79.3	0.22	0.015
87.1	0.20	0.012
94.7	0.26	0.017
112.1	0.30	0.033
116.8	0.42	0.023

Table A22. $^{12}C(^{3}He,p)^{14}N$
E_x = 10.43 ± 0.020 MeV

θcm. (deg)	dσ/dΩ (mb/sr)	Error (mb/sr)
9.8	2.19	0.083
12.1	1.98	0.079
14.5	2.16	0.070
14.5	2.11	0.085
18.0	1.97	0.076
23.7	1.80	0.038
27.2	1.29	0.062
29.5	0.97	0.054
31.8	0.91	0.044
35.3	0.68	0.043
41.0	0.52	0.020
46.6	0.48	0.025
47.1	0.43	0.029
52.3	0.42	0.023
57.8	0.38	0.023
63.3	0.31	0.020
63.8	0.27	0.022
63.8	0.34	0.013
68.8	0.26	0.018
74.2	0.21	0.017
79.5	0.16	0.013
87.2	0.13	0.009
94.9	0.15	0.012
112.2	0.14	0.023

Table A23. $^{12}C(^{3}He,p)^{14}N$
E_x = 10.81 ± 0.023 MeV

θcm. (deg)	dσ/dΩ (mb/sr)	Error (mb/sr)
9.8	0.27	0.029
12.2	0.27	0.029
18.0	0.31	0.030
23.8	0.30	0.015
31.9	0.25	0.023
31.9	0.29	0.031
35.4	0.32	0.030
41.1	0.28	0.015
46.8	0.31	0.020
47.2	0.29	0.023
52.4	0.25	0.018
58.0	0.22	0.017
63.9	0.16	0.017
63.9	0.20	0.010
68.9	0.15	0.014
74.3	0.16	0.015
79.7	0.17	0.013
87.4	0.19	0.011
95.1	0.18	0.014
112.4	0.10	0.019

Table A24. $^{12}C(^{3}He,p)^{14}N$
E_x = 12.40 ± 0.030 MeV

θcm. (deg)	dσ/dΩ (mb/sr)	Error (mb/sr)
10.0	2.55	0.088
12.3	2.04	0.079
14.7	2.31	0.071
14.7	2.58	0.093
18.2	1.90	0.073
24.1	1.27	0.031
27.6	1.17	0.058
30.0	1.00	0.058
32.3	0.89	0.043
35.8	0.83	0.047
41.6	0.62	0.021
47.3	0.50	0.025
47.8	0.57	0.032
53.0	0.68	0.030
58.6	0.66	0.030
64.2	0.58	0.027
64.7	0.72	0.036
64.7	0.70	0.019
69.7	0.65	0.029
75.1	0.54	0.027
80.5	0.39	0.020

Table A25. $^{12}C(^{3}He,p)^{14}N$
E_x = 12.50 ± 0.020MeV

θcm. (deg)	dσ/dΩ (mb/sr)	Error (mb/sr)
10.0	1.41	0.065
12.3	1.56	0.069
14.7	1.56	0.058
14.7	1.36	0.068
18.2	1.27	0.060
24.1	1.80	0.029
27.7	0.84	0.049
30.0	0.65	0.038
32.3	0.61	0.035
32.3	0.73	0.048
35.8	0.50	0.037
47.8	0.31	0.024
64.7	0.30	0.023
75.2	0.23	0.017

Table A26. $^{12}C(^{3}He,p)^{14}N$
E_x = 12.74 ± 0.030 MeV

θcm. (deg)	dσ/dΩ (mb/sr)	Error (mb/sr)
10.0	4.79	0.120
12.4	4.86	0.121
14.7	4.96	0.104
14.7	5.14	0.132
18.3	4.80	0.116
24.2	4.06	0.056
27.7	3.97	0.106
30.1	3.64	0.101
32.4	3.47	0.084
32.4	3.57	0.106
35.9	2.88	0.088
47.5	1.80	0.048
48.0	1.84	0.058
48.0	2.06	0.032
53.2	1.49	0.044
58.8	1.06	0.037
64.4	0.83	0.032
64.9	0.96	0.042
64.9	0.82	0.020
69.9	0.79	0.032
80.7	0.53	0.023

Table A27. $^{12}C(^{3}He,p)^{14}N$
E_x = 12.90 ± 0.025 MeV

θcm. (deg)	dσ/dΩ (mb/sr)	Error (mb/sr)
10.0	3.27	0.099
12.4	3.37	0.101
14.8	3.23	0.084
14.8	3.44	0.107
18.3	3.05	0.093
24.2	2.57	0.044
27.8	2.64	0.087
30.1	2.19	0.080
32.5	2.16	0.067
32.5	2.15	0.082
36.0	1.94	0.072
47.5	1.10	0.037
48.0	1.08	0.044
48.0	1.26	0.025
53.3	0.98	0.035
58.9	0.63	0.029
65.0	0.60	0.017
70.0	0.47	0.024

Table A28. $^{16}O(^{3}He,p)^{18}F$
E_x = 0.00 MeV

θcm. (deg)	dσ/dΩ (mb/sr)	Error (mb/sr)
8.8	2.86	0.058
11.1	2.72	0.110
14.4	1.58	0.029
16.6	1.14	0.029
18.8	0.67	0.029
22.0	0.48	0.053
27.5	0.81	0.032
29.6	0.78	0.057
31.8	1.05	0.115
32.9	1.05	0.040
35.1	1.04	0.075
37.3	0.97	0.042
39.4	0.79	0.045
42.7	0.58	0.083
43.7	0.61	0.028
48.0	0.46	0.033
53.4	0.26	0.026
59.7	0.23	0.017
64.0	0.21	0.020
70.2	0.18	0.014
75.4	0.17	0.015
79.5	0.17	0.017
85.7	0.16	0.015
94.8	0.11	0.013
104.7	0.20	0.017
110.6	0.14	0.014
125.0	0.10	0.012
128.8	0.08	0.010
132.5	0.12	0.013
142.8	0.10	0.011
150.2	0.12	0.011
152.9	0.12	0.012
170.2	0.20	0.009

Table A29. $^{16}O(^{3}He,p)^{18}F$
$E_x = 0.937 \pm 0.008$ MeV

θcm. (deg)	dσ/dΩ (mb/sr)	Error (mb/sr)
8.8	3.41	0.062
11.1	3.91	0.130
14.4	3.94	0.094
16.6	4.17	0.056
18.8	3.70	0.067
22.1	3.92	0.152
27.6	2.79	0.060
29.6	2.04	0.090
31.9	1.56	0.138
33.0	1.77	0.051
35.2	1.35	0.086
37.4	1.12	0.046
39.5	1.04	0.053
42.8	1.04	0.114
43.8	0.92	0.034
48.1	0.90	0.046
53.5	0.85	0.046
59.8	0.83	0.033
64.1	0.63	0.036
70.4	0.53	0.025
75.6	0.40	0.023
79.7	0.35	0.025
85.8	0.30	0.021
94.9	0.19	0.017
104.8	0.24	0.019
110.7	0.26	0.019
125.1	0.46	0.025
128.9	0.50	0.027
142.9	0.46	0.024
150.2	0.57	0.024
153.0	0.50	0.024
170.2	0.56	0.016

Table A30. $^{16}O(^{3}He,p)^{18}F$
$E_x = 1.111 \pm 0.007$ MeV

θcm. (deg)	dσ/dΩ (mb/sr)	Error (mb/sr)
8.8	0.68	0.027
11.1	1.09	0.066
14.4	1.03	0.049
16.6	0.89	0.026
18.8	1.04	0.036
22.1	1.02	0.076
27.6	1.36	0.042
29.6	1.44	0.078
31.9	1.17	0.121
33.0	1.67	0.050
35.2	1.68	0.098
37.4	1.65	0.055
39.5	1.49	0.063
42.8	1.55	0.130
43.8	1.33	0.042
48.2	1.06	0.049
53.5	0.90	0.048
59.9	0.66	0.029
64.1	0.61	0.034
70.4	0.61	0.028
75.6	0.63	0.028
79.7	0.60	0.033
85.8	0.58	0.029
94.9	0.52	0.028
104.8	0.46	0.027
110.7	0.52	0.028
125.1	0.58	0.028
128.9	0.67	0.027
142.9	0.92	0.033
150.2	0.91	0.030
153.0	1.07	0.034
170.2	1.13	0.022

Table A31. $^{16}O(^{3}He,p)^{18}F$
E_x = 1.680 ± 0.024 MeV

θcm. (deg)	dσ/dΩ (mb/sr)	Error (mb/sr)
8.8	0.32	0.020
11.1	0.29	0.034
14.4	0.20	0.021
16.6	0.17	0.012
18.8	0.17	0.014
27.6	0.10	0.011
29.7	0.09	0.019
32.0	0.08	0.031
33.1	0.09	0.012
35.2	0.12	0.026
37.4	0.10	0.013
39.6	0.11	0.017
42.8	0.13	0.039
43.9	0.09	0.011
48.2	0.10	0.015
53.6	0.07	0.013
60.0	0.07	0.010
64.2	0.06	0.011
70.5	0.06	0.009
75.7	0.06	0.009
79.8	0.05	0.009
85.9	0.05	0.008
95.0	0.05	0.008
104.9	0.03	0.006
110.8	0.03	0.007
125.2	0.05	0.009
129.0	0.05	0.009
132.8	0.05	0.008
143.0	0.06	0.008
150.3	0.05	0.007
153.0	0.05	0.007
170.2	0.03	0.004

Table A32. $^{16}O(^{3}He,p)^{18}F$
E_x = 2.096 ± 0.013 MeV

θcm. (deg)	dσ/dΩ (mb/sr)	Error (mb/sr)
8.8	0.12	0.012
11.2	0.08	0.018
14.5	0.10	0.015
16.7	0.09	0.008
18.9	0.11	0.012
22.2	0.08	0.021
27.6	0.19	0.015
29.7	0.17	0.027
32.0	0.20	0.050
33.1	0.22	0.018
35.3	0.29	0.041
37.5	0.26	0.022
39.6	0.26	0.026
42.9	0.28	0.058
44.0	0.26	0.018
48.3	0.20	0.021
53.6	0.27	0.025
60.0	0.22	0.017
64.2	0.18	0.019
70.5	0.18	0.014
75.7	0.15	0.014
79.9	0.17	0.018
86.0	0.16	0.015
95.1	0.13	0.014
105.0	0.09	0.012
110.9	0.07	0.010
125.3	0.09	0.011
129.0	0.11	0.012
132.8	0.13	0.012
143.0	0.11	0.011
150.3	0.15	0.012
153.1	0.18	0.014
170.2	0.17	0.009

Table A33. $^{16}O(^{3}He,p)^{18}F$
$E_x = 2.509 \pm 0.018$ MeV

θcm. (deg)	dσ/dΩ (mb/sr)	Error (mb/sr)
8.8	0.13	0.013
11.2	0.17	0.027
14.5	0.18	0.020
16.7	0.17	0.011
18.9	0.19	0.015
22.2	0.12	0.026
27.7	0.10	0.011
29.8	0.08	0.019
32.0	0.08	0.031
33.1	0.10	0.012
35.3	0.09	0.023
37.5	0.12	0.015
39.7	0.13	0.019
42.9	0.16	0.044
44.0	0.10	0.011
48.3	0.09	0.015
53.7	0.08	0.014
60.1	0.06	0.009
64.3	0.06	0.011
70.6	0.05	0.008
75.8	0.08	0.010
79.9	0.06	0.010
86.1	0.07	0.009
95.2	0.04	0.008
105.1	0.06	0.010
110.9	0.07	0.010
125.3	0.10	0.012
129.1	0.08	0.010
132.9	0.04	0.007
143.1	0.06	0.008
150.4	0.05	0.007
153.1	0.07	0.009
170.2	0.22	0.010

Table A34. $^{16}O(^{3}He,p)^{18}F$
$E_x = 3.062 \pm 0.015$ MeV

θcm. (deg)	dσ/dΩ (mb/sr)	Error (mb/sr)
8.9	1.94	0.046
11.2	2.79	0.110
14.5	2.36	0.073
16.7	2.11	0.040
18.9	1.86	0.047
22.2	1.55	0.093
27.7	1.01	0.035
29.8	0.72	0.052
32.1	0.51	0.080
33.2	0.60	0.030
35.4	0.51	0.054
37.6	0.42	0.027
39.7	0.39	0.031
43.0	0.41	0.069
44.1	0.42	0.024
48.4	0.50	0.034
53.8	0.46	0.033
60.2	0.46	0.025
64.4	0.38	0.028
70.7	0.30	0.019
75.9	0.31	0.020
80.0	0.30	0.023
86.2	0.31	0.021
95.3	0.30	0.021
105.2	0.24	0.019
111.0	0.20	0.018
125.4	0.14	0.014
129.2	0.16	0.016
132.9	0.21	0.016
143.1	0.16	0.013
150.4	0.17	0.013
153.2	0.18	0.014
170.3	0.13	0.008

Table A35. $^{16}O(^{3}He,p)^{18}F$
$E_x = 3.352 \pm 0.016$ MeV

θcm. (deg)	dσ/dΩ (mb/sr)	Error (mb/sr)
8.9	0.48	0.024
11.2	0.42	0.041
14.5	0.50	0.033
16.7	0.45	0.018
18.9	0.40	0.021
22.2	0.34	0.045
27.7	0.30	0.019
29.8	0.26	0.032
32.1	0.10	0.035
33.2	0.19	0.016
35.4	0.15	0.030
37.6	0.15	0.016
39.8	0.11	0.017
44.1	0.12	0.012
48.4	0.08	0.014
53.8	0.08	0.015
60.2	0.09	0.011
64.4	0.07	0.012
70.7	0.07	0.009
76.0	0.08	0.010
80.1	0.10	0.013
86.2	0.10	0.012
95.3	0.08	0.011
105.2	0.05	0.096
111.1	0.07	0.010
125.5	0.08	0.011
129.2	0.09	0.012
133.0	0.11	0.012
143.2	0.11	0.012
150.5	0.11	0.011
153.2	0.08	0.010

Table A36. $^{16}O(^{3}He,p)^{18}F$
$E_x = 3.732 \pm 0.030$ MeV

θcm. (deg)	dσ/dΩ (mb/sr)	Error (mb/sr)
11.2	0.88	0.060
14.5	1.11	0.049
16.7	0.86	0.026
18.9	0.78	0.030
22.2	0.42	0.049
27.7	0.66	0.029
29.8	0.69	0.063
32.1	0.55	0.082
33.2	0.48	0.027
35.4	0.40	0.048
37.6	0.36	0.025
39.8	0.39	0.032
43.0	0.14	0.041
44.1	0.41	0.023
48.4	0.15	0.019
53.8	0.06	0.013
60.2	0.13	0.013
64.5	0.32	0.025
76.0	0.21	0.016
80.1	0.38	0.026
86.3	0.28	0.019
95.4	0.15	0.015
105.3	0.13	0.014
111.1	0.19	0.017
125.5	0.36	0.022
129.3	0.55	0.028
133.0	0.37	0.022
143.2	0.31	0.019
150.5	0.19	0.014
153.2	0.44	0.022
170.3	0.33	0.012

Table A37. $^{16}O(^{3}He,p)^{18}F$
$E_x = 3.830 \pm 0.012$ MeV

θcm. (deg)	dσ/dΩ (mb/sr)	Error (mb/sr)
11.2	3.47	0.119
14.5	3.24	0.085
16.7	3.26	0.050
18.9	3.00	0.060
22.3	3.05	0.133
27.8	1.97	0.050
29.8	2.03	0.108
32.2	1.14	0.119
33.2	1.45	0.047
35.4	1.25	0.084
37.6	1.17	0.046
39.8	0.82	0.046
43.1	0.87	0.101
44.1	0.71	0.031
48.5	0.79	0.043
53.8	0.67	0.041
60.2	0.58	0.027
64.5	0.19	0.019
76.0	0.46	0.024
80.1	0.24	0.021
86.3	0.39	0.023
95.4	0.38	0.024
105.3	0.26	0.020
111.2	0.22	0.018
125.5	0.13	0.014
129.3	0.04	0.008
133.0	0.14	0.014
143.2	0.26	0.017
150.5	0.36	0.019
153.2	0.12	0.012
170.3	0.12	0.007

Table A38. $^{16}O(^{3}He,p)^{18}F$
$E_x = 4.134 \pm 0.011$ MeV

θcm. (deg)	dσ/dΩ (mb/sr)	Error (mb/sr)
11.2	0.63	0.051
14.5	0.55	0.035
16.7	0.42	0.018
19.0	0.41	0.022
22.3	0.23	0.037
27.8	0.27	0.018
29.9	0.37	0.046
32.2	0.18	0.047
33.3	0.22	0.018
35.5	0.22	0.035
37.7	0.18	0.018
39.8	0.17	0.021
43.1	0.09	0.033
44.2	0.17	0.015
48.5	0.16	0.019
53.9	0.16	0.020
60.3	0.17	0.015
64.5	0.16	0.018
76.1	0.17	0.014
80.2	0.17	0.017
86.3	0.17	0.015
95.4	0.16	0.016
105.4	0.09	0.012
111.2	0.06	0.009
125.6	0.10	0.012
129.3	0.10	0.012
133.1	0.13	0.013
143.2	0.16	0.014
150.5	0.20	0.014
153.3	0.17	0.014
170.3	0.25	0.011

Table A39. $^{16}O(^{3}He,p)^{18}F$
$E_x = 4.378 \pm 0.009$ MeV

θcm (deg)	dσ/dΩ (mb/sr)	Error (mb/sr)
11.2	0.81	0.058
14.5	0.65	0.038
16.8	0.63	0.022
19.0	0.53	0.025
22.3	0.39	0.048
27.8	0.44	0.023
29.9	0.48	0.052
32.2	0.26	0.057
33.3	0.44	0.025
35.5	0.32	0.043
37.7	0.39	0.027
39.9	0.38	0.031
43.1	0.37	0.066
44.2	0.36	0.022
48.5	0.33	0.027
53.9	0.41	0.032
60.3	0.40	0.023
64.6	0.31	0.025
76.1	0.29	0.019
80.2	0.24	0.020
86.4	0.18	0.016
95.5	0.18	0.017
105.4	0.20	0.018
111.3	0.20	0.017
125.6	0.24	0.018
129.4	0.22	0.018
133.1	0.18	0.015
143.3	0.21	0.016
150.6	0.28	0.017
153.3	0.29	0.018
170.3	0.30	0.012

Table A40. $^{16}O(^{3}He,p)^{18}F$
$E_x = 4.651 \pm 0.012$ MeV

θcm. (deg)	dσ/dΩ (mb/sr)	Error (mb/sr)
11.2	1.23	0.071
14.6	1.20	0.051
16.8	1.22	0.030
19.0	1.20	0.038
22.3	1.22	0.084
27.8	1.11	0.037
29.9	1.29	0.086
32.2	0.78	0.098
33.3	1.03	0.039
35.5	0.85	0.069
37.7	0.95	0.041
39.9	0.84	0.047
43.2	0.63	0.080
44.3	0.61	0.028
48.6	0.39	0.030
54.0	0.25	0.025
60.4	0.14	0.014
64.6	0.12	0.016
76.2	0.17	0.014
80.3	0.20	0.018
86.5	0.21	0.017
95.6	0.17	0.016
105.5	0.16	0.016
111.3	0.22	0.018
129.4	0.19	0.017
133.2	0.20	0.016
143.3	0.15	0.013
150.6	0.27	0.017
153.3	0.28	0.018
170.3	0.52	0.015

Table A41. $^{16}O(^{3}He,p)^{18}F$
$E_x = 4.843 \pm 0.012$ MeV

θcm. (deg)	dσ/dΩ (mb/sr)	Error (mb/sr)
11.2	0.43	0.046
14.6	0.44	0.031
16.8	0.41	0.018
19.0	0.41	0.022
22.3	0.43	0.049
27.9	0.37	0.021
29.9	0.45	0.057
32.3	0.36	0.062
33.4	0.39	0.024
35.6	0.45	0.054
37.7	0.35	0.027
39.9	0.38	0.031
43.2	0.41	0.066
44.3	0.35	0.021
48.6	0.36	0.024
54.0	0.28	0.026
60.4	0.20	0.016
64.7	0.12	0.017
76.2	0.12	0.012
80.4	0.10	0.013
86.5	0.13	0.013
95.6	0.22	0.018
105.5	0.09	0.012
111.4	0.21	0.017
129.5	0.16	0.015
133.2	0.12	0.013
143.3	0.16	0.014
150.6	0.20	0.014
153.3	0.24	0.016
170.3	0.31	0.012

Table A42. $^{16}O(^{3}He,p)^{18}F$
$E_x = 4.967 \pm 0.021$ MeV

θcm. (deg)	dσ/dΩ (mb/sr)	Error (mb/sr)
11.2	0.29	0.028
16.8	0.29	0.015
19.0	0.29	0.019
27.9	0.23	0.017
30.0	0.22	0.024
32.3	0.22	0.058
33.4	0.21	0.018
35.6	0.28	0.025
37.8	0.13	0.011
39.9	0.12	0.018
43.2	0.13	0.046
44.3	0.12	0.012
48.6	0.09	0.021
60.5	0.05	0.008
64.7	0.05	0.006
76.2	0.08	0.010
80.4	0.06	0.011
105.5	0.11	0.013
125.7	0.12	0.013
129.5	0.04	0.008
133.2	0.03	0.006
143.4	0.10	0.011
150.6	0.03	0.006

Table A43. $^{16}O(^{3}He,p)^{18}F$
$E_x = 5.601 \pm 0.012$ MeV

θcm (deg)	dσ/dΩ (mb/sr)	Error (mb/sr)
11.3	1.26	0.071
14.6	1.23	0.052
16.8	1.35	0.032
19.1	1.31	0.039
22.4	1.09	0.079
27.9	1.16	0.038
30.0	1.42	0.090
32.3	0.88	0.104
33.5	0.95	0.037
35.7	0.73	0.064
37.8	0.77	0.037
40.0	0.66	0.041
43.3	0.60	0.084
44.4	0.63	0.029
48.7	0.45	0.032
54.2	0.43	0.033
60.6	0.29	0.020
64.8	0.21	0.020
76.4	0.23	0.017
80.5	0.16	0.017
86.7	0.22	0.017
95.8	0.19	0.017
105.7	0.18	0.017
111.6	0.19	0.017
125.9	0.19	0.016
129.6	0.20	0.017
133.4	0.20	0.016
143.5	0.23	0.017
150.7	0.26	0.016
153.4	0.26	0.017
170.4	0.34	0.013

Table A44. $^{16}O(^{3}He,p)^{18}F$
$E_x = 6.105 \pm 0.008$ MeV

θcm. (deg)	dσ/dΩ (mb/sr)	Error (mb/sr)
11.3	3.64	0.121
14.6	3.32	0.085
16.9	3.11	0.048
19.1	2.80	0.057
22.4	2.25	0.113
28.0	2.02	0.050
30.1	2.13	0.110
32.4	1.49	0.135
33.5	1.60	0.049
35.7	1.45	0.090
37.9	1.35	0.049
40.1	1.25	0.057
43.4	0.69	0.090
44.5	1.07	0.037
48.8	0.87	0.044
54.2	0.91	0.048
60.7	0.74	0.031
64.9	0.59	0.034
76.5	0.57	0.027
80.7	0.49	0.029
86.8	0.55	0.027
95.9	0.37	0.024
105.8	0.40	0.025
111.7	0.38	0.024
126.0	0.46	0.026
129.7	0.43	0.025
133.5	0.40	0.023
143.6	0.46	0.024
150.8	0.51	0.023
153.5	0.47	0.023
170.4	0.34	0.013

Table A45. $^{16}O(^{3}He,p)^{18}F$
$E_x = 6.265 \pm 0.013$ MeV

θcm. (deg)	dσ/dΩ (mb/sr)	Error (mb/sr)
11.3	1.90	0.087
14.7	1.66	0.060
16.9	1.74	0.036
19.1	1.54	0.042
22.5	1.52	0.093
28.0	1.22	0.039
30.1	1.06	0.077
32.4	0.99	0.110
33.5	0.90	0.036
35.7	0.69	0.062
37.9	0.88	0.040
40.1	0.58	0.039
43.4	0.60	0.084
44.5	0.63	0.028
48.9	0.56	0.036
54.3	0.43	0.033
60.7	0.45	0.024
65.0	0.44	0.029
76.5	0.38	0.022
80.7	0.38	0.026
86.9	0.28	0.019
96.0	0.42	0.025
105.9	0.31	0.022
111.7	0.28	0.020
126.0	0.20	0.017
129.8	0.21	0.018
133.5	0.32	0.021
143.6	0.25	0.018
150.8	0.26	0.016
153.5	0.28	0.018
170.4	0.36	0.013

Table A46. $^{16}O(^{3}He,p)^{18}F$
$E_x = 6.779 \pm 0.007$ MeV

θcm. (deg)	dσ/dΩ (mb/sr)	Error (mb/sr)
11.3	5.16	0.144
14.7	6.02	0.114
16.9	4.12	0.055
19.2	3.72	0.065
22.5	2.55	0.120
28.1	2.74	0.058
30.2	2.87	0.127
32.5	2.26	0.166
33.6	2.34	0.059
35.8	2.03	0.106
38.0	1.98	0.059
40.2	1.86	0.069
43.5	1.74	0.141
44.6	1.49	0.044
49.0	1.13	0.051
54.4	1.25	0.056
60.8	0.96	0.035
65.1	0.82	0.040
76.7	0.57	0.027
80.8	0.58	0.032
87.0	0.54	0.027
96.1	0.41	0.025
106.0	0.41	0.025
111.9	0.50	0.027
126.2	0.46	0.026
129.9	0.47	0.026
133.6	0.36	0.022
143.7	0.40	0.022
150.9	0.45	0.022
153.6	0.46	0.023
170.4	0.57	0.016

Table A47. $^{16}O(^{3}He,p)^{18}F$
$E_x = 7.206 \pm 0.009$ MeV

θcm. (deg)	dσ/dΩ (mb/sr)	Error (mb/sr)
11.3	1.27	0.071
14.7	1.30	0.053
17.0	0.96	0.027
19.2	2.83	0.057
22.5	0.80	0.067
28.1	0.62	0.028
30.2	0.59	0.058
32.6	0.86	0.102
33.7	0.67	0.031
35.9	0.75	0.065
38.1	0.72	0.036
40.3	0.64	0.040
43.6	0.41	0.069
44.7	0.56	0.027
49.1	0.39	0.029
54.5	0.59	0.038
60.9	0.45	0.024
65.2	0.46	0.030
76.8	0.45	0.024
81.0	0.29	0.022
87.1	0.35	0.022
96.2	0.32	0.022
106.1	0.30	0.022
112.0	0.44	0.026
126.3	0.39	0.023
130.0	0.31	0.021
133.7	0.38	0.023
143.8	0.31	0.019
151.0	0.30	0.018
153.6	0.28	0.018
170.4	0.32	0.012

Table A48. $^{16}O(^{3}He,p)^{18}F$
$E_x = 7.646 \pm 0.014$ MeV

θcm. (deg)	dσ/dΩ (mb/sr)	Error (mb/sr)
11.4	2.48	0.099
14.7	2.18	0.068
17.0	2.07	0.039
19.2	2.02	0.048
28.2	1.49	0.043
30.3	1.56	0.094
32.6	1.58	0.138
33.7	1.41	0.045
36.0	1.17	0.080
38.2	1.10	0.044
40.4	1.09	0.053
43.7	0.95	0.104
44.8	0.86	0.033
49.1	0.62	0.037
54.6	0.59	0.038
61.1	0.40	0.023
65.3	0.43	0.029
76.9	0.38	0.022
81.1	0.28	0.022
87.3	0.38	0.023
96.4	0.24	0.019
106.3	0.26	0.020
126.4	0.27	0.020
130.1	0.25	0.019
133.8	0.36	0.022
143.8	0.29	0.019
151.0	0.25	0.016
153.7	0.21	0.015
170.5	0.57	0.016

Table A49. $^{16}O(^{3}He,p)^{18}F$
$E_x = 7.874 \pm 0.022$ MeV

θcm. (deg)	dσ/dΩ (mb/sr)	Error (mb/sr)
106.4	0.18	0.017
11.4	2.33	0.096
14.8	2.39	0.071
17.0	1.92	0.038
19.3	1.85	0.046
22.6	2.07	0.108
28.2	1.38	0.041
30.3	1.25	0.084
32.7	1.51	0.135
33.8	1.16	0.041
36.0	1.23	0.082
38.2	1.09	0.044
40.4	0.93	0.049
43.7	0.78	0.094
44.8	0.69	0.030
49.2	0.47	0.033
54.7	0.50	0.035
61.1	0.51	0.026
65.4	0.43	0.029
77.0	0.44	0.023
81.2	0.41	0.027
87.3	0.43	0.024
96.5	0.34	0.023
126.5	0.17	0.016
130.2	0.22	0.018
133.9	0.32	0.021
143.9	0.23	0.017
151.1	0.29	0.017
153.8	0.32	0.019
170.5	0.38	0.013

Table A50. $^{16}O(^{3}He,p)^{18}F$
$E_x = 9.145 \pm 0.032$ MeV

θcm. (deg)	dσ/dΩ (mb/sr)	Error (mb/sr)
11.5	2.44	0.097
14.9	1.99	0.065
17.1	2.21	0.040
19.4	1.87	0.046
22.8	1.67	0.096
28.4	1.27	0.039
30.6	1.65	0.095
32.9	1.81	0.147
34.0	1.83	0.051
36.3	0.80	0.066
38.5	0.71	0.035
40.7	0.73	0.043
45.1	0.48	0.025
49.5	0.43	0.031
55.0	0.36	0.030
61.5	0.29	0.019
65.8	0.29	0.024
77.5	0.27	0.018
81.6	0.23	0.020
87.8	0.18	0.016
96.9	0.23	0.019
106.8	0.18	0.017
112.7	0.22	0.018
126.9	0.18	0.016
130.6	0.15	0.015
134.3	0.35	0.022
144.2	0.27	0.018
151.3	0.29	0.017

Table A51. $^{16}O(\alpha,d)^{18}F$
E_x = 0.00 MeV

θcm. (deg)	dσ/dΩ (mb/sr)	Error (mb/sr)
10.4	0.27	0.024
12.9	0.25	0.012
19.1	0.15	0.017
25.2	0.17	0.009
31.3	0.20	0.017
37.4	0.18	0.008
43.4	0.17	0.016
49.4	0.20	0.009
55.2	0.22	0.021
61.1	0.20	0.012
72.4	0.11	0.009
83.5	0.11	0.013
94.1	0.10	0.013

Table A52. $^{16}O(\alpha,d)^{18}F$
E_x = 0.934 ± 0.014 MeV

θcm. (deg)	dσ/dΩ (mb/sr)	Error (mb/sr)
10.5	1.40	0.055
13.0	1.33	0.027
19.2	1.14	0.046
25.4	0.80	0.019
31.5	0.34	0.022
37.6	0.23	0.010
43.6	0.31	0.022
49.6	0.29	0.011
55.5	0.34	0.025
61.4	0.31	0.015
72.8	0.21	0.013
83.9	0.32	0.021
94.5	0.19	0.018

Table A53. $^{16}O(\alpha,d)^{18}F$
E_x = 1.119 ± 0.016MeV

θcm. (deg)	dσ/dΩ (mb/sr)	Error (mb/sr)
10.5	6.57	0.118
13.0	5.90	0.053
19.2	3.86	0.081
25.4	2.87	0.037
31.5	2.66	0.061
37.6	2.57	0.031
43.7	2.17	0.057
49.7	1.73	0.026
55.6	1.20	0.048
61.5	0.87	0.026
72.9	0.66	0.022
83.9	0.63	0.030
94.6	0.69	0.033

Table A54. $^{16}O(\alpha,d)^{18}F$
E_x = 1.716 ± 0.018 MeV

θcm. (deg)	dσ/dΩ (mb/sr)	Error (mb/sr)
10.5	0.11	0.015
13.0	0.09	0.007
19.3	0.05	0.009
25.5	0.05	0.005
31.7	0.04	0.008
37.8	0.04	0.004
43.9	0.02	0.006
49.9	0.02	0.003
55.8	0.02	0.006
61.7	0.02	0.004
73.2	0.01	0.003
84.2	0.01	0.004
94.9	0.02	0.006

Table A55. $^{16}O(\alpha,d)^{18}F$
E_x = 2.100 ± 0.011 MeV

θcm (deg)	dσ/dΩ (mb/sr)	Error (mb/sr)
10.6	0.30	0.026
13.1	0.28	0.012
19.3	0.14	0.016
25.5	0.10	0.007
31.7	0.07	0.009
37.9	0.07	0.005
44.0	0.07	0.010
50.0	0.06	0.005
56.0	0.04	0.009
61.8	0.03	0.004
73.3	0.01	0.002
84.4	0.02	0.005
95.1	0.01	0.004

Table A56. $^{16}O(\alpha,d)^{18}F$
E_x = 2.541 ± 0.019 MeV

θcm. (deg)	dσ/dΩ (mb/sr)	Error (mb/sr)
10.6	0.07	0.012
13.1	0.04	0.005
19.4	0.03	0.007
25.6	0.02	0.003
31.9	0.02	0.006
38.0	0.03	0.003
44.1	0.03	0.006
50.2	0.03	0.003
56.1	0.02	0.005
62.0	0.01	0.003
73.6	0.01	0.003
84.7	0.01	0.004
95.3	0.01	0.003

Table A57. $^{16}O(\alpha,d)^{18}F$
E_x = 3.122 ± 0.014 MeV

θcm (deg)	dσ/dΩ (mb/sr)	Error (mb/sr)
10.6	0.07	0.012
13.2	0.05	0.005
25.7	0.06	0.005
32.0	0.07	0.010
38.2	0.05	0.004
44.3	0.02	0.006
50.4	0.02	0.003
56.4	0.02	0.006
62.3	0.02	0.004
73.8	0	0
85.0	0.01	0.004
95.7	0.01	0.004

Table A58. $^{16}O(\alpha,d)^{18}F$
E_x = 3.363 ± 0.020 MeV

θcm. (deg)	dσ/dΩ (mb/sr)	Error (mb/sr)
10.7	0.26	0.023
13.2	0.23	0.011
19.5	0.13	0.015
25.8	0.10	0.007
32.1	0.07	0.010
38.3	0.04	0.004
44.4	0.03	0.006
50.5	0.03	0.003
56.5	0.02	0.006
62.4	0.02	0.004
74.0	0.03	0.004
85.1	0.03	0.007
95.8	0.01	0.005

Table A59. $^{16}O(\alpha,d)^{18}F$
E_x = 3.808 ± 0.012 MeV

θcm. (deg)	dσ/dΩ (mb/sr)	Error (mb/sr)
10.7	0.35	0.027
13.2	0.29	0.013
19.6	0.18	0.018
25.9	0.18	0.009
32.2	0.21	0.018
38.4	0.27	0.010
44.6	0.24	0.019
50.7	0.21	0.009
56.7	0.15	0.017
62.6	0.11	0.009
74.2	0.14	0.010
85.4	0.14	0.014
96.1	0.10	0.013

Table A60. $^{16}O(\alpha,d)^{18}F$
E_x = 4.140 ± 0.012 MeV

θcm. (deg)	dσ/dΩ (mb/sr)	Error (mb/sr)
10.7	0.15	0.018
13.3	0.14	0.009
19.6	0.07	0.011
26.0	0.10	0.007
32.3	0.12	0.013
38.5	0.08	0.005
44.7	0.08	0.011
50.8	0.08	0.006
56.8	0.08	0.011
62.8	0.08	0.008
74.4	0.09	0.008
85.6	0.07	0.010
96.3	0.05	0.009

Table A61. $^{16}O(\alpha,d)^{18}F$
E_x = 4.393 ± 0.009 MeV

θcm. (deg)	dσ/dΩ (mb/sr)	Error (mb/sr)
10.8	0.32	0.026
13.3	0.30	0.013
19.7	0.28	0.022
26.0	0.23	0.010
32.3	0.15	0.014
38.6	0.11	0.006
44.8	0.08	0.011
50.9	0.07	0.005
57.0	0.05	0.010
62.9	0.09	0.008
74.6	0.07	0.007
85.8	0.07	0.010
96.5	0.09	0.012

Table A62. $^{16}O(\alpha,d)^{18}F$
E_x = 4.852 ± 0.010 MeV

θcm. (deg)	dσ/dΩ (mb/sr)	Error (mb/sr)
10.8	0.21	0.021
13.4	0.20	0.010
19.8	0.12	0.015
26.2	0.11	0.007
32.5	0.08	0.010
38.8	0.09	0.006
45.0	0.11	0.012
51.1	0.12	0.007
57.2	0.13	0.015
63.2	0.12	0.009
74.9	0.10	0.009
86.1	0.05	0.009
96.8	0.05	0.009

Table A63. $^{16}O(\alpha,d)^{18}F$
$E_x = 5.590 \pm 0.027$ MeV

θcm. (deg)	dσ/dΩ (mb/sr)	Error (mb/sr)
10.9	0.27	0.024
13.5	0.24	0.011
19.9	0.15	0.016
26.4	0.11	0.007
32.7	0.07	0.010
39.1	0.08	0.006
45.3	0.06	0.009
51.5	0.05	0.004
57.6	0.07	0.011
63.7	0.07	0.007
75.4	0.05	0.006
86.7	0.03	0.007
97.4	0.05	0.009

Table A64. $^{16}O(\alpha,d)^{18}F$
$E_x = 6.139 \pm 0.012$ MeV

θcm. (deg)	dσ/dΩ (mb/sr)	Error (mb/sr)
11.0	0.53	0.033
13.6	0.57	0.017
20.1	0.40	0.026
26.5	0.34	0.012
32.9	0.33	0.021
39.3	0.39	0.012
45.6	0.39	0.024
51.8	0.37	0.012
58.0	0.32	0.024
64.0	0.30	0.015
75.8	0.24	0.013
87.1	0.28	0.020
97.9	0.28	0.021

Table A65. $^{16}O(\alpha,d)^{18}F$
$E_x = 6.807 \pm 0.010$ MeV

θcm. (deg)	dσ/dΩ (mb/sr)	Error (mb/sr)
11.1	0.37	0.027
13.7	0.43	0.015
20.2	0.55	0.030
26.7	0.46	0.014
33.2	0.33	0.021
39.6	0.28	0.010
46.0	0.20	0.017
52.2	0.16	0.007
58.4	0.15	0.016
64.5	0.16	0.011
76.4	0.17	0.011
87.7	0.13	0.014
98.6	0.14	0.015

Table A66. $^{16}O(\alpha,d)^{18}F$
$E_x = 7.191 \pm 0.008$ MeV

θcm. (deg)	dσ/dΩ (mb/sr)	Error (mb/sr)
11.1	0.21	0.021
13.7	0.21	0.011
26.9	0.18	0.009
33.4	0.16	0.014
39.8	0.15	0.007
46.2	0.17	0.015
52.5	0.17	0.008
58.7	0.18	0.018
64.8	0.25	0.014
76.7	0.25	0.013
88.1	0.21	0.017
99.0	0.33	0.023

Table A67. $^{16}O(\alpha,d)^{18}F$
E_x = 7.434 ± 0.013 MeV

θcm. (deg)	dσ/dΩ (mb/sr)	Error (mb/sr)
11.1	0.18	0.019
13.8	0.19	0.010
20.4	0.19	0.018
27.0	0.17	0.008
33.5	0.15	0.014
40.0	0.13	0.007
46.4	0.10	0.012
52.7	0.08	0.005
58.9	0.08	0.012
77.0	0.06	0.006
88.4	0.09	0.011
99.3	0.11	0.013

Table A68. $^{16}O(\alpha,d)^{18}F$
E_x = 7.658 ± 0.012 MeV

θcm. (deg)	dσ/dΩ (mb/sr)	Error (mb/sr)
11.2	0.19	0.019
13.8	0.19	0.010
20.5	0.19	0.017
27.1	0.16	0.008
33.6	0.14	0.013
40.1	0.10	0.006
46.5	0.12	0.013
52.8	0.10	0.006
59.1	0.07	0.011
77.2	0.06	0.006
88.6	0.05	0.009

Table A69. $^{16}O(\alpha,d)^{18}F$
E_x = 7.871 ± 0.011 MeV

θcm. (deg)	dσ/dΩ (mb/sr)	Error (mb/sr)
11.2	0.19	0.019
13.9	0.19	0.010
20.5	0.15	0.016
27.1	0.13	0.007
33.7	0.08	0.010
40.2	0.13	0.007
46.7	0.11	0.012
53.0	0.09	0.005
59.3	0.07	0.011
65.4	0.13	0.009
77.4	0.07	0.007
88.9	0.05	0.009

Table A70. $^{16}O(\alpha,d)^{18}F$
E_x = 9.494 ± 0.015 MeV

θcm. (deg)	dσ/dΩ (mb/sr)	Error (mb/sr)
11.6	0.43	0.028
14.3	0.36	0.013
21.1	0.34	0.022
28.0	0.33	0.011
34.7	0.31	0.019
41.4	0.34	0.011
48.0	0.30	0.020
54.5	0.34	0.011
61.0	0.29	0.022
67.3	0.32	0.015
79.5	0.30	0.015
91.2	0.23	0.018
102.2	0.29	0.022

Table A71. $^{16}O(\alpha,d)^{18}F$
E_x = 10.541 ± 0.010 MeV

θcm (deg)	dσ/dΩ (mb/sr)	Error (mb/sr)
11.9	0.43	0.027
14.7	0.38	0.013
21.7	0.32	0.022
28.7	0.26	0.010
35.6	0.23	0.016
42.4	0.19	0.008
49.2	0.17	0.015
55.9	0.17	0.007
62.5	0.17	0.017
68.9	0.23	0.012
81.4	0.25	0.013

REFERENCES

1. Norman K. Glendenning, Phys. Rev. 137, B102 (1965).
2. B. G. Harvey, J. Cerny, R. H. Pehl, and E. Rivet, Nucl. Phys. 39, 160 (1962).
3. E. Rivet, R. H. Pehl, J. Cerny, and B. G. Harvey, Phys. Rev. 141, 1021 (1966).
4. E. J-M. Rivet, Investigation of Highly Populated Levels of the $(d5/2)^2_5$ and $(f7/2)^2_7$ Configurations of the (α,d) Reaction, UCRL-11341, March 1964; and private communication, 1965.
5. F. Pühlhofer and R. Bock, Phys. Letters (to be published).
6. M. Gell-Mann and M. L. Goldberger, Phys. Rev. 91, 398 (1953).
7. G. R. Satchler, Some Topics in the Theory of Direct Nuclear Reactions, Lectures in Theoretical Physics, Vol. VIII C, edited by P. D. Kunz, D. A. Lind, and W. E. Brittin (The University of Colorado Press, Boulder, 1966), p. 73.
8. G. R. Satchler, Nucl. Phys. 55, 1 (1964).
9. Norman K. Glendenning, Ann. Rev. Nucl. Sci. 13, 191 (1963).
10. Ernest M. Henley and David U. L. Yu, Phys. Rev. 133, B1445 (1964).
11. W. Tobocman, Theory of Direct Nuclear Reactions (Oxford University Press, London, 1961), Chap. III.
12. J. R. Rook, Nucl. Phys. 61, 219 (1965).
13. L. R. Dodd and K. R. Greider, Phys. Rev. 146, 675 (1966).
14. G. Rakavy, Nucl. Phys. 7, 553 (1958).
15. D. G. Fleming, J. Cerny, and N. K. Glendenning, Phys. Rev. (to be published).
16. J. C. Hardy and I. S. Towner, Effects of a Spin-Dependent Interaction Potential in the DWBA Analysis of Two-Nucleon Transfer Reactions, Nuclear Physics Laboratory, University of Oxford, Ref: 25.67, 1967; and J. C. Hardy (University of Oxford), private communication, July 1967.
17. R. H. Bassel, Phys. Rev. 149, 791 (1966).
18. V. S. Mathur and J. R. Rook, Nucl. Phys. A91, 305 (1967).
19. J. R. Rook, Nucl. Phys. A97, 217 (1967).
20. R. H. Bassel, R. M. Drisko, and G. R. Satchler, The Distorted-Wave theory of Direct Nuclear Reactions, ORNL-3240, February 1962.

21. S. K. Penny and G. R. Satchler, Nucl. Phys. 53, 145 (1964).
22. N. K. Glendenning, Nucl. Phys. 29, 109 (1962).
23. H. C. Newns, Proc. Phys. Soc. (London) 76, 489 (1960).
24. M. El-Nadi and H. Sherif, Nucl. Phys. 55, 489 (1964).
25. A. Y. Abul-Magd and M. El-Nadi, Nucl. Phys. 77, 182 (1966).
26. Ching Liang Lin and Shiro Yoshida, Progr. Theoret. Phys. (Kyoto) 32, 885 (1964).
27. Ching Liang Lin, Progr. Theoret. Phys. (Kyoto) 36, 251 (1966).
28. J. Jänecke, Nucl. Phys. 48, 129 (1963).
29. B. Bayman, Nuclear-Structure Information From Many-Particle Transfer Reactions, in Nuclear Spectroscopy with Direct Reactions II. Proceedings, edited by F. E. Throw, ANL-6878, March 1964, p. 335.
30. J. R. Rook and D. Mitra, Nucl. Phys. 51, 96 (1964).
31. S. Yoshida, Nucl. Phys. 33, 685 (1962).
32. M. Moshinsky, Nucl. Phys. 13, 104 (1959).
33. J. C. Hiebert, E. Newman, and R. H. Bassel, Phys. Rev. 154, 898 (1967).
34. L. L. Lee, Jr., J. P. Schiffer, B. Zeidman, G. R. Satcher, R. M. Drisko, and R. H. Bassel, Phys. Rev. 136, B971 (1964).
35. William R. Smith, Nucl. Phys. A94, 550 (1967).
36. R. N. Glover and A. D. W. Jones, Nucl. Phys. 81, 277 (1966).
37. Gy. Bencze and J. Zimányi, Nucl. Phys. 81, 76 (1966).
38. R. E. Schenter, Phys. Rev. Letters 18, 465 (1967).
39. R. E. Schenter, Nucl. Phys. A94, 408 (1967).
40. W. T. Pinkston and G. R. Satchler, Nucl. Phys. 72, 641 (1965).
41. N. Austern, Phys. Rev. 136, B1743 (1964).
42. G. R. Satchler, Distorted-Wave Calculations and Spectroscopic Factors, in Nuclear Spectroscopy With Direct Reactio II. Proceedings, edited by F. E. Throw, ANL-6878, March 1964, p. 23.
43. R. H. Bassel, R. M. Drisko, and G. R. Satchler, Memorandum to the users of the code JULIE, Oakridge National Laboratory, June 1966 (Unpublished).
44. E. Rost, Phys. Letters 21, 87 (1966).
45. Norman K. Glendenning, Phys. Rev. 156, 1344 (1967).
46. R. A. Broglia and C. Riedel, Nucl. Phys. A92, 145 (1967).
47. R. M. Drisko and F. Rybicki, Phys. Rev. Letters 16, 275 (1966).

48. N. K. Glendenning (Lawrence Radiation Laboratory, Berkeley, California), private communication, 1967.
49. Seldon Keith Penny, Inelastic Effects in Stripping and Other Direct Reactions (Ph.D. Thesis), University of Tennessee (1966).
50. B. Kozlowsky and A. De-Shalit, Nucl. Phys. 77, 215 (1966).
51. F. S. Levin, Phys. Rev. 147, 715 (1966).
52. P. J. Iano and N. Austern, Phys. Rev. 151, 853 (1966).
53. R. Bock, H. H. Duhm, R. Rüdel, and R. Stock, Phys. Letters 13, 151 (1964).
54. Georege L. Strobel, Phys. Rev. 154, 941 (1967).
55. Richard H. Pehl, Studies in Nuclear Spectroscopy By Two-Nucleon Transfer Reactions (Ph.D. Thesis), UCRL-10993, August 1963.
56. M. K. Banerjie, The Theory of Stripping and Pickup Reactions, in Nuclear Spectroscopy Part B, edited by Fay Ajzenberg-Selove (Academic Press, New York, 1960), p. 695.
57. N. Austern, Direct Reactions and Nuclear Structure, in Nuclear Spectroscopy With Direct Reactions II, Proceedings, edited by F. E. Throw, ANL-6878, March 1964, p. 1.
58. E. L. Kelly, Nucl. Instr. Methods 18,19, 33 (1962).
59. B. G. Harvey, E. J-M. Rivet, A. Springer, J. R. Meriwether, W. B. Jones, J. H. Elliott, and P. Darriulat, Nucl. Phys. 52, 465 (1964).
60. J. B. Ball, Computation of Losses Due to Multiple Scattering of Charged Particles in Thin Foils, ORNL-3311, January 1963.
61. B. G. Harvey, J. R. Meriwether, J. Mahoney, A. Bussiere de Nercey, and D. J. Horen, Phys. Rev. 146, 712 (1966).
62. C. Williamson and J. P. Boujot, Tables of Range and Rate of Energy Loss of Charged Particles of Energy 0.5 to 150 MeV, Rapport CEA 2189, 1962.
63. F. S. Goulding, D. A. Landis, J. Cerny, and R. H. Pehl, Nucl. Instr. Methods 31, 1 (1964).
64. F. S. Goulding, D. A. Landis, J. Cerny, and R. H. Pehl, IEEE (Inst. Elec. Electron Engrs.) Trans. Nucl. Sci. 13, No. 3, 514 (1966).
65. F. S. Goulding, Nucl. Instr. Methods 43, 1 (1966).

66. F. S. Goulding and D. Landis, Linear Amplifier, Gating and Timing System, in Instrumentation Techniques in Nuclear Pulse Analysis, National Research Council Publication 1184, 1964, p. 124.
67. L. B. Robinson and F. S. Goulding, An On-Line Computer Installation at Lawrence Radiation Laboratory, Berkeley, UCRL-11458, July 1967.
68. The computer program VFIT was written originally by Arthur Springer and later extensively modifed by David L. Hendrie.
69. The computer program LORNA was written by Creve Maples, Jr..
70. C. Maples, G. W. Goth, and J. Cerny, Nuclear Reaction Q-Values, Nucl. Data Tables (to be published)(UCRL-16964, July 1966).
71. C. H. Holbrow, R. Middleton, J. Parks, and J. Bishop, in Nuclear Spin-Parity Assignments, edited by N. B. Gove and R. L. Robinson (Academic Press, New York, 1966), p. 354.
72. J. R. Priest, D. J. Tendam, and E. Bleuler, Phys. Rev. 119, 1295 (1960).
73. S. Hinds and R. Middleton, Proc. Phys. Soc. (London) 75, 745 (1960).
74. H. W. Fulbright, W. Parker Alford, O. M. Bilaniuk, V. K. Deshpande, and J. W. Verba, Nucl. Phys. 70, 553 (1965).
75. D. R. Osgood, J. R. Patterson, and W. E. Titterton, Nucl. Phys. 60, 503 (1964).
76. V. K. Deshpande, H. W. Fulbright and J. W. Verba, Nucl. Phys. 52, 457 (1964).
77. J. H. Manley, Phys. Rev. 130, 1475 (1963).
78. H. C. Bryant, J. G. Berry, E. R. Flynn and W. T. Leland, Nucl. Phys. 53, 97 (1964).
79. D. Eccleshall and M. J. L. Yates, U.K.A.E.A.-A.W.R.E. report NR/P-7/61.
80. S. Hinds and B. M. Hinds, Nucl. Phys. 48, 690 (1963).
81. S. Hinds and R. Middleton, Proc. Phys. Soc. (London) 74, 762 (1959).
82. J. Aguilar, J. de la Rubia, A. Sanchez, and R. Martinez, An. Real Soc. Espan. Fis. Quin. (Madrid), Ser. A, 62, 279 (1966).
83. Falk Pühlhofer, Die Auslegung eines Breitbandspektrographen Grenzschichtzahlern und Messung der 2-Nukleon-Transfer-Reaktionen $^{16}O(^{3}He,p)^{18}F$ Und $^{40}Ca(^{3}He,p)^{42}Sc$ (Ph.D. Thesis), Ruprecht-Karl-Universitat zu Heidelberg, 1966.
84. J. H. Manley and W. E. Stein, Phys. Rev. 144, 956 (1966).

85. P. H. Stelson and L. Grodzins, Nucl. Data A-1, 21 (1965).

86. T. Lauritsen and F. Ajzenberg-Selove, Nuclear Data Sheets, edited by K. Way, et al. (Printing and Publishing Office, National Academy of Sciences--National Research Council, Washington 25, D. C., 1962), NRC 61-5,6.

87. William W. True, Phys. Rev. 130, 1530 (1963); and W. W. True (University of California, Davis, California), private communication to N. K. Glendenning (Lawrence Radiation Laboratory Berkely, California).

88. S. Cohen and D. Kurath, Nucl. Phys. 73, 1 (1965); and D. Kurath, Argonne National Laboratory, Argonne, Illinois, private communications, May and July, 1966.

89. R. W. Detenbeck, J. C. Armstrong, A. S. Figuera, and J. B. Marion, Nucl. Phys. 72, 552 (1965).

90. C. D. Zafiratos, J. S. Lilley, and F. W. Slee, Phys. Rev. 154, 887 (1967); and C. D. Zafiratos (University of Colorado, Boulder) private communication, September, 1966.

91. R. H. Pehl, E. Rivet, J. Cerny and B. G. Harvey, Phys. Rev. 137, B114 (1965).

92. V. A. Latorre and J. C. Armstrong, Phys. Rev. 144, 891 (1966).

93. E. Kashy, R. R. Perry, R. L. Steele, and J. R. Risser, Phys. Rev. 122, 884 (1961).

94. E. K. Warburton and W. T. Pinkston, Phys. Rev. 118, 733 (1960).

95. I. Talmi and I. Unna, Ann. Rev. Nucl. Sci. 10, 353 (1960).

96. G. C. Ball and J. Cerny, Phys. Letters 21, 551 (1966).

97. D. A. Bromley, E. Almqvist, H. E. Gove, A. E. Litherland, E. B. Paul, and A. J. Ferguson, Phys. Rev. 105, 957 (1957).

98. S. Gorodetzky, R. M. Freeman, A. Gallmann, and F. Haas, Phys. Rev. 149, 801 (1966).

99. Gordon C. Ball and Joseph Cerny, Phys. Rev. 155, 1170 (1967).

100. C. H. Holbrow, R. Middleton, and B. Rosner, Phys. Rev. 152, 970 (1966).

101. H. J. Rose, W. Trost and F. Riess, Nucl. Phys. 44, 287 (1963).

102. J. O. Newton, R. S. Blake, D. J. Jacobs and J. P. Shapira, Nucl. Phys. 71, 113 (1965).

103. E. K. Warburton, J. S. Lopes, R. W. Ollerhead, A. R. Poletti, and M. F. Thomas, Phys. Rev. 138, B104 (1965).

104. C. P. Swann, Phys. Rev. 148, 1119 (1966).
105. D. E. Alburger, A. Gallmann, J. B. Nelson, J. T. Sample, and E. K. Warburton, Phys. Rev. 148, 1050 (1966).
106. R. N. Glover and A. D. W. Jones, Nucl. Phys. 84, 673 (1966).
107. R. R. Carlson, Phys. Rev. 148, 991 (1966).
108. F. Riess and W. Trost, Nucl. Phys. 78, 385 (1966).
109. M. W. Sachs, C. Chasman and D. A. Bromley, Phys. Rev. 139, B92 (1965).
110. H. J. Rose, F. Riess and W. Trost, Nucl. Phys. 52, 481 (1964).
111. L. J. Parish, J. A. Rawlins, and Y. M. Shin, Bull. Am. Phys. Soc. 11, 27 (1966).
112. J. P. Elliott and B. H. Flowers, Proc. Roy. Soc. (London) A229, 536 (1955).
113. Martin G. Redlich, Phys. Rev. 110, 468 (1958).
114. G. E. Brown and A. M. Green, Nucl. Phys. 75, 401 (1966).
115. T. Engeland, Nucl. Phys. 72, 68 (1965).
116. P. Federman and I. Talmi, Phys. Letters 15, 165 (1965).
117. P. Federman, Nucl. Phys. A95, 443 (1967).
118. G. E. Brown and A. M. Green, Nucl. Phys. 85, 87 (1966).
119. A. Arima, H. Horiuchi, and T. Sebe, Phys. Letters 24B, 129 (1967).
120. T. T. S. Kuo and G. E. Brown, Nucl. Phys. 85, 40 (1966).
121. M. Harvey, Phys. Letters 3, 209 (1963).
122. R. W. Ollerhead, J. S. Lopes, A. R. Poletti, M. F. Thomas, and E. K. Warburton, Nucl. Phys. 66, 161 (1965).
123. A. R. Poletti and E. K. Warburton, Phys. Rev. 137, B595 (1965).
124. J. A. Kuehner, E. Almqvist, and D. A. Bromley, Phys. Rev. 122, 908 (1961).
125. J. W. Olness and E. K. Warburton, Phys. Rev. 151, 792 (1966).
126. J. W. Olness and E. K. Warburton, Phys. Rev. 156, 1145 (1967).
127. E. K. Warburton, J. W. Olness and A. R. Poletti, Phys. Rev. 155, 1164 (1967).
128. R. Moreh and T. Daniels, Nucl. Phys. 74, 403 (1965).
129. A. R. Poletti, Phys. Rev. 153, 1108 (1967).
130. P. R. Chagnon, Nucl. Phys. 81, 433 (1966).
131. S. Gorodetzky, R. M. Freeman, A. Gallmann, F. Haas and B. Heusch, Phys. Rev. 155, 1119 (1967).